Chapter One
Introduction and Historical Review

1.1 Introduction

Ultra-short pulses are very important research field. Today short pulsed laser systems find numerous applications in areas of fundamental research as well as for medical and industrial applications, depending on the wavelength and pulse width.

They could be used as sources in spectroscopic tools in the laboratory for time-resolved studies of fast nonlinear phenomena in semiconductors, or as a source in eye-safe laser radar (LIDAR).They could also be used as a source for a pulsed optical-fiber gyroscope or as a seed pulse for another laser in medical applications. Other medical related applications are eye laser surgery and dentist drills. In the industry, ultra-short lasers are used for micro-machining and marking.

Another important field for ultra-short pulses is in high-speed optical communication systems, an optical short pulse source with a high repetition rate is very important for high-bit rate systems. [1, 2] For these wide applications, ultra-short pulses became very important field.

Mode-locked lasers have a number of potential applications, depending on the wavelength and pulse width.

In fiber lasers, an optical rare-earth doped fiber is used as a gain medium to produce laser. The produced laser could be Q-switched [3,7] or mode-locked either : actively or passively . In Active mode-locking a modulator is used to control the cavity losses and induces pulsed operation

[8, 9]. In Passive Mode-locking technique intensity fluctuation acts with a nonlinear medium inside the cavity is used to modulate the cavity loss without external control [10, 11].

The shortest pulses which can be obtained from active mode-locking are in the range of a few pico- seconds. This because it is limited by the speed of the electronics used to drive the modulators. While for passive mode-locking, a femto-seconds regime could be produced, and so, it is the preferred technique for obtaining the shortest pulses [12].

However, active mode-locking, allows operation at frequencies much higher than the fundamental repetition rate, which is important for communications applications [13,1].

1.2 Mode-Locking Fiber Laser

The generation of ultrashort pulses, that is pulses of the order of picoseconds and femtoseconds in duration, is made possible by the technique of mode-locking, first demonstrated in the mid-1960s [1]. The essence of mode-locking is the ability to combine several longitudinal modes oscillating in phase in a laser resonator. It is possible to have more than one longitudinal mode oscillation simultaneously if the gain bandwidth, which is associated with the emission line-width of the laser transition, is greater than that of the longitudinal mode spacing technique of:

$$\Delta\nu = {}^{c}/_{2nL} \quad \text{..... (1.1)}$$

Where: c is the speed of light, n is the refractive index of the cavity medium and L is the separation between the cavity mirrors [3].

In general, these modes oscillate simultaneously, all having a slightly different frequency and without fixed amplitude or phase relationships

between one another. Each mode has its own phase with respect to other modes randomly distributed from $-\pi$ to π and the resulting temporal output from the laser is a statistical time-averaged value characteristic of thermal noise.[6]

Mode-locking is achieved when a number of distinct longitudinal modes of a laser oscillate in phase. When this is the case, a short pulse is formed by constructive interference of the many longitudinal modes that are held in phase in the laser resonator. Various techniques have been employed, usually grouped under the terms "active" and "passive" mode-locking. In active mode-locking intra-cavity amplitude or phase modulators are used to force the cavity modes to couple, whereas in passive mode-locking, the coupling is done by optical nonlinear effects in the cavity [3].

1. 2.1 Active mode-locking

Active mode-locking is the process in which gain or loss is modulated by an external driving source. This principle essentially involves placing a very fast shutter in the laser cavity. Mode locking takes place if the shutter opens only for a very short period of time, every time the light pulse makes a complete roundtrip in the cavity. This results in the constructive interference of the laser modes for a short duration of time, and destructive interference of the modes at all other times. It is, however, not necessary to fully close the shutter. A sinusoidal transmission modulation with a modulation frequency equal to the mode frequency separation $\nu_m = c/2L$ causes the attenuation of any radiation not arriving at the time of peak transmission. Two coupling mechanisms for lasers are: amplitude

modulation and phase modulation. These produce additional electric field components called sidebands on each side of the mode closest to the centre of the laser gain profile. Energy is transferred from the central mode to these side modes at each pass through the modulator. If the laser has gain at these frequencies, these side modes remain "locked" and will, in turn, transfer power to modes further out which will still be locked to the central mode [3].

1.2.1.1 AM Mode-Locking

Amplitude modulation (AM) relies on either the acousto-optic or electro-optic effect in appropriate crystal. An acousto –optic is based on a suitable crystal diffractive properties obtained by applying a sound wave across the crystal , where the electro –optic effect produces a refractive index term that varies with the applied electric field[10].AM modulator by using electro-optic effect uses Mach-Zehndar Interferometer(MZI) .An optical pulse passing through it will first spilt into two halves ,then travel through different sections of fiber ,at which they will interfere at the output coupler .The interference is constructive or destructive depending on path length difference between two arms of the device .By using electro-optic crystal in one arms of this MZI we can change the optical bath length of that arm. This change in the type of interference at the output depends on applied field and results in device losses [14].

1.2.1.2 FM Mode-Locking

Active mode-locking also works with a periodic phase modulation, even though this leads to chirped pulses [8, 11].This technique is called frequency modulation (FM) mode-locking .In both types of active mod-

locking, for stable operation the roundtrip time of the cavity must quite precisely match the period of the modulator signal.

MZI is an electro-optic modulator (EOM) device. Frequency mode-locking involving the periodic modulation of the roundtrip phase change [14,15], is achieved using an electro-optic modulator, such as Mach-Zehnder , that often are used as phase modulators.

They are based on the linear electro-optic effect (also called Pockels effect), i.e., the modification of the refractive index of a nonlinear crystal by an electric field in proportion to the field strength. When an electric field is applied to the crystal via electrodes, refraction index will change linearly with the strength of an externally applied electric field E.

As a result changes in the phase delay of a laser beam will take place. MZI allows controlling the power, phase or polarization of a laser beam with an electrical control signal. In most cases, the achieved pulse duration is governed by a balance of pulse shortening through the modulator and pulse broadening via other effects, such as the limited gain bandwidth [4].

1.2.2 Passive mode-locking

In passive mode-locking, no external source is needed to modulate gain or loss in the cavity. Instead, passive mode-locking utilizes a passive intra-cavity element that favors the high peak power characteristic of mode-locked pulses. Different techniques exist are based on this principle.

1.2.2.1 Colliding pulse mode-locking

The colliding pulse mode-locked dye laser was the first laser capable of generating ultrashort pulses of less than 100 fs duration [16]. Colliding

pulse mode-locking is produced by the interaction of two counter-propagating pulses in a thin SA, such as a dye, installed within a ring laser cavity. Coherent interference of the two colliding pulses produces a standing-wave grating pattern over the thickness of the SA, which effectively increases the intensity of the laser at that location, which thereby increases the bleaching effect even further.

1.2.2.2 Additive pulse mode-locking

In additive pulse mode-locking, also known as coupled cavity mode-locking, pulse shortening results from the interference of pulses with different amount of self-phase modulation. This technique uses an externally coupled resonant cavity in which part of the pulses is given some phase modulation through an optical fiber, such that the leading edge of the pulse is red-shifted and its trailing edge is blue-shifted. The phase-modulated pulse is then re-injected inside the cavity, where the leading edge interferes constructively and the trailing edge interferes destructively with the cavity pulse [17,18]. This process repeatedly compresses the pulse until it reaches the bandwidth limit of the gain medium.

1.2.2.3 Additive Semiconductor saturable absorber mirrors

The mode-locking force of APM is in essence equivalent to a fast saturable absorber [19]. Fiber lasers have also been passively mode locked in a linear-cavity configuration that employs a semiconductor structure for the fast saturable absorber [20] .A semiconductor saturable absorber device incorporates an epitaxial grown pair of InGaAs quantum wells and a low-loss Bragg reflector structure to produce a saturable Bragg reflector (SBR)

[21] . The advantage of semiconductor saturable absorbers over other passive mode locking techniques such as Kerr lens mode locking or APM is their extremely low saturation energies, permitting efficient femtosecond mode locking of low-gain coefficient or short-gain-length lasers. Yt-doped fiber lasers mode locked with the SBR have achieved higher repetition rates (by factors of 3 or more) than APM mode-locked fiber lasers in a single pulse per round-trip configuration. These results are promising for high speed networks that require broadband and stable sources [21].

Semiconductor saturable absorber mirrors(SESAMs)are becoming important devices for short optical pulse generation and all optical switching .Exploiting these SESAM as additive cavity mirror in fiber laser makes it possible to construct compact size, environmentally stable, and ultra short pulse laser that can cover a wide range of wavelengths, generating optical pulse from picoseconds to femto second [22].

1.2.2.4 Kerr lens mode-locking

The most important mode-locking technique was termed self-mode-locking or Kerr-lens mode-locking (KLM). The essential difference between self-mode-locking and previously established mode-locking techniques is the absence of an additional intra-cavity mode-locking element.

The optical Kerr effect, also called Kerr-lensing , is a third-order nonlinear effect which results in a change of the refractive index of a material in the presence of a high-intensity electric field. The behavior of the refractive index under the Kerr effect is intensity dependent and can be described by: [23]

$$n(I) = n_0 + n_2 I \quad \ldots\ldots\ldots\ldots\ldots\ldots \qquad (1\text{-}2)$$

where: [3]

n_0 is the linear refractive index, n_2 is the nonlinear refractive index, and

I is the instantaneous beam intensity.

For typical solid-state materials, the nonlinear index n_2 is on the order of $\sim 10^{-16}$ cm^2/W. So it becomes considerable only for the high-intensity light pulses. Consequently, for a pulse more intense at the center than at effect the edges, the index of refraction of the material becomes higher at the center than at the edges. In the spatial domain, this effect creates a lens (also called a Kerr-lens) that slightly focuses the beam within the material. This is named self-focusing. In the time domain, the index change causes a temporal delay or phase shift for the most intense parts of a beam that induces a red shift of the leading part of the pulse, and a blue shift in the trailing part. This effect is named self-phase modulation (SPM)[23].

It is important to note that SPM generates an extra bandwidth, thus spectrally broadening the pulse. In KLM, the self-focusing effect is used to favor the pulsed mode-locked operation rather than CW operation by one of two possible techniques [23]. In hard aperture mode-locking, a physical aperture is placed inside the cavity near the mirror, which provides relatively high loss to the CW mode. However, during mode-locked operation, a pulse of light with higher intensity than the CW beam will produce self-focusing as it propagates through the medium, which will reduce its diameter as it emerges from the medium. It will thus pass through the aperture with lower loss than for the CW mode, thereby providing a more favorable environment

for pulse operation than for CW operation (Figure 1.1a). Soft aperture mode-locking also uses the difference between the pulsed mode and the CW mode. In this case, the cavity is adjusted such that there is a better overlap between the pump beam and the mode-locked beam, than with the CW beam (Figure 1. 1b).

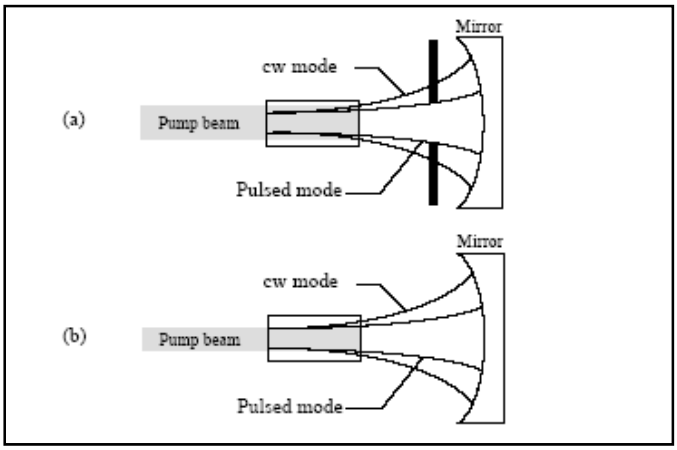

Figure (1.1) Two techniques for achieving Kerr-lens mode-locking. (a) hard aperture mode-locking and (b) soft aperture mode-locked.[24]

KLM requires an initial pulse of sufficient intensity to initiate the effects described above and therefore the mode-locked pulse sequence.

1.2.2.5 Hybrid Mode-Locking

Hybrid mode locking is a combination of active and passive mode locking, where both an RF signal and a passive medium are used to produce ultra-short pulses. It takes advantage of active mode-locked stability and the saturable absorber's pulse shortening mechanisms [6].

1.3 Fiber lasers

Fiber lasers, where an optical rare-earth doped fiber is used as again medium, could be Q-switched or mode-locked either: actively or passively.

If ultrafast optics is to gain grounds on much wider commercial markets, solutions to these limitations must be found. The potential of making compact, rugged laser systems with low power consumption at relative low price make amplified fiber lasers a very promising alternative to classical solid state lasers. The key properties that make rare-earth doped fibers attractive as laser gain media are the high single pass gain combined with broad gain bandwidths and excellent beam quality. Tese qualities make fibers attractive as gain media in mode-locked lasers [6].

1.4 Historical Review

The first mode locking laser was demonstrated by Gürs and Müller in 1963 on Ruby laser using an internal modulator driven by an external periodic wave. The mechanism of mode locking was first clearly explained by M.DiDomenico and Jr.Yariv[10] , which is referred later as active mode-locking.

Since then mode-locking technique and hence generating Ultra-short pulse with high repetition, found wide area of applications, this made the scientists to investigate this field deeply [24,25, 26,27].

In this section a brief literature survey will be concerned to explore efforts and studies that have been done to understand and investigate mode-locking technique.

G. Geister and R. Ulrich [28] reported in 1988 the first FM mode-locked fiber laser.

Implementation of APM mode locking was demonstrated by M.Hofer *et al.in* 1991[29] by using an elliptically polarized pulse inside stander single –mode fiber. In this laser a linear polarized pulse is converted into

elliptically polarized pulse using wave plates or other rotation device. The two polarization components of the pulse then propagate under the influence of self-and cross-phase modulation in optical fiber inside cavity.

In1992,K.Tamura *et al* [30]constricted the first all-fiber, unidirectional, mode-locked ring laser using the non-linear polarization rotation mechanism, NLPR. In the same year, 5-ps pulses were demonstrated in another fiber laser mode locked at a higher repetition rate, 20 GHz.

M. E. Fermann, *et al.* [31]technique employs nonlinear polarization evolution in conjunction with a polarizer which also provides ultrafast amplitude modulation.

S.Longhi *et al* [32] demonstrated in1994 *a* 2.5-GHz FM mode locked laser with a pulse width of 9.6 ps. It is interesting to note that the pulses obtained from FM mode-locked lasers are generally shorter than those obtained from AM mode-locked lasers.

F.X.Kartner *et al.* [33] analytically tried in1995 to include not only the effect of dispersion and nonlinearity in an AM mode-locked laser, but the effect of the modulator as well.

Using rational harmonic mode locking, E.Yoshida and M.Nakazawa[34] demonstrated in 1996 one of the highest repetition rates to-date with a FM mode-locked erbium doped fiber laser operating at 80–200 GHz. However, this method, suffers from pulse-train non-uniformity, jitter, and stability

B. C. Collings *et al.* [35] were presented short cavity erbium/ytterbium fiber lasers that are passively mode-locked with a saturable Bragg reflector. The lasers produce sub-500-fs pulses at

fundamental cavity repetition rates as high as 300 MHz. Stable passive harmonic operation increases the repetition rate to 2.0 GHz.

J. Nathan Kutz *et al.* developed a theoretical model for the pulse dynamics in a fiber laser mode locked by a saturable Bragg reflector and operating in regimes beyond the scope of the master mode-locking equation The model employed allows, direct comparison (with no free parameters) of the theoretical predictions of the pulse spectral and temporal profiles with M. E. Fermann, *et al.* [31]technique employs nonlinear polarization evolution in conjunction with a polarizer which also provides ultrafast amplitude modulation.

S.Longhi *et al* [32] demonstrated in1994 *a* 2.5-GHz FM mode locked laser with a pulse width of 9.6 ps. It is interesting to note that the pulses obtained from FM mode-locked lasers are generally shorter than those obtained from AM mode-locked lasers.

F.X.Kartner *et al.* [33] analytically tried in1995 to include not only the effect of dispersion and nonlinearity in an AM mode-locked laser, but the effect of the modulator as well.

Using rational harmonic mode locking, E.Yoshida and M.Nakazawa[34] demonstrated in 1996 one of the highest repetition rates to-date with a FM mode-locked erbium doped fiber laser operating at 80–200 GHz. However, this method, suffers from pulse-train non-uniformity, jitter, and stability

B. C. Collings *et al.* [35] were presented short cavity erbium/ytterbium fiber lasers that are passively mode-locked with a saturable Bragg reflector. The lasers produce sub-500-fs pulses at

fundamental cavity repetition rates as high as 300 MHz. Stable passive harmonic operation increases the repetition rate to 2.0 GHz.

J. Nathan Kutz *et al.* developed a theoretical model for the pulse dynamics in a fiber laser mode locked by a saturable Bragg reflector and operating in regimes beyond the scope of the master mode-locking equation The model employed allows, direct comparison (with no free parameters) of the theoretical predictions of the pulse spectral and temporal profiles with experimental results in both the normal and anomalous dispersion regimes [12]. Fig (1-2) was shown mode-locking fiber laser.

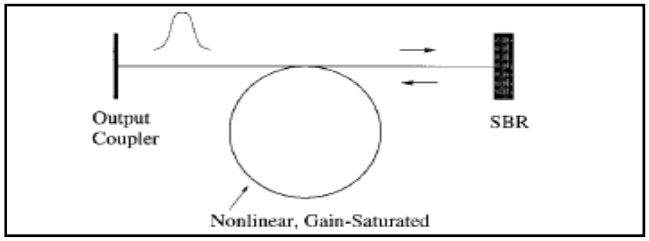

Fig(1- 2) Schematic of mode-locking fiber laser[12].

A.B.Grudinin and S.Gray [36]used in1997 a semiconductor saturable absorber mirror (SESAM) to help increase the repetition rate to (> 2 GHz); this laser operated at its 369th harmonic .

K.S. Abedin *et al.* [37]investigated in1999 a higher-order FM mode locking in a series of papers where they demonstrated 800-fs transform limited pulse trains at repetition rates as high as 154 GHz. The schematic diagram is shown in fig (1-3).

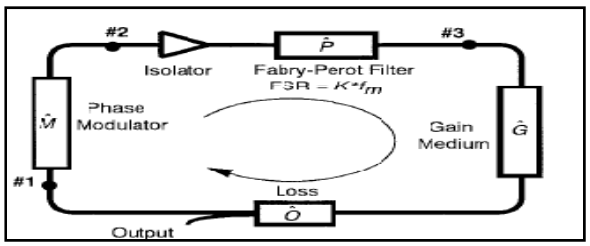

Fig(1-3) Schematic diagram of the higher order FM mode locking[37].

C.X.Yu *et al.* [38]used in 2000 an FM modulator in conjunction with fiber nonlinearity to produce 500-fs pulses at a 1-GHz repetition rate.

L.Q.Huy and L.N.Binh [5]presented the implementation of several mode-locked fiber lasers employing active harmonic mode locking, rational harmonic mode locking, and regenerative mode locking techniques. The effects of the cavity settings on the characteristic of the lasers have been studied. It is found that pulse train with short pulse width can be obtained by modulating the light wave with high modulation frequency, deep modulation depth and incorporating a wide bandwidth filter into the ring cavity. High pump power and long fiber length ring cavity also help to shorten the pulse via the soliton effect. Fig(1-4) is shown the setup of active mode-locking.

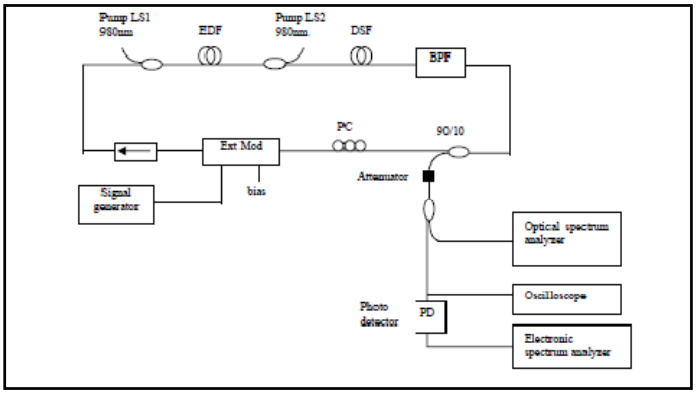

Fig(1- 4) Active harmonic mode-locked fiber laser experiment setup[5].

Ori Katz *et al* [39] is described a robust, self starting picosecond pulse source based on ytterbium (Yb3+) doped fiber laser**.** Utilizing a chirped-fiber-Bragg-grating (C-FBG) for dispersion control, solitary mode-locking .A semiconductor saturable absorber (SESAM) is used for stable self-starting. 3.6ps pulses were produced, with 45MHz basic repetition-rate and mW scale average output power at 1060nm. The cavity configuration shown in fig(1-5).

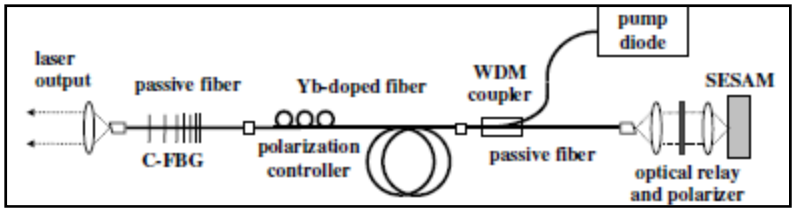

Fig(1-5) Fiber-laser cavity configuration[36]

Nielsen and Andersen [40] presented a theoretically analysis of the Additive pulse mode lock design based on the master equation. Using the analytical theory developed for the master equation it is possible to determine and compare the round trip loss for mode locked. The coupled cavity Fabry–Perot APM fiber laser is shown in fig (1-6).

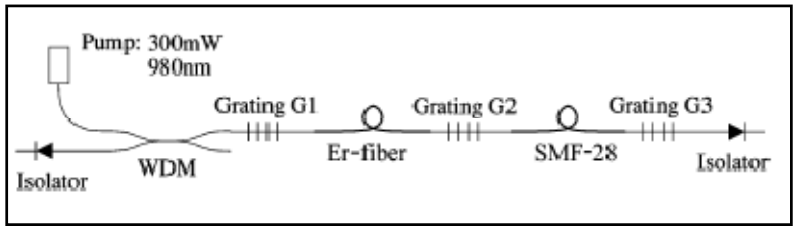

Fig(1- 6) Schematic of a coupled cavity Fabry–Perot all-fiberAPM laser[40].

N.G.Usechak and G.P.Agrawal [41] presented a semi analytic approach based on the moment method used for investigating pulse evolution in mode-locked lasers in which intracavity dispersive and nonlinear effects play a significant role. Its application to an FM mode-locked laser allows us to perform fast parametric studies while predicting the important pulse parameters. When third-order dispersive effects are negligible, a fully analytic treatment is developed that predicts how cavity parameters affect the final steady state. The pulse width obtained in anomalous regime 0.7ps and 2.7ps in normal regime.Then a semi-analytic tool was developed for investigating pulse dynamic in mode lock lasers. It provides aset of three rate equations for pulse energy, width, and chirp. It is

application to an AM mode lock .The AM Mode-lock laser record pulse width of 3.73ps in normal regime and 0.8ps in anomalous regime [42].

The current fiber laser records 33 fs is held by an ytterbium fiber laser built by J.R.Buckley *et al.*, in 2006 [43].

N.G.Usechak and G.P.Agrawal [13] presented experimental FM mode lock operating in the Auto soliton regime at high repation rate in ytterbium fiber laser by using phase modulator. They concluded a pulse width equal to 0.857ps.

N.G.Usechak *et al.*, [44] presented a ytterbium fiber laser mode locked at its 281st harmonic, which corresponds to a repetition rate greater than 10 GHz. The laser produces linearly polarized, 2-ps pulses with up to 38-mW of average output power. Fig(1-7) is shown the setup of laser cavity

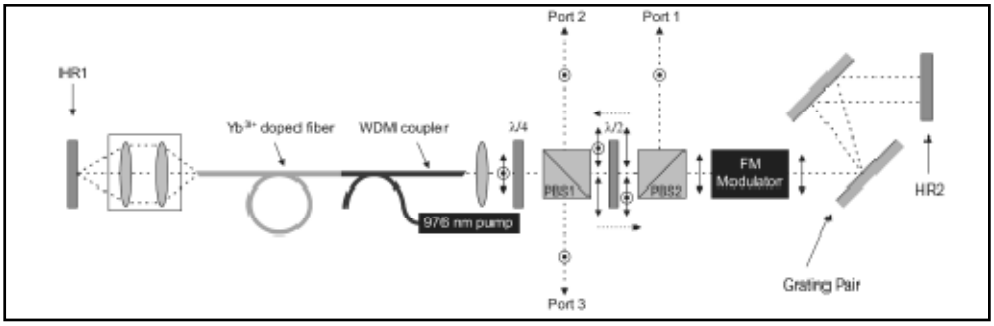

Fig(1-7) Laser cavity configuration[13].

X. Zhou *et al.*, [45] An ultrashort-pulse, mode-locked ytterbium-doped fiber laser has been developed. The group-delay dispersion was compensated with a grating pair inside the cavity. A broad spectrum from 1000-nm to 1120-nm was obtained without intracavity compensation of third-order dispersion. A 0.7-nJ pulse as short as 28.3 fs was obtained with a repetition rate of 80MHz.

H. Sayinc *et al.* [46], We report on a passively mode-locked ytterbium-doped fiber laser with a repetition rate of 1.8 MHz. The laser was hybridly modelocked by nonlinear polarization evolution and a semiconductor saturable absorber mirror. It generated chirped 3.8 ps long pulses with a pulse energy of 1.0 nJ which could be dechirped to a pulse duration of 93 fs.

M. A. Abdelalim *et al.* [47],introduceed Stable mode-locked operation in a simple normal-cavitydispersion laser oscillator that consists of only Yb-doped fiber and saturable absorber is studied. The Yb-doped fiber design parameters group velocity dispersion (GVD), nonlinearity coefficient, bandwidth (Yb-BW), length and gain are considered to be the controlling parameters of the laser cavity.The pulse characteristics such as the temporal width, spectrum and pulse energy as a function of these elements were reported. A pulse spectrum transition from M-like to Π-like and then to parabolic-like shape is observed with different values of the controlling parameters which are similar to that has been observed before in a solid-state laser. The stability limits in the domain of the Yb-BW and length are studied. The stability dependence on GVD, nonlinearity coefficient and gain of the Yb-doped fiber are elucidated. The stability dependence on GVD, nonlinearity coefficient and gain of the Yb-doped fiber are elucidated fig (1-8).

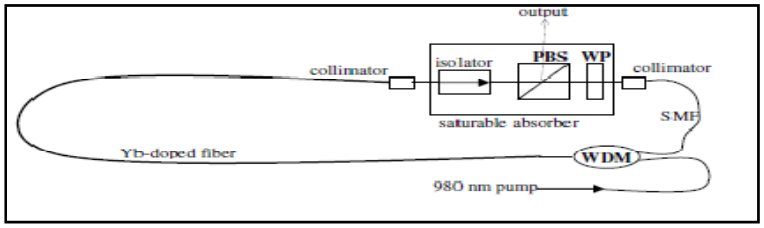

Fig(1-8) Fiber Laser cavity configuration[47].

1.6 Aim of This Thesis

- The aim of this project is to obtain the basic equation that governs propagation of optical pulses in single-mode fibers. Then the equations that govern the evolution of pulse parameters during each roundtrip will be introduced by moment methods. These equations will be solved numerically using fourth-fifth order Runge-Kutta numerical method.
- Study the effect of Chanchiang input parameter such as(Fr,Lr,β2 ,and nonlinearity) on the output pulse parameter of the FM Mode locking at normal and anomalous regime.
- Solve the master equation specially for AM Mode locking by the moments method to track the o/p laser pulse parameter(E,Ω,ζ,q and pulse width)at each round trip, then study the effect of Chanchiang input parameters at the output pulse in normal and a anomalous regime.
- Solve the SBR Mode locking Master Equation by the moment method to gives five o/p pulse parameter(E,Ω,ζ,q and pulse width),then study the effect of Chanchiang i/p parameter (Fr,Lr,β2,Δsa and nonlinearity) on the o/p pulse.

1.7 Thesis Layout

In chapter two, a general description of optical fiber will be investigated and how it is used as gain medium after doping it with one of rare-earth atoms such as Yt^{+3}or Er^{+3} and the characteristics of ytterbium doped fiber are shown .

Parameters that effect on pulse propagation inside doped fiber such as losses, dispersion, and nonlinearity are investigated.

In chapter three, theory and equations that govern pulse prorogation through optical fiber starting from Maxwell's equations and based on Non-Linear Schrödinger Equation NLSE, are demonstrated.

Mode-locking fiber laser master equation is then introduced after setting the basic equations and assumptions. Based on master equation and modified Ginzburg-Landau equation, pulse parameters evolution equations are introduced using moment method.

In chapter four, a numerical simulation is done to solve the evolution equations using fourth-fifth order Runge-Kutta method for FM,AM and APM mode-locked ytterbium fiber laser .Then a study and analysis for results are done.

In chapter five, conclusion and future work are shown.

Chapter Two
Theoretical &Basic Concept

2.1 Introduction

Optical fiber is commonly used as a transmission medium in communications where often referred to as a passive fiber. When this fiber is doped with one of rare-earth atoms such as erbium or ytterbium and pumped by optical source, it becomes active and could be used as a laser source or optical amplifier.

Doped optical fibers are an attractive gain material for lasers and amplifiers. They are solid-state and do not have to be water-cooled, and they can be pumped easily with wavelength-division-multiplexing fiber couplers. Doped fibers provide both the gain and the cavity since the light is guided by the single-mode core [6].

Fiber lasers can be mode-locked actively, where a modulator controls the cavity losses and induces pulsed operation, or passively, where an intensity fluctuation acts in conjunction with a nonlinear medium inside the cavity to modulate the cavity loss without external control. The shortest pulses which can be obtained from active mode-locking tend to be limited to approximately 1 psec by the speed of the electronics used to drive the modulators, and so passive mode-locking is the preferred technique for obtaining the shortest pulses[3].

2.2 Fiber Amplifiers

Although fiber amplifiers were made as early as 1964, their use became practical only after 1986 when the techniques for fabrication and characterization of low-loss, rare-earth-doped fibers were perfected. The rare earths form a group of 14 similar elements with atomic numbers in the range

from 58 to 71. When these elements are doped in silica or other glass fibers, they become triply ionized [6]. Many different rare-earth ions, such as erbium, holmium, neodymium, samarium, thulium, and ytterbium, can be used to make fiber amplifiers that operate at wavelengths covering a wide range. Fiber amplifiers are commonly used to overcome transmission losses and restore the optical signal in such systems.

2.3 Fiber Grating

Silica fibers can change their optical properties permanently when they are exposed to intense radiation from a laser operating in the blue or ultraviolet spectra region.

This photosensitive effect can be used to induce periodic changes in the refractive index along the fiber length, resulting in the formation of an intracore Bragg grating. Fiber gratings can be designed to operate over a wide range of wavelengths extending from the ultraviolet to the infrared region.

Fiber lasers are very closely related to fiber amplifiers, since they are lasers with active medium which is made of rare earth doped fiber [6].

A section of rare-earth doped fiber is used as the gain medium (cavity) of the laser, while the mirrors can be made in various ways but the use of Fiber Bragg Gratings (FBGs) which is very attractive because of their wavelength-selective nature [48]

The laser is pumped with light of a wavelength appropriate to the lasing medium, (as an example: 980 nm or 1480 nm for erbium).In Figure (2.1), a simple example of a fiber laser is constructed from two FBGs and a length of erbium doped fiber. It is an optical amplifier with mirrors on the end of the fiber to form a cavity.

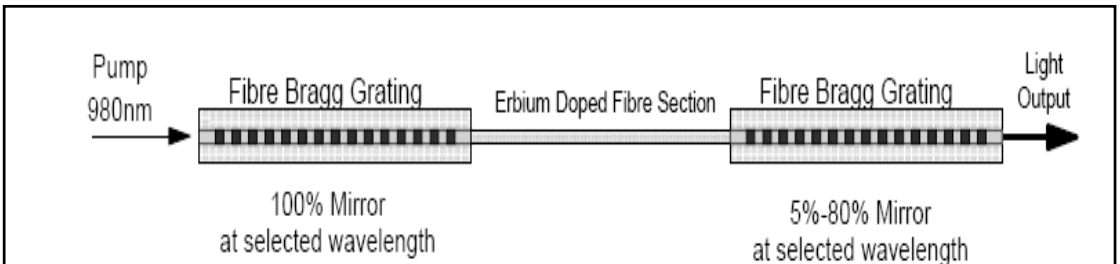

Fig. (2.1): Fiber laser using FBGs [6].

Pumped laser of 980 nm wavelength enters the cavity through the left-hand FBG. Both FBGs are resonant (reflective) at a very specific chosen wavelength in the 1550 band and so the 980 nm light will pass straight through the FBG without attenuation [6].Due to optical pumping, atoms will be excited to higher levels.

Consequently a spontaneous emission will begin in the erbium doped fiber very quickly. Since spontaneous emission is random in direction, so most of it will not be in the guided mode and will leave the cavity quite quickly.

Also, it is random in wavelengths, so will not be at exactly the right wavelength to be reflected by the FBGs and will pass out of the cavity straight through the FBG mirrors. But some spontaneous emission will (by chance) have exactly the right wavelength and will happen to be in the guided mode.

In this case, lasing will begin, since these emissions will be reflected by the FBGs and amplified in the cavity [48].

2.4 Factors affecting on fiber Laser Characteristics.

There are some factors which affect on fiber laser characteristics such as:

1. Lasers could be produced in different wavelength bands, depending on rare earth dopants [6,49] .Fig(2-2shows the wavelength ranges accessible from the different rare-earth dopants in silica glass fibers.

   Nd^{+3} at 0.9 μm , Nd^{+3} at 1.08 μm , Pr^{+3} at 1.06 μm , Er^{+3} at 1.55 μm and Yt^{+3} at 1055

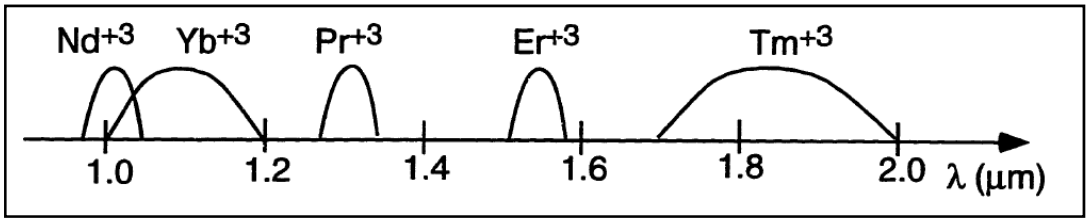

Fig(2.2) Diagram of wavelength ranges which be obtained dopants in silica fibers[3].

Also the level of rare earth dopant used in the glass is another factor which affect on fiber laser. Some glass hosts cannot be doped to very high concentrations.

2. Another factor affects on operational characteristics of the lasing medium is the type and composition of glass used in the "host" fiber. This is because the host plays a part in the energy state transitions necessary to support stimulated emission.
3. The characteristics of used grating determine the exact output wavelength.

2.4.1 Rare-Earth Doped Fibers significant properties

Rare-earth doped fibers are attractive as laser gain media due to the following significant properties: [6, 36]

1. High power output (in hundreds or even several kilowatts), due to high gain and high efficiency.

2. Broad gain bandwidth
3. Excellent beam quality
4. Directly pumped by laser diodes
5. Low noise
6. Tunability
7. Very narrow line-width, a 10 kHz line-width has been produced.
8. Good soliton generation
9. External modulation.
10. Preselected wavelengths, since FBGs can be manufactured to very accurate wavelength tolerances
11. Low cost

These qualities make doping optical fibers as fiber lasers sources , very important components in modern communication systems (for their ability to generate transform-limited pulses) and , hence attractive as a gain medium in mode-locked lasers [50].

2.4.1.1 Erbium-doped silica fiber

Due to current interest in all-optical communications, erbium-doped fiber is probably the most well-known of all the rare-earth doped fibers. Er^{+3}-doped fiber amplifiers are beginning to replace repeaters in undersea transmission systems, and Er^{+3}-doped fiber lasers may someday have a role as a pulsed source in a communications network. Many excellent references exist on the characteristics of Er^{+3}-doped fiber including [51], and so only brief comments are included here.

Erbium-doped silica fiber is a three-level system with pump absorption bands at 800 nm, 980 nm, and 1480 nm and broadband emission near 1.55 µm as shown in Fig.(2-3).

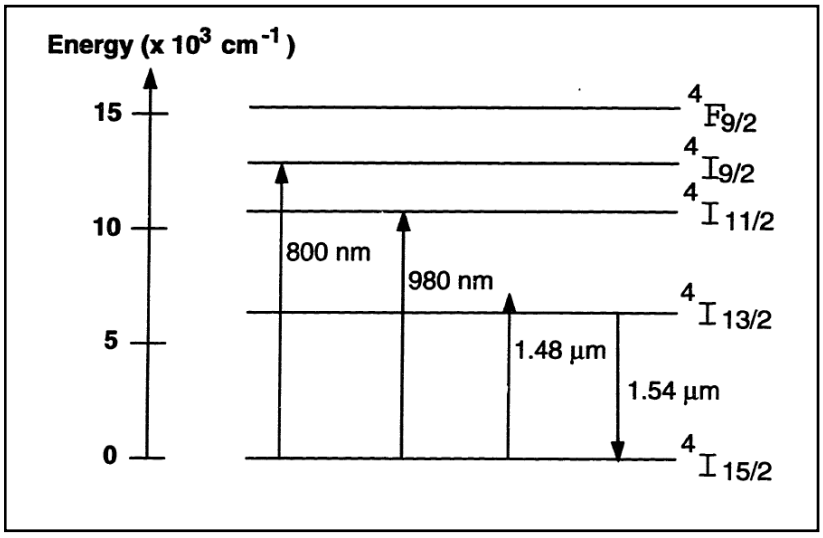

Fig(2.3)Energy levels of silica-glass fiber. Pump bands are at 800nm, 980nm and1.48µm Er^{+3} with brode band emission near 1.55µm [3].

For erbium-doped silica fiber, the most convenient pump wavelength would be 800 nm due to the availability of high power AlGaAs diodes, but pump excited-state absorption occurs which seriously degrades the pumping efficiency. 980 nm and 1480 nm are then the preferred pump wavelengths, and diode lasers are available at both wavelengths: strain-layer InGaAs diodes at 980 nm and InGaAsP diodes at 1480 nm. Pumping at 980 nm has shown higher gains and better noise performance [52].

2.4.1.2 Ytterbium doped fibers

The significant features of ytterbium-doped fiber made it attractive as optical amplifier and laser source. It has broad-gain bandwidth, high efficiency and broad absorption band [10]. Its high quantum efficiency (~ 95

%), since lasing band is very close to the pump wavelength [6] .Very high doping concentrations are possible in ytterbium doped fibers, enabling very high single pass gains and high slope efficiencies of up to ~ 80 %.

Ytterbium has a high absorption at (976 nm), and for this wavelength there have been a large development of both single mode fiber pigtailed diode pump lasers and high power diode pump lasers. Single mode pump lasers at (976 nm) have primarily been developed for use with Erbium in the telecommunication industry. Ytterbium absorption band extends from below (850 nm) to (980 nm) and from (1010 nm) to above (1070 nm), and has peak absorption at 976 nm as shown for the emission and absorption spectrum in Fig.(2.4).Therefore they can generate many wavelengths of general interest, e.g. for spectroscopy or for pumping other fiber lasers.[6,11].

Yb^{+3} Spectroscopy is very simple in comparison with other rare-earth doped fibers .It is considered as two main level systems (ground and excited levels) with other sublevels as shown in Fig. (2.5)[36].

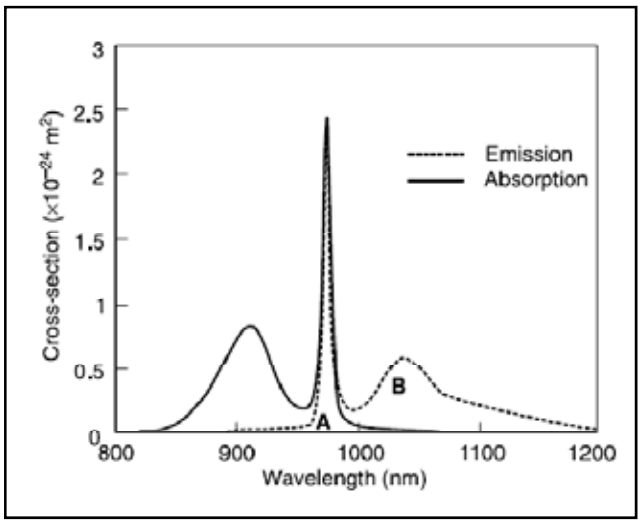

Fig.2.4 Absorption (solid) and emission (dotted) cross sections of Yb $^{+3}$ [6].

When Yb^{+3} doped fiber is typically pumped into the higher sublevels, it behaves as a true three-level system for wavelengths below about (990 nm),

as shown in Fig. (2.5). While at the longer wavelengths, from (~1000 to ~1200 nm), it behaves as a quasi-four-level system.

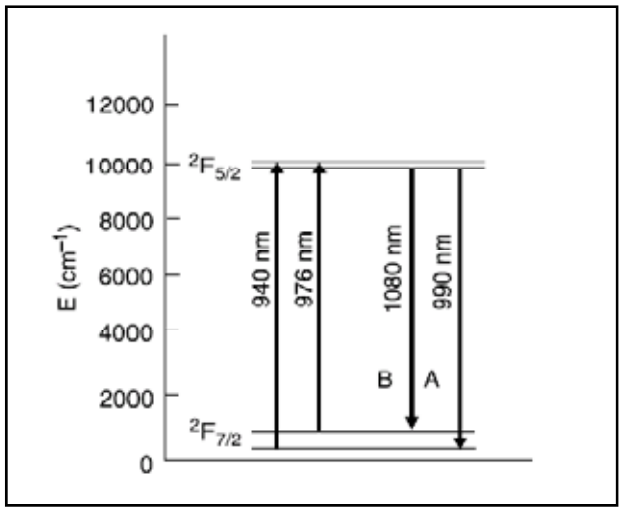

Fig. (2.5): Energy level of Ytterbium doped silica fibers.

Yb^{+3} Doped fibers are very efficient sources. The emission wavelength can be more or less selected by a careful choice of the pump wavelength. The gain of an ytterbium doped fiber can be well modeled by a Gaussian function with FWHM of (~40 nm) and with a central wavelength at (1030 nm).

2.5 Losses, Dispersion and Nonlinearity in Doped Fiber

When light enters one end of the fiber it travels (confined within the fiber) until leaving the fiber at the other end. It will emerge (depending on the distance) much weaker, lengthened in time, and distorted.

In the following section, a brief study for these parameters which are mainly: losses, dispersion and nonlinearity, that affect on pulse propagated in optical fiber .

2.5.1 Fiber Losses

Losses are referred to the attenuation of the pulse propagated through the optical fiber .This attenuation is defined as the reduction in the output signal power as it travels in distance through the optical fiber[53].

This attenuation is due to several factors such as, material absorption losses, Rayleigh scattering losses and bending losses which are contributing dominantly**.** Other mechanisms for scattering light are a result of the existence of in homogeneities in the materials based on compositional fluctuations or the presence of bubbles and strains introduced in the process of jacketing or cabling the fiber [54].

A brief description for each type of losses will be investigated in the following section.

2.5.1.1 Material absorption

When light travels through the fiber it will be weaker because all glass absorbs light. In fact, the glass itself does not absorb light, but the impurities in the glass absorb light at the wavelengths of interest (infrared region).However, even a relatively small amount of impurities can lead to significant absorption in that wavelength window [55].

Generally the OH ions are the most important impurity affecting fiber loss, as shown in Fig (2.6).

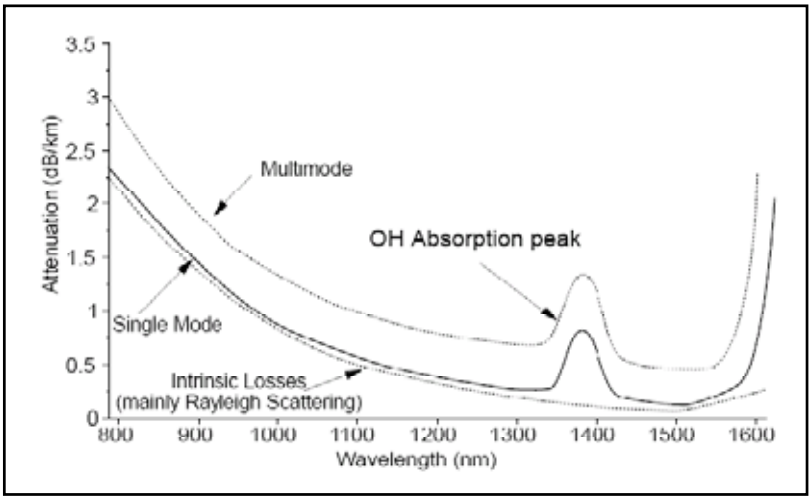

Fig.(2.6)Typical Fiber Infrared Absorption Spectrum [55].

Also the figure displays losses in single and multimode fiber and Rayleigh scattering .

Measuring power loss is an important fiber parameter during transmission of optical signals inside the fiber. Due to high technology used in producing optical fiber, a significant reduction in material losses is achieved as shown in Fig. (2.7).

As shown in Fig.(2.6) and (2.7) , the fiber exhibits a minimum loss of about (0.2 dB/km) near (1.55 μm). Then losses are considerably high at wavelengths shorter and higher than (1.55 μm), reaching a level of a few dB/km in the visible region. In Fig. (2.7, three windows (or bands) are shown to facilitate losses–wavelength dependency study.

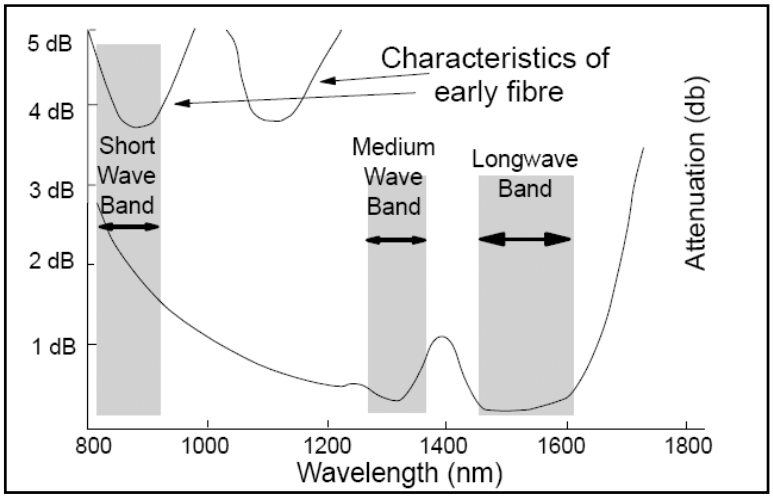

Fig. (2.7) Transmission Windows [55].

If P_0 is the power launched at the input of a fiber of length *l*, then the transmitted power P_T is given by: [55]

$$P_T = P_o \, exp(-\alpha l) \qquad \ldots\ldots\ldots\ldots\ldots\ldots \qquad (2.1)$$

Where the attenuation constant (α) is a measure of total fiber losses from all sources. Usually (α) is expressed in units of dB/km using the following relation:[54]

$$\alpha_{dB} = -\frac{10}{l} log\left(\frac{P_T}{P_o}\right) = 4.343\,\alpha \qquad \ldots\ldots\ldots \qquad (2.2)$$

Where Eq. (2.2) was used to relate α_{dB} and α , where the later is wavelength dependant.

2.5.1.2 Rayleigh scattering

Most light loss in a modern fiber is caused by scattering . Rayleigh scattering is a fundamental loss mechanism, caused by the interaction of light and the granular appearance of atoms and molecules on a microscopic scale [4].

Rayleigh scattering originates from density fluctuations frozen into the fused silica during manufacturing, resulting local fluctuations in the refractive index, causing to scatter light in all directions [21] .It varies as λ^{-4} and is dominant at short wavelengths. Since this loss is intrinsic to the fiber, it sets the ultimate limit on fiber loss. The intrinsic loss level (shown by a dashed line in Fig. (2.6) is estimated to be (in dB/km) as in the following relation:

$$\alpha_R = \frac{C_R}{\lambda^4} \qquad \ldots\ldots\ldots\ldots\ldots\ldots\ldots\ldots\ldots\ldots \qquad (2.3)$$

Where the constant C_R is in the range (0.7–0.9 dB/(km-μm^4)) depending on the constituents of the fiber core.

As α_R = 0.12–0.15 dB/km near λ= 1.55 μm, losses in silica fibers are dominated by Rayleigh scattering. Another reason for this type of losses is the variations in the uniformity of the glass cause scattering of the light. Both rate of light absorption and amount of scattering are dependent on the wavelength of the light and the characteristics of the particular glass.

2.5.1.3 Bending Losses

Another type of losses arises from bending optical fiber .At the bend , the propagation conditions alter and the light rays which would propagate in a straight fiber are lost in the cladding[6].

Two classes of fiber losses arise from either large-radii bends or small fiber curvatures with small periods. These bending effects are called macro-bending losses (due to tight bend) and micro-bending losses (due to microscopic fiber deformation, commonly caused by poor cable design), respectively.

If a fiber is bent from the straight position, the light may be radiated away from the guide, causing optical leakage. As the radius of curvature of the fiber bend decreases, the bending loss will increase exponentially [55].

2.5.2 Dispersion

It is defined as the broadening in the optical pulse due to the variation of refractive index with wavelength as the pulse of light spreads
out during transmission on the fiber [10,56].

When the pulse propagates inside the fiber, each spectral component travels independently, and hence suffers from time delay or group delay per unit length in the direction of propagation [55].The broad bandwidth frequency components of a transform limited pulse experience an index of refraction based on their frequency n(ω).A short pulse becomes longer due to broadening and ultimately joins with the pulse behind, making recovery of a reliable bit stream impossible as shown in Fig. (2.8).

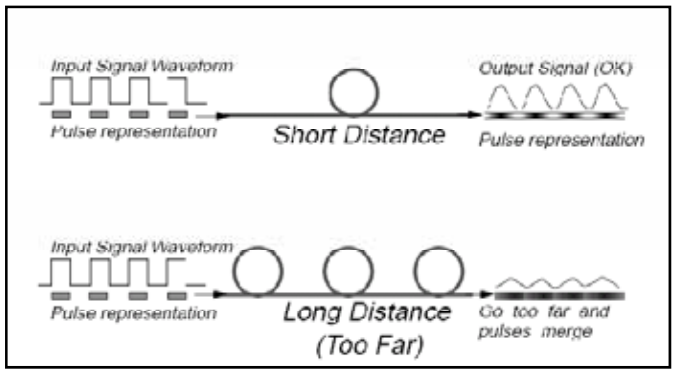

Fig. (2.8)Dispersion effect on propagated pulses .The circles in the figure represent fiber loops [55].

In communication systems as bit rates increase, dispersion becomes a critical aspect and limits the available bandwidth. This because dispersion broadening effect will make bit interval longer. Consequently fewer bits transmitted and hence low bit rare .

There are many kinds of dispersion, each of type works in a different way, but the most important three are discussed below.

2.5.2.1 Chromatic Dispersion

A chromatic dispersion is a sum of two types of dispersions which are: [55, 56]

a. Material dispersion

It is intrinsic to the optical fiber itself, which arises from the variation of refractive index with wavelength.

b. Waveguide dispersion

Which is a function of design of the core and cladding of the fiber, and arises from the dependence of the fiber's properties on the wavelength.

2.5.2.2 Material Dispersion

Material dispersion could be explained as following :

The bound electrons of a dielectric (optical fiber) interact with an electromagnetic wave propagated inside it , causing to the medium to response , depending on the optical frequency ω□. This response is called as a material dispersion, arising from the frequency dependence of the refractive index *n(*□ω).

Essentially, the origin of material dispersion is related to the characteristic resonance frequencies at which the medium absorbs the electromagnetic radiation through oscillations of bound electrons [48].

Since lasers and LEDs produce a range of optical wavelengths (a band of light) rather than a single narrow wavelength, therefore the fiber has different refractive index characteristics at different wavelengths and hence each wavelength will travel at a different speed in the fiber .

Thus, some wavelengths arrive before others and hence, a signal pulse disperses[55].Fig (2.9), shows a change in refractive index due to different wavelengths spectrum .The refractive index could be well approximated by the Sellmeier equation [56]

$$n^2(\omega) = 1 + \sum_{i=1}^{m} \frac{B_j \omega_j^2}{\omega_i^2 - \omega^2} \qquad \ldots\ldots\ldots\ldots\ldots \qquad (2.4)$$

Where $\omega_i$is the resonance frequency and B_i is the strength of jth resonance.

Dispersion plays very important role in propagation of short optical pulses since different spectral components associated with the pulse travel at different speeds given by c / n□λ□.

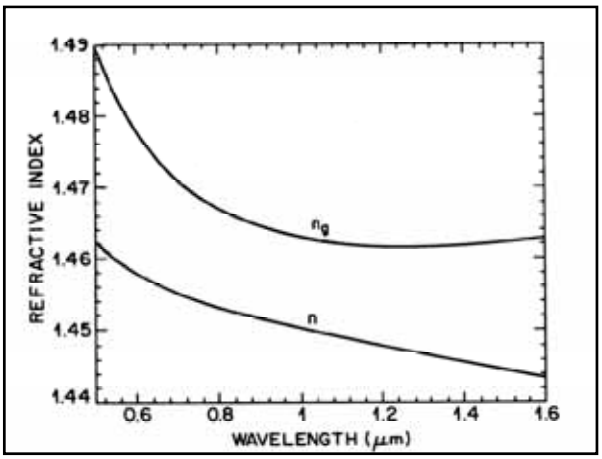

Fig. (2.9): Refractive index n and Group index n_g versus wavelength for fused silica[55].

Dispersion-induced pulse broadening can be harmful for optical communication systems, even when the nonlinear effects are not important [55 ,56].

The combination of dispersion and nonlinearity can result in a qualitatively different behavior, when system is brought into nonlinear regime.

By expanding the mode-propagation constant β in a Taylor series about the frequency ω_0 at which the pulse spectrum is centered, the effects of fiber dispersion could be accounted mathematically,

$$\beta(\omega) = n(\omega)\frac{\omega}{c} = \beta_0 + \beta_1(\omega - \omega_0) + \frac{1}{2}\beta_2(\omega - \omega_0)^2 + \cdots \quad \ldots\ldots \quad (2.5)$$

Where:

$$\beta_m = \left(\frac{d^m\beta}{d\omega^m}\right)_{\omega=\omega_0} \quad (m = 0, 1, 2) \quad \ldots\ldots\ldots\ldots \quad (2.6)$$

β_1 and β_2 are related to the refractive index n and their derivatives are:

$$\beta_1 = \frac{1}{v_g} = \frac{n_g}{c} = \frac{1}{c}\left(n + \omega\frac{dn}{d\omega}\right) = GD = \acute{K}(\omega) \quad \ldots\ldots\ldots \quad (2.7)$$

$$\beta_2 = \frac{1}{c}\left(2\frac{dn}{d\omega} + \omega\frac{d^2n}{d\omega^2}\right) = GVD = K''(\omega) \quad \ldots\ldots\ldots \quad (2.8)$$

Where:

v_g : the group velocity,

n_g : the group index.

C : the light speed.

From physics point of view, the envelope of an optical pulse moves at the group velocity while the parameter β_2 represents dispersion of the group velocity and is responsible for pulse broadening [55]. Hence this effect is called as the group-velocity dispersion (GVD), and β_2 is the GVD parameter.

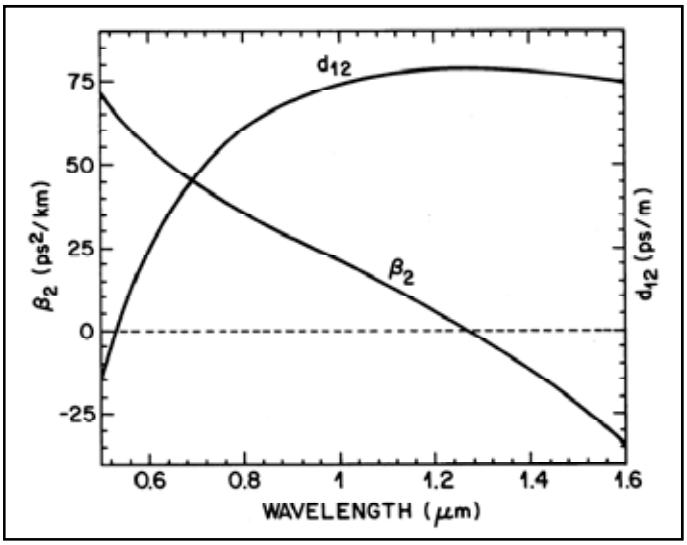

Fig.(2.10) : β_2 and d_{12} as a function of wavelength for fused silica [56].

Studying Fig. (2.10), it is obvious that β_2 vanishes (becomes zero) at a wavelength of about (1.27 μm) and then becomes negative for longer wavelengths. This wavelength is referred to as the zero-dispersion wavelength and is referred to as λ_D.

When $\lambda=\lambda_D$,this doesn't mean that dispersion becomes zero , however, another term of dispersion appears and must be considered. This new term is called third order dispersion TOD or β_3 , which is the cubic term in Eq.(2.5) [56].

This higher-order dispersive effects can distort ultra-short optical pulses by asymmetrically broaden pulses [54] both in the linear and nonlinear regimes. Adding it, is necessary only when the wavelength λ approaches λ_D to within a few nanometers. Fig.(2.11) demonstrates λ normal and anomalous dispersion regime as functions of wavelength in single-mode fiber.

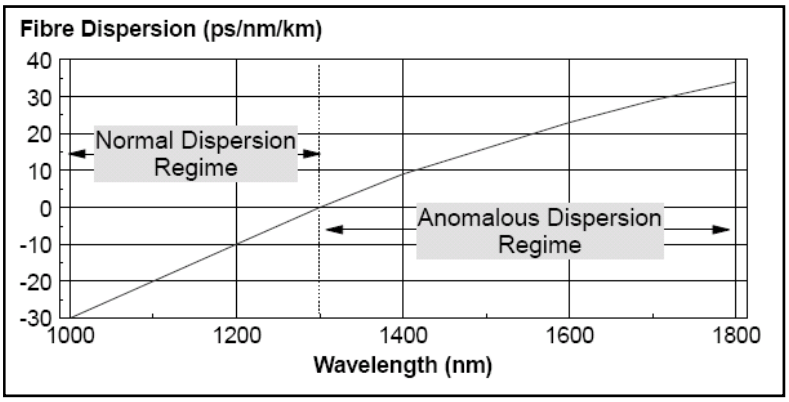

Fig.(2.11) Dispersion in standard single-mode fiber[55].

2.5.2.3 Normal and Anomalous Dispersion

Depending on the sign of the GVD parameter, nonlinear effects in optical fibers can exhibit qualitatively different behaviors. As shown in Fig. (2.12) when $\lambda < \lambda_D$ where $\lambda_D \approx 1.3\mu m$) the fiber is in so-called normal dispersion regime as $\beta_2 > 0$. In this regime, high-frequency (blue-shifted) components of an optical pulse travel slower than low-frequency (red-shifted) components of the same pulse[55].

In the anomalous dispersion regime when $\beta_2 < 0$, the opposite occurs. Optical fibers exhibit anomalous dispersion when the light wavelength exceeds the zero-dispersion wavelength $\lambda > \lambda_D$ as shown in Fig. (2.11) .

Anomalous-dispersion regime is very important in study of nonlinear effects since in this regime, the optical fibers support solitons through a balance between dispersion and nonlinearity.

Fig. (2.11) is for bulk-fused silica, while the dispersive behavior of actual glass fibers deviates from that shown in these figures due to following two reasons :

1. In fiber laser ,where fiber are used as gain medium , the fiber core may have small amounts of rare earth dopants such as (Er^{+3}, Yb^{+3}) so , dopants effect should be added to Eq.(2.4).
2. Due to dielectric wave-guiding, the effective mode index is slightly lower than the material index n□(ω) of the core, reduction itself being ω dependent. Hence, a waveguide contribution must be considered and added to the material contribution to calculate the total dispersion.

2.5.2.3 Waveguide dispersion

In spite of a very complex effect of a waveguide dispersion which is caused by the shape and index profile of the fiber core, this can be controlled by careful design .In fact; waveguide dispersion can be used to counteract material dispersion [6].

Waveguide effect on β_2 is relatively small except near the zero-dispersion wavelength λ_D where the two become comparable. The waveguide effect is mainly to shift λ_D slightly toward longer wavelengths, where ($\lambda_D \approx$ ~1.31 μm) for standard fibers.

The dispersion parameter D that is commonly used in the fiber-optics instead of β_2. It is related to β_2 by the relation:[55]

$$D = \frac{d\beta_1}{d\lambda} = -\frac{2\pi c}{\lambda^2}\beta_2 \approx \frac{\lambda}{c}\frac{d^2n}{d\lambda^2}. \quad \ldots\ldots\ldots\ldots \qquad (2.9)$$

2.5.2.4 Polarization Mode Dispersion (PMD)

Conventional optical fiber is cylindrically symmetric but it contains imperfections, so light travelling down such a fiber is changed in polarization. When light transmitted in a single mode fiber, it travels in two orthogonal polarization modes. In a perfect fiber, both modes travel at the same speed, and the polarization modes are said to be degenerated.

While in the case where the two modes travel at different speeds, the fiber can be described as birefringent [57].

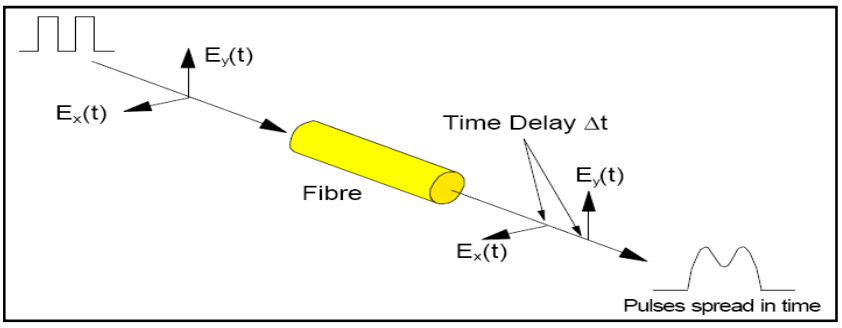

Fig. (2.12) :Polarization mode dispersion[58]

Over a length of the fiber , the polarization states travel at different speeds, so the states will be unsynchronized, which results that the signal energy reaches the fiber end at different point in time , and hence pulse spreading or dispersion arises as shown in Fig (2.12).

Polarization mode dispersion PMD is directly proportional with square root of distance. When operating fibers near zero chromatic dispersion, PMD effects become crucial [55].

2.6 Non-linear effects in Optical Fibers

All the previous discussed effects are considered as power independent (i.e. mainly depend upon wavelength), while now, effects (behavior) that are power dependent will be considered. Such behavior depends on the power (intensity) of light propagating inside the fiber is called non-linear optical effect, which includes the following phenomena:[58]

1. Nonlinear Refraction effects:

a. Self Phase Modulation (SPM)

A phenomena occurs as a result of intensity dependence of refractive index in nonlinear optical media which leads to spectral broadening of optical pulses, and hence distortion. [34] Self-phase modulation (SPM) is the intensity dependent phase shift and resulting spectral broadening which arises when a pulse passes through a medium with an intensity dependent index of refraction .The index *n* is expressed as

$$n\big(I(t)\big) = n_2 + n_2 I(t) \quad \ldots\ldots\ldots\ldots\ldots\ldots \qquad (2.10)$$

where n_o is the linear index, n_2 is the nonlinear index, and I(t) is the pulse intensity. The index is assumed to respond instantaneously to changes in intensity.

b. Cross Phase Modulation (XPM).

A phenomenon occurs when two or more optical fields having different wavelengths propagate simultaneously inside a fiber. As a result of interaction between them, new waves are generated.

Cross-phase modulation is always accompanied by self-phase modulation (SPM) and occurs, since the effective refractive index seen by an optical beam in a nonlinear medium depends not only on the intensity of that beam but also on the intensity of other co propagating beams.

XPM is responsible for asymmetric spectral broadening of co-propagating optical pulses. An important feature of XPM is that, for equally intense optical fields of different wavelengths, the contribution of XPM to the nonlinear phase shift is twice that of SPM [55].

Stimulated Scattering, where is subdivided into two types as shown in Fig.(2.13):

a. Stimulated Brillouin Scattering (SBS)

b. Stimulated Raman Scattering (SRS)

When the light intensity increases, the response of any dielectric becomes nonlinear for intense electromagnetic fields, and so optical fibers do.Stimulated inelastic scattering is a nonlinear effect results from in which the optical field transfers part of its energy to the nonlinear medium. While, elastic effect is for no energy exchanged between the electromagnetic field and the dielectric medium.

Increasing intensity above a threshold causes a stimulated scattering which is defined as a transferring energy from the incident wave to a wave at lower frequency (longer wavelength) with the small energy difference being released in the form of phonons[59].

SBS and SRS as an inelastic scattering, the main difference between them is that: optical phonons participate in SRS while acoustic phonons participate in SBS. In a simple quantum-mechanical picture applicable to both SRS and SBS, a photon of the incident field (called the pump) is annihilated to create a photon at a lower frequency and a phonon with the right energy and momentum to conserve the energy and the momentum.

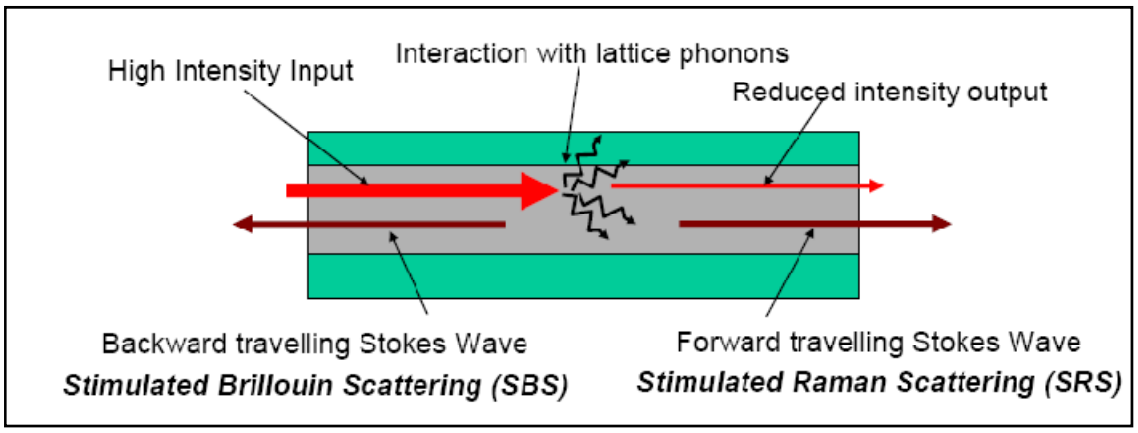

Fig.(2.14) Stimulated Scattering Even though SRS and SBS are very similar in their origin, different dispersion relations for acoustic and optical phonons [58]

2.7 Parameters Limiting Pulse Duration

There are many parameters that govern pulse width among them are: the optical cavity length, nd, and the number of oscillating modes, N.

Generating shortest pulse duration is related to these parameters as in the following relation:

$$\Delta t_{p,min} = \frac{2nd}{Nc} = \frac{2\pi}{\Delta\omega N} = \frac{1}{\Delta v_{sep} N} \geq \frac{1}{\text{gain bandwidth}} \quad \ldots\ldots (2.11)$$

Where, $\Delta v_{sep} N \leq$ gain bandwidth.

So, large number of longitudinal modes means wide bandwidth, hence shorter pulse width [6].

2.8 Time-Bandwidth Product

When pulse duration is equal to the inverse of the gain bandwidth, it is often referred to as bandwidth-limited pulses. Also could be defined as the shortest pulses that can be obtained from a given amplitude spectrum [58].

As an example, in case of pulses with a Gaussian temporal shape, the minimum pulse duration as in the following relation:

$$\Delta t_{p,min} = \frac{0.441}{N\Delta\nu_{sep}} \qquad \ldots\ldots\ldots\ldots\ldots\ldots \qquad (2.12)$$

The value (0.441) is known as the time-bandwidth product and depends on the pulse shape. The minimum attainable time-bandwidth product of a secant hyperbolic squared pulse shape is (0.315) and (0.11) for a single sided exponential shape.

2.9 Dispersion compensation and compression methods

Controlled amounts of positive or negative GVD can be forced upon a femtosecond pulse with the proper geometric arrangement of diffractive elements. Several designs using prism and grating pairs have been proposed where the first element of the pair disperses a pulse spectrally, while the second element cancels the angular dispersion of the first one. The different frequency components of the pulse will then travel parallel path but will be delayed with respect to each other. The most important schemes are described in this section.

2.9.1 Prism pair

The prism pair method is a well-known technique for GVD compensation inside a laser cavity since the insertion loss can virtually be zero. This arrangement creates a longer optical path length through the prism material for the red wavelengths than for the blue wavelengths, introducing negative GVD (Figure 2.15). The amount of GVD can be adjusted by varying the prism separation l_p (defined tip-to-tip). The prism apex angle β is cut such that, at minimum deviation of the center wavelength, the angle of incidence is

the Brewster angle. In this case, the Fresnel reflection losses are minimized and the system is virtually loss free[3].

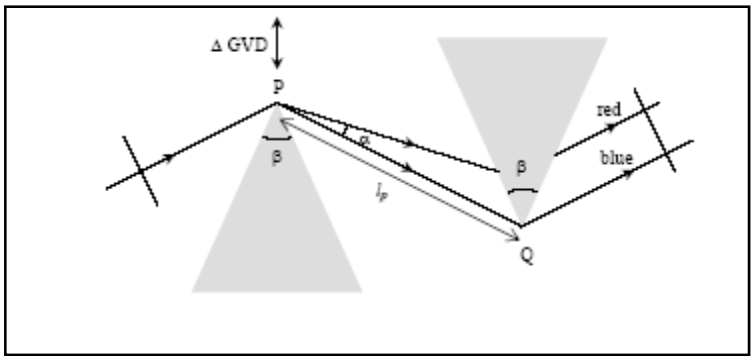

Figure (2.12) Prism pair arrangement introducing GVD without net angular dispersion[3].

It can be shown [15] that the optical path length *P* that the different frequency components travel through the prism pair can be expressed in this equation:

$$P = 1_p cos\alpha \qquad \ldots\ldots\ldots\ldots\ldots\ldots\ldots\ldots \qquad (2.13)$$

Where:
1_p: prism separation
α: dispersion angle

The dispersion is obtained by twofold derivation of the phase φ with respect to ω expressed in terms of the optical path length P. At minimum deviation angle (symmetrical beam path through the prism) and with the apex angle chosen such that the Brewster condition is satisfied (minimum reflection losses With a prism pair arrangement such as the one described above) [6].

2.10.2 Grating pair

Gratings can produce much larger angular dispersion than prisms. However, their high diffraction losses generally limit their use to extra-cavity arrangements. Similarly to the prism pair arrangement, the grating pair arrangement consists of two identical elements, where the first grating is used to spectrally disperse an incident beam and the second grating cancels the

angular dispersion of the first grating, so that the different frequency components of the spectrum travel parallel but geometrically separated paths (Figure 2.13). The resulting negative GVD was first utilized by Treacy to compress pulses of a Nd:glass laser [60].

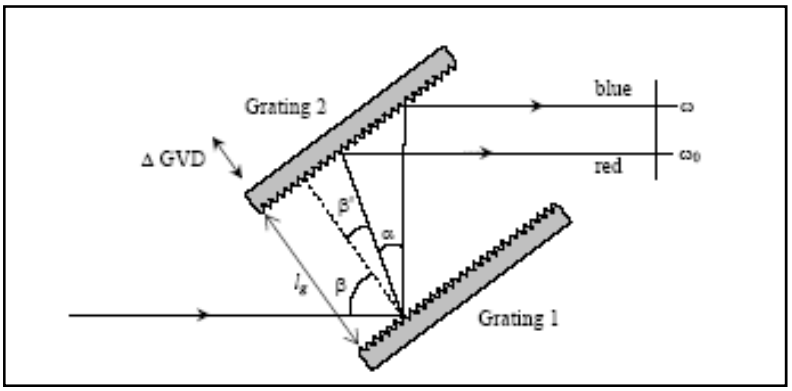

Fig (2.13) Grating pair arrangement introducing GVD without net angular dispersion [3]

The dispersion is obtained by calculating the frequency dependent optical path length between the first grating and an output wavefront taken after the second grating. The optical path length *P* can be expressed by [3]:

$$P = l_g/cos(\beta' + \alpha)[1 + \cos(\beta + '\beta + \alpha)] \quad \ldots. \qquad (2.14)$$

Where: β the angle of incidence, β′+α : the diffraction angle for the frequency component ω and l_g : the normal separation between the two gratings.

Considering the first diffraction order, the angle of incidence and the diffraction angle are related through the grating equation:

$$\sin\beta - \sin(\beta' + \alpha) = {}^{2\pi c}/_{\omega d} \qquad \ldots\ldots\ldots \qquad (2.15)$$

where : d the groove spacing.

The desired amount of GVD is obtained by changing the grating separation l_g.

2.9.3 Chirped mirrors

Another major development pushing the performance of ultrafast lasers further to their theoretical limits is dispersion compensated or chirped mirrors. Chirped mirrors are able to provide second- and third-order compensation using a scheme where each frequency components is reflected at different depth through the dielectric coating, which consists of multiple stacks of varying thickness. The longer wavelength light penetrates deeper into such mirrors than the shorter wavelength light, which leads to a negative group delay dispersion [3]. The chirped mirrors have rather uniform GDD and very high reflectivity in the relevant wavelength range of 700 – 900 nm (Figure 2.14), allowing efficient intra-cavity use.

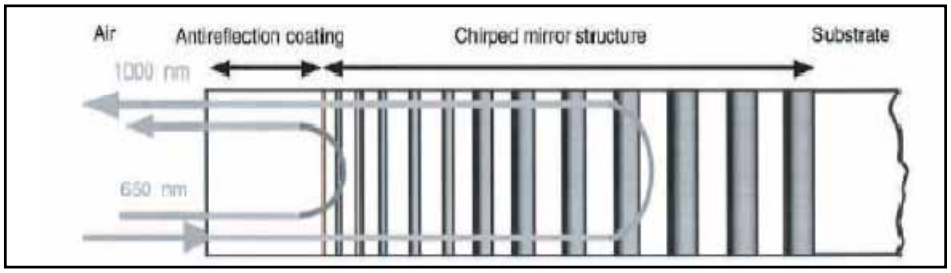

ig(2.14) Chirped mirrors construction[3].

A thick piece of glass, such as a window or a lens tends to induce strong positive GVD. To overcome this problem, the pulse can be negatively pre-chirped, so that it attains its minimal duration (net GVD=0) only after passing through the lens. Chirped mirrors provide very robust and compact arrangements for the design of ultrafast lasers and are expected to become more common, as they become more available commercially.

Chapter Three

Theory analysis

3.1 Introduction

High speed optical networks require sources producing ultrashort pulses with the ability of increasing repetition rates and average output powers. The 1550-nm wavelength region in silica fiber represents the lowest attenuation window where efficient; nearly quantum limited amplification is provided by Er-doped fiber amplifiers and soliton pulse propagation is supported. To be practical, these sources must be compact, reliable and require minimal power consumption. Mode-locked Er,Yt doped fiber lasers provide potentially attractive short pulse sources possessing some key advantages over modulated continuous-wave (CW) sources including large optical bandwidths, high intensities and powers, short coherence lengths and high timing stability. The spectral bandwidth generated from a single mode-locked source can be partitioned to form a large number of wavelength-division multiplexed (WDM) channels.The mode-locking mechanism is central to the development of a competitive source [56]. It is well known that the propagation of ultrashort pulses in optical fibers is governed by the nonlinear Schrödinger equation (NLSE) [3]. In the anomalous-dispersion regime, this equation allows for the fundamental-soliton solution that represents an optical pulse whose shape and

width are invariant under propagation. In the fiber lasers, the NLSE must be modified to account for loss, gain, gain filtering, and a mode locking element, although the resulting equation has no closed form solution [2].

To describe mode-locked fiber lasers and hence setting the master equation that governs this technique, it is necessary to consider the theory of electromagnetic wave propagation in dispersive, nonlinear media [55].Pulse propagation in optical fibers is governed by the Nonlinear Schrodinger Equation (NLSE), which must generally be solved numerically since it has no analytic solution [61].

To avoid dispersion and nonlinearity in a laser, both amplitude modulation (AM) and frequency modulation (FM) mode-locking techniques must be used in order to produce Gaussian pulses .FM mode-lockers interact with self-phase modulation (SPM) in a direct manner, whereas AM mode-lockers affect the cavity loss and literally carve pulses out of CW light. As a consequence, FM mode lockers do not require biasing while their AM counterparts do [10].

In this study we present Numerical studies of fiber laser mode-Locked by a derivative mode locked methods .A description of the pulse interaction of FM,AM and SBR are also included .The comparison is made for fiber laser operating in both the normal and anomalous dispersion regimes.

The purpose of this chapter is to obtain the basic equation that governs propagation of optical pulses in single-mode fibers. Then the equations that govern the evolution of pulse parameters during each roundtrip will be introduced. These equations will be solved numerically using fourth order Runge-Kutta numerical method.

The Runge-Kutta numerical method for solving boundary value problems was chosen for this task because it is easy to be implemented from scratch in MATLAB and because of its high accuracy.

Since deriving mode-locking master equation and all details related are beyond the scope of this thesis, only general procedures and steps will be shown to give an idea of how to implement these derivations and all assumptions and approximations.

3.1.1 Maxwell Equations

Starting with Maxwell four equations, which are very well-known equations that govern the propagation of electromagnetic waves NLSE, will be obtained. Electromagnetic waves consist of two orthogonal components of electric field vector $\bar{E}$ and magnetic field vector H[21,40,23].

Maxwell equations are:

1. Faraday's law:

$$\nabla \times \bar{E} = -\frac{\partial \bar{B}}{\partial t} \quad \ldots\ldots\ldots\ldots\ldots\ldots\ldots\ldots\ldots\ldots\ldots\ldots \quad (3.1)$$

2. Ampere's circuital law

$$\nabla \times \bar{H} = \bar{J} + \frac{\partial \bar{D}}{\partial t} \quad \ldots\ldots\ldots\ldots\ldots\ldots\ldots\ldots\ldots\ldots\ldots\ldots \quad (3.2)$$

3. Gauss's law

$$\nabla \cdot \bar{D} = \rho_v \quad \ldots\ldots\ldots\ldots\ldots\ldots\ldots\ldots\ldots\ldots\ldots\ldots \quad (3.3)$$

4. No magnetic monopole

$$\nabla \cdot \bar{B} = 0 \quad \ldots\ldots\ldots\ldots\ldots\ldots\ldots\ldots\ldots\ldots\ldots\ldots \quad (3.4)$$

Where:

$\bar{J}$: The current density vector,

ρ_v : The charge density,

$\bar{D}$: The electric flux density,

$\bar{B}$: The magnetic flux density.

Due to the electric and magnetic fields $\bar{E}$ and $\bar{H}$ propagation inside the medium, an electric and magnetic flux densities $\bar{D}$ and $\bar{B}$ will arise in response to this propagation respectively and are related to them through the following relations: [55, 61]

$$\bar{D} = \varepsilon_o \bar{E} + \bar{P} \quad \ldots\ldots\ldots\ldots\ldots\ldots\ldots\ldots\ldots\ldots\ldots\ldots \quad (3.5)$$

$$\bar{B} = \mu_o \bar{H} + \bar{M} \quad \ldots\ldots\ldots\ldots\ldots\ldots\ldots\ldots\ldots\ldots\ldots\ldots \quad (3.6)$$

Where, ε_0 represents permittivity of free space , μ_0 , permeability of free space , $\bar{\mathbf{P}}$, induced electric polarization , $\bar{\mathbf{M}}$ induced magnetic polarization , and , $\mu_0 \varepsilon_0 = 1/c^2$, where c is light speed in vacuum .

Electromagnetic field propagation is governed by Eqs. (3.1) (3.4), therefore, we must take in consideration all effects of these equations to describe the propagation of an optical pulse.

Since fiber is an optical media, therefore, it is free from electric sources and also it is nonmagnetic, hence:

$\bar{\mathbf{J}} = \bar{\mathbf{M}} = 0$

For optical fibers medium, there are no free charges and hence:

$\rho_v = 0$

For pulse widths in the range ~10 ns to 10 fs, as in our case study propagating inside optical fiber, both dispersive and nonlinear effects will influence their shape and spectrum [55, 62].

Due to nonlinear effect, (power dependant refractive index) the induced polarization consists of two parts, linear and nonlinear contributions

[39] as in the following relation [55,10]

$$\bar{\mathbf{P}}(\vec{r}, t) = \bar{\mathbf{P}}_L(\vec{r}, t) + \bar{\mathbf{P}}_{NL}(\vec{r}, t) \quad \text{.....} \quad (3.7)$$

Which is related to the electric field through the optical susceptibility (χ), through the following relation:

$$\bar{P} = \varepsilon_0 \chi_e \bar{E} \quad \ldots\ldots\ldots\ldots\ldots\ldots\ldots\ldots\ldots\ldots \quad (3.8)$$

Where χ_e is electric susceptibility, which in linear regime is independent on $\bar{E}$ while in non-linear regime is dependent on $\bar{E}$ [55].

From the privious equations , the effect of wavelength and power refractive index dependancy and also losses due to absorption have been considered . Consequently , second order dispersion , Thrid order dispersion , nonlinearity and attenuation have been considered and will appear later in mode-locking master equation.

Since optical fiber is used here as a gain medium (amplifier), the gain saturation which, is another parameter must be considered. Usually the gain medium in rare-earth-doped fibers, and most solid-state materials, responds much slower than that of the pulse width. Moreover the losses in such lasers are small and equally distributed [63].

For this reason, saturation gain,$\bar{g}$, could be approximated as in following relation:[55,64]

$$\bar{g} = \bar{g}_0/(1+P_{ave}/P_{sat}) \quad \ldots\ldots\ldots\ldots\ldots\ldots\ldots\ldots\ldots\ldots \quad (3.9)$$

Where, P_{sat} represents the saturation power of the gain medium , $\bar{g}_0$ the average small-signal gain, and, P_{ave} the average power over one pulse slot of duration T_m, which could be calculated as in the following equation:[13,54]

$$P_{ave} = \frac{1}{T_m} \int_{-T_m/2}^{+T_m/2} |A(t,z)|^2 dt \quad \ldots\ldots\ldots\ldots\ldots\ldots\ldots\ldots \quad (3.10)$$

The term $A(t,z)$, represents the slowly varying envelope of the electric field and the pulse slot is calculated as follows:

$$T_m = 1/F_r = T_R/N \quad \ldots\ldots\ldots\ldots\ldots\ldots\ldots\ldots\ldots\ldots\ldots\ldots \quad (3.11)$$

Where F_r is the frequency at which the laser is mode-locked, which is often denoted F_m as modulation frequency. N is an integer (≥ 1) representing the harmonic at which the laser will mode locked. T_R , is the roundtrip and will be identified in next sections.

The gain medium's finite bandwidth is assumed to have a parabolic filtering effect with a spectral full width at half-maximum (FWHM). It is given by the following relation: [55, 13,65]

$$\Delta_\omega = 2/T_2. \quad \ldots\ldots\ldots\ldots\ldots\ldots\ldots\ldots\ldots\ldots\ldots\ldots \quad (3.12)$$

Where:

T_2 : Spectral width of the finite gain bandwidth.

3.2 Mode-locking Fiber Laser Master Equation

Based on previous equations and assumptions , a general" master" equation used to model mode-locking fiber laser system is introduced.

This equation (3.13) is in fact a Generalized Non-Linear Schrödinger Equation GNLSE [3,63] which generally describes all types of

mode-locking fiber lasers by just changing the term $M(A,t)$ that represents the mode-locker technique. The mode-lock master equation is:[55,59]

$$T_R\frac{\partial A}{\partial T}+\frac{i}{2}\left(\bar{\beta}_2+i\bar{g}T_2^2\right)L_R\frac{\partial^2 A}{\partial t^2}-\frac{\bar{\beta}_3}{6}L_R\frac{\partial^3 A}{\partial t^3}=\bar{\gamma}L_R|A|^2A+\frac{1}{2}(\bar{g}-\bar{\alpha})L_RA$$

$$+M(A,t) \quad \ldots\ldots\ldots\ldots\ldots\ldots\ldots\ldots\ldots\ldots\ldots\ldots\ldots\ldots \quad (3.13)$$

In the following all the terms of Mode-Locking master equation will be identified.

3.2.1 Identifying Mode-Locking Master Equations Terms

For full mathematical model to be able to describes mode locking for optical pulse propagating through optical fiber , all parameters that affect pulse propagation must be considered as described in the previous chapter .To verify this fact, let's examine the master Eq. (3.13) to identify each term, starting from the left side [16,55].

1st term describes the basic propagation of the optical field in z direction,

2nd term describes the effect of second order dispersion,

3rd term describes the effect of third order dispersion,

4th term describes the effect of nonlinearity,

5th term describes the effect of gain and intensity-dependent losses,

6th term represents the mode locker effect which will be identified later.

The term, $i\bar{g}T_2^2$, results from the gain . The physical origin of this contribution is related to the finite gain bandwidth of the doping fiber and is referred to as gain dispersion ($\bar{g}T_2^2$) since it originates from the frequency dependence of the gain [41].

The term A (T, t) is the slowly varying envelope of the electric field in term of T, the propagation time, which is given by the following relation:

$T = z/v_g$ ……. (3.14)

Where:

z: the propagation distance in z direction,

v_g: The group velocity.

In the master equation eq.(3-13), there are two time scales that represent:

1. The time (t), measured in the frame of the moving pulse and,

2. The propagation time (T).

Since we averaged over a single roundtrip is considered (T) is measured in terms of the roundtrip time:

$T_R = L_R/v_g = c / 2nL_R$ …… (3.15)

Where:

L_R : Cavity length,

C: speed of light,

n :refractive index.

The pulse time scale is assumed to be sufficiently smaller than T_R and hence, the two times are essentially decoupled [8].Also this treatment is valid for most mode-locked lasers for which T_R exceeds 1 ns and pulse widths are typically less than 100 ps. The over bar in Eq. (3.13) refers to the averaged value of the corresponding parameter. For example, $\bar{\beta}_2$, $\bar{\beta}_3$, $\bar{\alpha}$ and $\bar{\gamma}$ represent the second-order dispersion, TOD, loss, and nonlinearity, respectively, averaged over the cavity length.

Figure (3-1) shows the mathematical meaning of every term in the master equation.

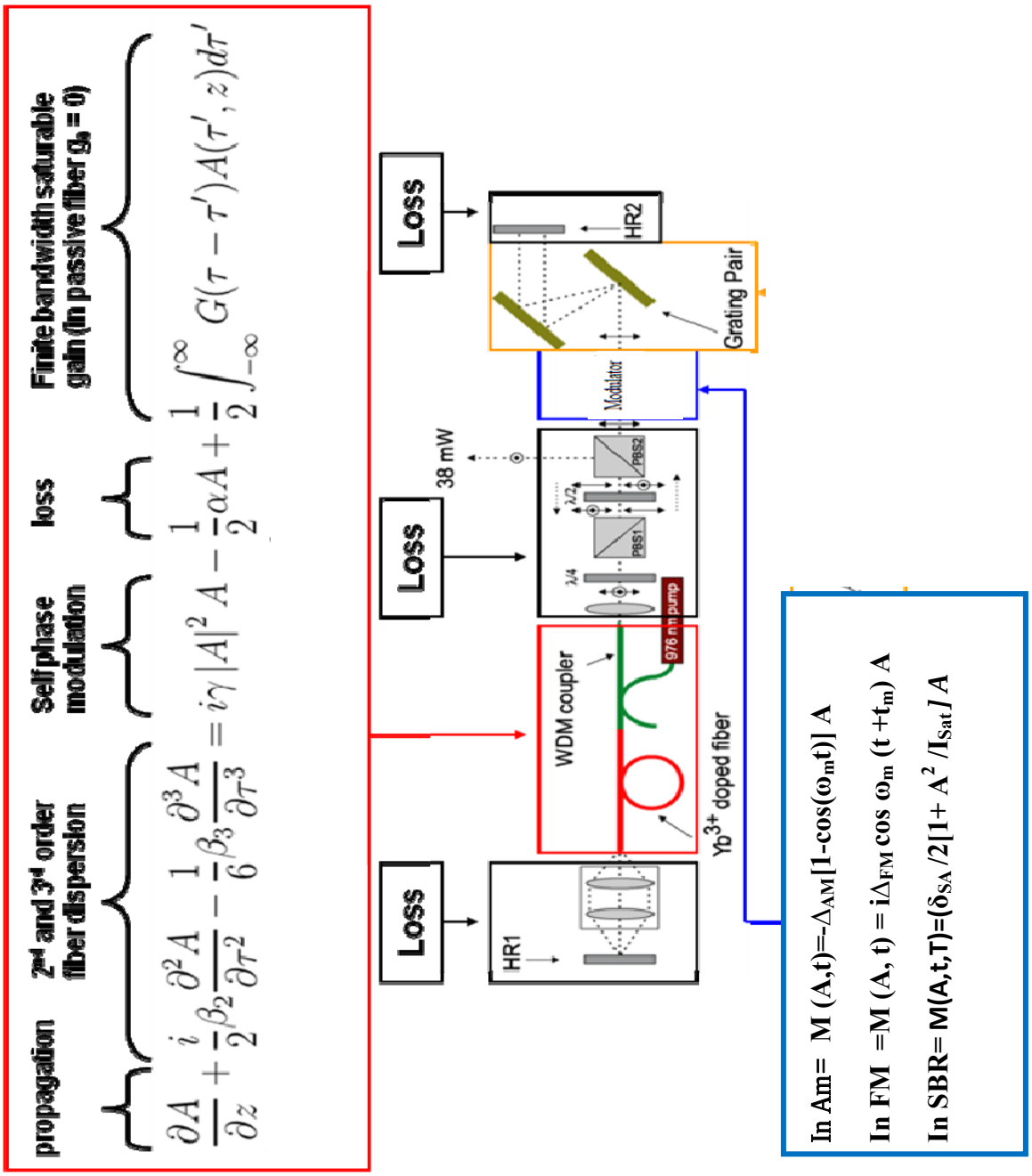

Fig (3-1) Block diagram and mathematical relation for each part of mode locked.

3.3 Moment Method

As shown in previous sections(3-2) , mode-locked fiber lasers are governed by nonlinear partial differential equation Eq.(3.13) , which generally, does not possess analytic solution [67] , hence the produced pulse can not be modeled .Another drawback ,it gives the final pulse shape , it does not explain how does the pulse evolves during each roundtrip. Also, to solve it numerically by one of numerical solution method such as split or wavelet method [66], all parameters need to be considered including TOD and mode-locker effect .These last two parameters have great effect on pulse shape and stability as mentioned in the previous chapter.

As a result, to solve such third order partial deferential equation, initial conditions and boundary conditions need to be known .Moreover, a long time is required for computer program to implement such numerical solution.

It is useful to convert this third order partial differential equation to a set of ordinary differential equations that describe the evolution of pulse parameters during each roundtrip [44].These pulse parameters evolution equations are obtained using the so-called moment method [68].

By using the moment method pulse parameters equations, it is possible to study the pulse evolution process under the effect of Eq. (3.13), which does not need a full numerical simulation.

3.4 Pulse Parameters Evolution Equations

Depending on master equation Eq.(3.13) , and using the assumed pulse shapes for both dispersion regimes after modifying Ginzburg–Landau Equation , GLE , by adding TOD and mode-locker effects, the extended solution will be as in the following relations [13,45, 44,68] .

a. Normal regime:

$$A(T,t) = a\left(\exp\left(-\frac{(t-\xi)^2}{2\tau^2}\right)\right)^{1+iq} \times \exp(i\Omega(t-\xi) + ikT + i\varphi_0) \quad \ldots. \quad (3.16)$$

b. Anomalous regime:

$$A(T,t) = a\left(\operatorname{sech}\left(\frac{t-\xi}{\tau}\right)\right)^{1+iq} \times \exp(i\Omega(t-\xi) + ikT + i\varphi_0) \quad \ldots.. \quad (3.17)$$

Where pulse parameters for both profiles are:

(a) represents pulse amplitude,

(ξ) Temporal shift,

(τ) pulse width,

(q) chirp,

(Ω) frequency shift,

$ikT + i\varphi_0$ Represent the phase and rarely is of physical interest in lasers producing picoseconds pulses, and will be ignored [13].

The relations of pulse parameters with temporal pulse profile are as following: [41, 42]

$$E(T)=\int_{-\infty}^{+\infty} |A(T,t)|^2 \, dt \quad \ldots\ldots\ldots\ldots\ldots\ldots\ldots \quad (3\text{-}18)$$

$$\xi(T) = \frac{1}{E}\int_{+\infty}^{-\infty} t\,|A(T,t)|^2 \, dt \quad \ldots\ldots\ldots\ldots\ldots\ldots\ldots \quad (3\text{-}19)$$

$$\Omega(T) = \frac{i}{2E}\int_{+\infty}^{-\infty}\left[A^* \frac{\partial A}{\partial t} - A\frac{\partial A^*}{\partial t}\right]dt \quad \ldots\ldots\ldots\ldots\ldots\ldots\ldots \quad (3\text{-}20)$$

$$q(T) = \frac{i}{E}\int_{+\infty}^{-\infty}(t-\xi)\left[A^* \frac{\partial A}{\partial t} - A\frac{\partial A^*}{\partial t}\right]dt \quad \ldots\ldots\ldots\ldots\ldots\ldots\ldots \quad (3\text{-}21)$$

$$\tau^2(T)=\frac{2\sigma}{E}\int_{+\infty}^{-\infty}(t-\xi)\,|A(T,t)|^2 \, dt \quad \ldots\ldots\ldots\ldots\ldots\ldots\ldots \quad (3\text{-}22)$$

3.4.1 AM Mode Locking

Mode locking through amplitude modulation, commonly known as AM mode locking, is conceptually the easiest of all mode-locking techniques. It is achieved by placing an AM modulator inside a laser cavity and matching the frequency with which it is driven to a harmonic of the cavities fundamental frequency. The setup for such a laser is shown in Fig. (3.2).

The laser used in this research is a 976-nm-pumped linear cavity. The model studied, uses ytterbium-doped, single mode fiber pumped by 976 nm laser source with 150 mW pumping power to produce 1055 nm output laser. Amplitude Modulation was used the electro-optic effect the fiber-based Mach-Zehnder AM modulator.

The effect of an AM modulator on the optical field is given by[55]

$$M(A,t)=-\Delta_{AM}[1-\cos(\omega_m t)]\,A \quad \ldots\ldots\ldots\ldots\ldots\ldots\ldots\ldots \quad (3\text{-}23)$$

Where:

Δ_{AM}: modulation depth ,and

ω_m: Modulation frequency

$\omega_m=2\pi\,(F_r)$

The modulator effect is substituted in equation (3-13),and so pulse propagation in such a laser is modeled by

$$T_R\frac{\partial A}{\partial T}+\frac{1}{2}\left(\bar{\beta}_2+i\bar{g}T_2^2\right)L_R\frac{\partial^2 A}{\partial t^2}-\frac{\bar{\beta}_3}{6}L_R\frac{\partial^3 A}{\partial t^3}=\bar{\gamma}L_R|A|^2A+\frac{1}{2}(\bar{g}-\bar{\alpha})L_RA$$

$$-\Delta_{AM}[1-\cos(\omega_m t)]\,A \quad \ldots\ldots\ldots\ldots\ldots\ldots\ldots\ldots\ldots\ldots\ldots\ldots \quad (3\text{-}24)$$

The moment method is applied to an AM mode locked laser. This gives us so-called five AM mode-locking rate equations, compared with the three AM-Mode locking rate equations that were obtained in[42]. By these five equations we can study the pulse parameters .

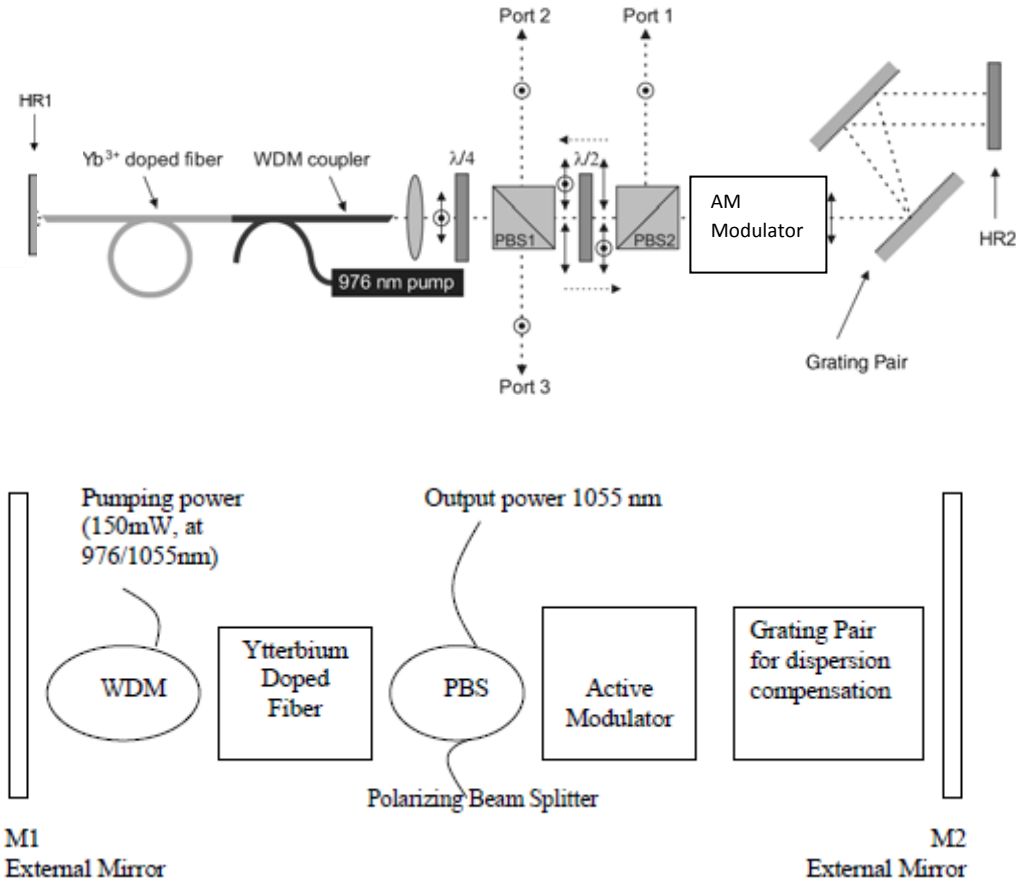

Figure (3-2) AM mode-locked, HR1, HR2, high-reflectivity mirrors; PBS, polarizing beam splitter.

$$\frac{T_R}{L_R}\frac{dE}{dT}=(\bar{g}-\bar{\alpha})E-\frac{\bar{g}T_2^2}{2\tau^2}[C_0(1+q^2)+2\Omega^2\tau^2]E+\frac{2\Delta_{AM}}{L_R}\Psi_0\cos[\omega_m(\xi-t)]E \quad \ldots\ldots \quad (3\text{-}25)$$

$$\frac{T_R}{L_R}\frac{d\xi}{dT}=\bar{\beta}_2\Omega-\bar{g}T_2^2 q\Omega+\frac{\bar{\beta}_3}{4\tau^2}[C_0(1+q^2)+2\Omega^2\tau^2] -\frac{\Delta_{AM}\tau}{L_R}\Psi_1\sin[\omega_m(\xi-t_s)] \quad \ldots\ldots\ldots\ldots \quad (3\text{-}26)$$

$$\frac{T_R}{L_R}\frac{d\Omega}{dT} = -[C_0(1+q^2)+2\Omega^2\tau^2] - \frac{\Delta_{AM}}{L_R} q\Psi \sin[\omega m(\xi - ts)] \quad \ldots\ldots\ldots\ldots\ldots \quad (3\text{-}27)$$

$$\frac{T_R}{L_R}\frac{dq}{dT} = \frac{\overline{\beta}_2}{\tau^2}[C_0(1+q^2)+2\Omega^2\tau^2] - \frac{\overline{g}T_2^2}{\tau^2} q[C_1(1+q^2)+2\Omega^2\tau^2] +$$

$$C_2 \frac{\overline{\gamma}E}{\sqrt{2\pi}\tau} + \frac{\overline{\beta}_3\Omega}{\tau^2}\left[\frac{3}{2C_0}(1+q^2)+\Omega^2\tau^2\right] \quad \ldots\ldots\ldots\ldots\ldots \quad (3\text{-}28)$$

$$-\frac{\Delta_{AM}\tau}{L_R}\Psi_1\{qk\cos[\omega_m(\xi - t_s)] + 2\Omega \sin[\omega_m(\xi - t_s)]\}$$

$$\frac{T_R}{L_R}\frac{d\tau}{dT} = C_3\frac{\overline{\beta}_2}{\tau} q + C3\frac{\overline{\beta}_3}{\tau} q\Omega + C_0C_3\frac{\overline{g}T_2^2}{2\tau}(C_4 - q^2) - \frac{\Delta_{AM}\tau}{2L_R}\Psi_2\cos[\omega_m(\xi - t_s)] \quad (3\text{-}29)$$

$$\Psi_0 = \exp(-\omega_m^2\tau^2/4) \quad \ldots\ldots\ldots\ldots\ldots\ldots\ldots\ldots\ldots\ldots \quad (3\text{-}30)$$

$$\Psi_1 = \omega_m\tau\Psi_0 \quad \ldots\ldots\ldots\ldots\ldots\ldots\ldots\ldots\ldots\ldots \quad (3\text{-}31)$$

$$\Psi_2 = \omega_m\tau^2\Psi_0 \quad \ldots\ldots\ldots\ldots\ldots\ldots\ldots\ldots\ldots\ldots \quad (3\text{-}32)$$

In these equations, the Gaussian pulse is introduced where the constants C_n (n=0 to 4) are,

1. $C_0 = C_1 = C_2 = C_3 = C_4 = 1$

and for the autosoliton.

1. $C_0 = 2/3$,
2. $C_1 = 1/3$,
3. $C_2 = \sqrt{2\pi}/3$,
4. $C_3 = 6/\pi^2$,

5. C4=2

$$\Psi_0 = (\pi\omega_m\tau/2)\operatorname{csc} h(\pi\omega_m\tau/2) \quad \text{.....} \quad (3\text{-}33)$$

$$\Psi_1 = [\pi\coth(\pi\omega_m\tau/2) - 2/(\omega_m\tau)]\Psi_0 \quad \text{.....} \quad (3\text{-}34)$$

$$\Psi_2 = \{2 + 3\operatorname{csc} h2(\pi\omega_m\tau/2)[3 + \cosh(\pi\omega_m\tau) - 4/(\pi\omega_m\tau)\sinh(\pi\omega_m\tau)]\}\Psi_0 \quad (3\text{-}35)$$

To illustrate pulse dynamics ,we solve the five pulse parameters elevation equations numerically for AM type of mode locked ,equations(3. 24,25,26,27.28), MATLAB 7.0 program has been written by using fourth-fifth order Runge-kutta method which uses the function ODE-45.This method is used to solve ordinary differentional equations numerically.

MATLAB 7.0 program uses the constants in table 3-1,with the following initial values for pulse parameters [42,41] .

E(0)=1fJ, $\zeta(0)=0$, $\Omega(0)=0$, q(0)=0, $\tau(0)=0.5$ ps

The flow chart of the MATHLAB main program used to solve the master equation is shown in fig (3-3), then study the effect of change input parameters on the output laser such as: frequency, cavity length, dispersion and nonlinearity. The flow chart described these studies shown in fig (3-4).

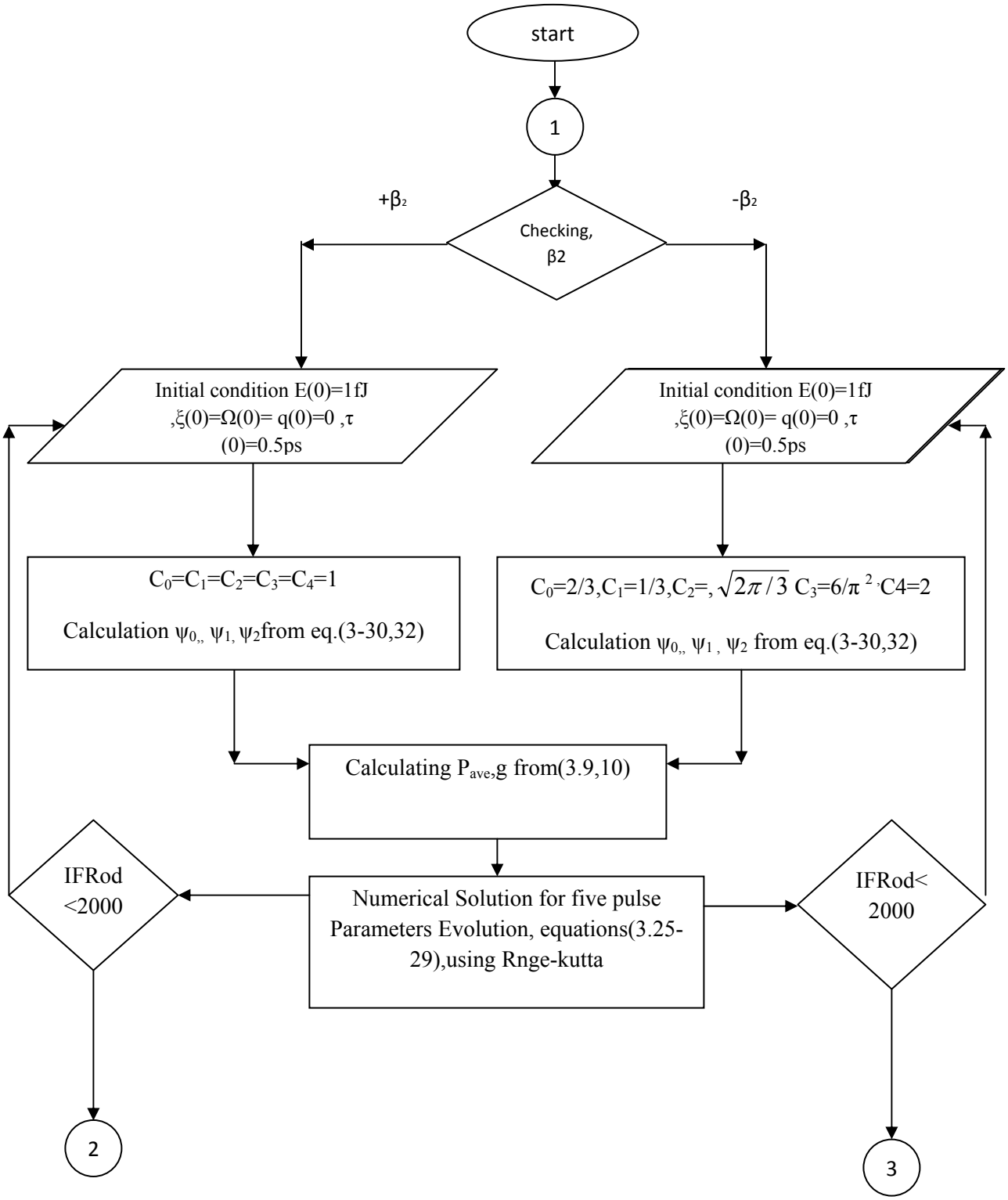

Fig (3-3) Flow chart of the main program for AM mode-Locking.

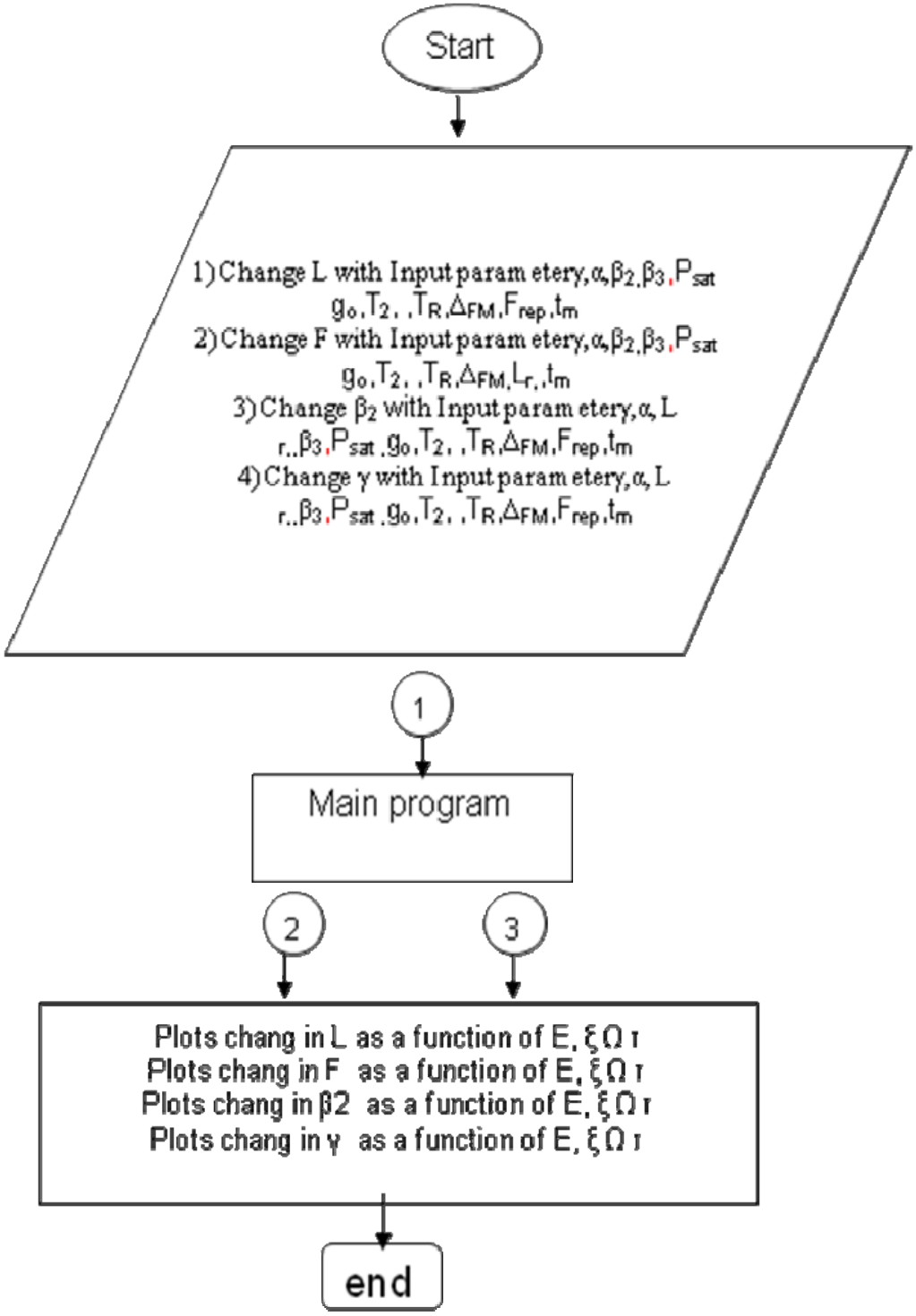

Fig(3-4) Flow chart of the program for study the varying Fr,Lr,γ,β_2 for mode-Locking.

3.4.2 FM Mode-Locker Effect

The same laser in AM Mode-locked is used in FM Mode-locked and Frequency Modulation Harmonically Mode-Locked by MZI optical modulator.

The laser configuration is shown in Fig.3-5 (a) where the combination of a half-wave plate (λ/2) and polarizing beam splitter (PBS2) not only provide variable output coupling, but also sets a linear polarization for the FM modulator and the grating pair.

A block diagram is shown in Fig. (3-5)(b) describing the numerically modeled laser configuration. Since the work is below zero dispersion, (the used laser wavelength is 1.55 μm) where normal dispersion GVD must be compensated, a grating pair was usually used to drive the system into anomalous regime [11, 13]. This will achieve the balancing between negative GVD and nonlinearity leading to pulse compression [41,44].

The effect of FM mode-locker on the field is sinusoidal as in the following expression: [10, 41]

$$M(A, t) = i\Delta_{FM} \cos \omega_m (t + t_m) A \quad \ldots\ldots\ldots\ldots\ldots\ldots\ldots\ldots \quad (3.36)$$

Where:

Δ_{FM} : Modulation depth,

t_m : The delay between the center of the modulation cycle and the temporal window in which the pulses are viewed, and

ω_m: Modulation frequency

$\omega_m = 2\pi (F_r)$.

This term is substituted in master equation (3.13)

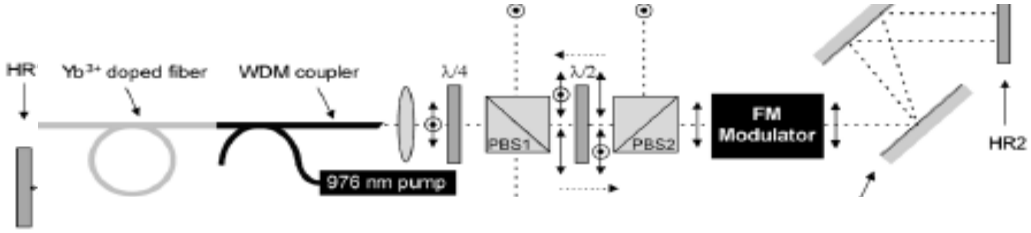

(a)

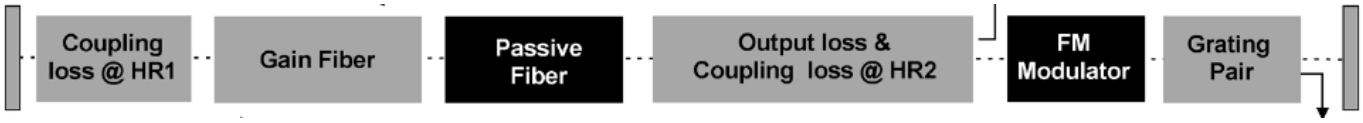

(b)

Fig (3-5) :(a) FM mode-locked, HR1, HR2, high-reflectivity mirrors. (b) Numerically modeled laser configuration: the coupling losses take into account all cavity losses at the respective cavity ends, including the laser outputs.

The moment method was applied to an FM mode locked laser. This gives us the so-called FM mode-locking rate equations. A set of five

equations are introduced describing pulse parameters evolution during each roundtrip [44, 55]

$$\frac{T_R}{L_R}\frac{dE}{dT} = (\bar{g} - \bar{\alpha})E\frac{\bar{g}T_2^2}{2\tau^2}(C_0(1+q^2) + 2\Omega^2\tau^2)E \quad \ldots\ldots\ldots\ldots \quad (3.37)$$

$$\frac{T_R}{L_R}\frac{d\xi}{dT} = \bar{\beta}_2\Omega - \bar{g}T_2^2 q\Omega + \frac{\bar{\beta}_2}{4\tau^2}(C_0(1+q^2) + 2\Omega^2\tau^2) \quad \ldots\ldots\ldots \quad (3.38)$$

$$\frac{T_R}{L_r}\frac{d\Omega}{dT} = -C_0\frac{\bar{g}T_2^2}{\tau^2}(1+q^2)\Omega + \frac{\Delta_{FM}\omega_m}{L_R}\psi_0 \times \sin(\omega_m(\xi - t)) \quad \ldots\ldots \quad (3.39)$$

$$\frac{T_R}{L_r}\frac{dq}{dT} = \frac{\bar{\beta}_2}{\tau^2}(C_0(1+q^2) + 2\Omega^2\tau^2) - \frac{\bar{g}T_2^2}{\tau^2}q(C_1(1+q^2) + 2\Omega^2\tau^2)) + C_2\frac{\sqrt{E}}{\sqrt{2\pi\tau}}$$

$$+ \frac{\bar{\beta}_2\Omega}{\tau^2}\left[\frac{2}{2C_0}(1+q^2) + \Omega^2\tau^2\right] + \frac{\Delta_{FM}\omega_m\tau}{L_R}\psi_1 \cos(\omega_m(\xi - t)) \quad \ldots\ldots\ldots \quad (3.40)$$

$$\frac{T_R}{L_r}\frac{d\tau}{dT} = C_3\frac{\bar{\beta}_2}{\tau}q + C_3\frac{\bar{\beta}_2}{\tau}q\Omega + C_0C_3\frac{\bar{g}T_2^2}{2\tau}(C_4 \quad q^2) \quad \ldots\ldots\ldots\ldots\ldots \quad (3.41)$$

Where the constants C_n (n=0 to 4) are introduced.

In case of Gaussian pulse:

1. $C_0 = C_1 = C_2 = C_3 = C_4 = 1$

2. $\psi_0 = \exp\left(-\frac{\omega_m^2\tau^2}{4}\right)$ ..... (3.42)

3. $\psi_1 = \omega_m\tau\psi_0$ ..... (3.43)

In the case of an autosoliton,

1. C_0=2/3,

2. C_1=1/3,

3. C_2=$\sqrt{2\pi}$ /3,

4. $C_3=6/\pi^2$,

5. C4=2.

6. $\psi_0 = \left(\frac{\pi\omega_m\tau}{2}\right)\operatorname{csch}\left(\frac{\pi\omega_m\tau}{2}\right)$ ..... (3.44)

7. $\psi_1 = \left(\pi\coth\left(\frac{\pi\omega_m\tau}{2}\right) - 2/(\omega_m\tau)\right)\psi_0$ ..... (3.45)

Since the accuracy of this approach depends upon the knowledge of exact pulse shape, master equation Eq.(3.13) must be solved numerically to obtain minimum deviation. A numerical solution for these five equations, using the fourth order Runge-Kutta method demonstrates that steady-state values obtained deviate from the values obtained by directly solving Eq. (3.13) [44,13].Hence, these results justify the use of the moment method and the pulse shapes assumed.

To solve the five pulse parameters elevation equations numerically for FM type of mode locked ,equations(3.37,38,39,40,41), MATLAB 7.0 program has been written by using fourth-fifth order Runge-kutta method which uses the function ODE-45.This method is used to solve ordinary differentional equations numerically. Ytterbium doped fiber pumped by 976nm laser source is used with 150mw pumping power to produce 1055nm output laser [13].

MATLAB 7.0 program uses the constants in table 3-1, with the following initial values for pulse parameters [41, 42].

E(0)=1fJ, $\zeta(0)=0$, $\omega(0)=0$, $q(0)=0$, $\tau(0)=0.5$ ps

Table. 3.1 Constant for numerical solution [41, 13] for FM and AM mode –locked.

Parameter	Value	Parameter	Value
$\bar{\beta}_2$	$\pm 1.4\times10^{4}$ fs^2/m	$\bar{\beta}_3$	30×10^{4} fs^3/m
$\bar{\gamma}$	$0.012(W/m)^{-1}$	$\bar{\alpha}$	$0.17m^{-1}$
g	0.55/m	T2	47 fs/rad
P	25mW	L	4m
T_R	40ns	Fr	10 GHz
Δ_{FM}	0.45	tm	0
Δ_{AM}	0.3	λ	1055 nm

The flow chart of the main MATHLAB program used to solve the master equation was shown Fig (3-6) and the study of the effect of change input parameters on the output laser such as: frequency, cavity length, dispersion and nonlinearity shown in fig (3-7).

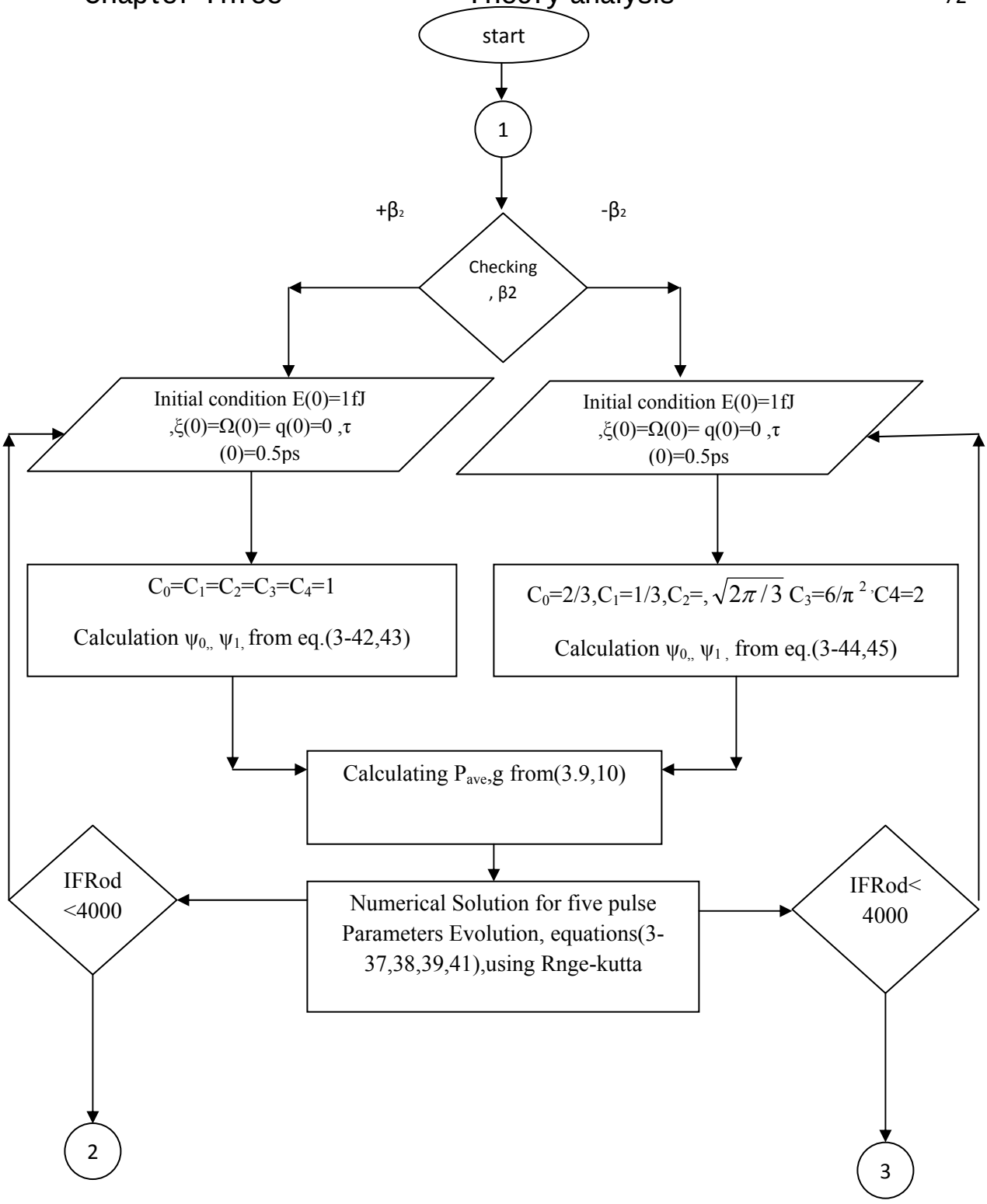

Fig (3-6) Flow chart of the main program for FM mode Locking.

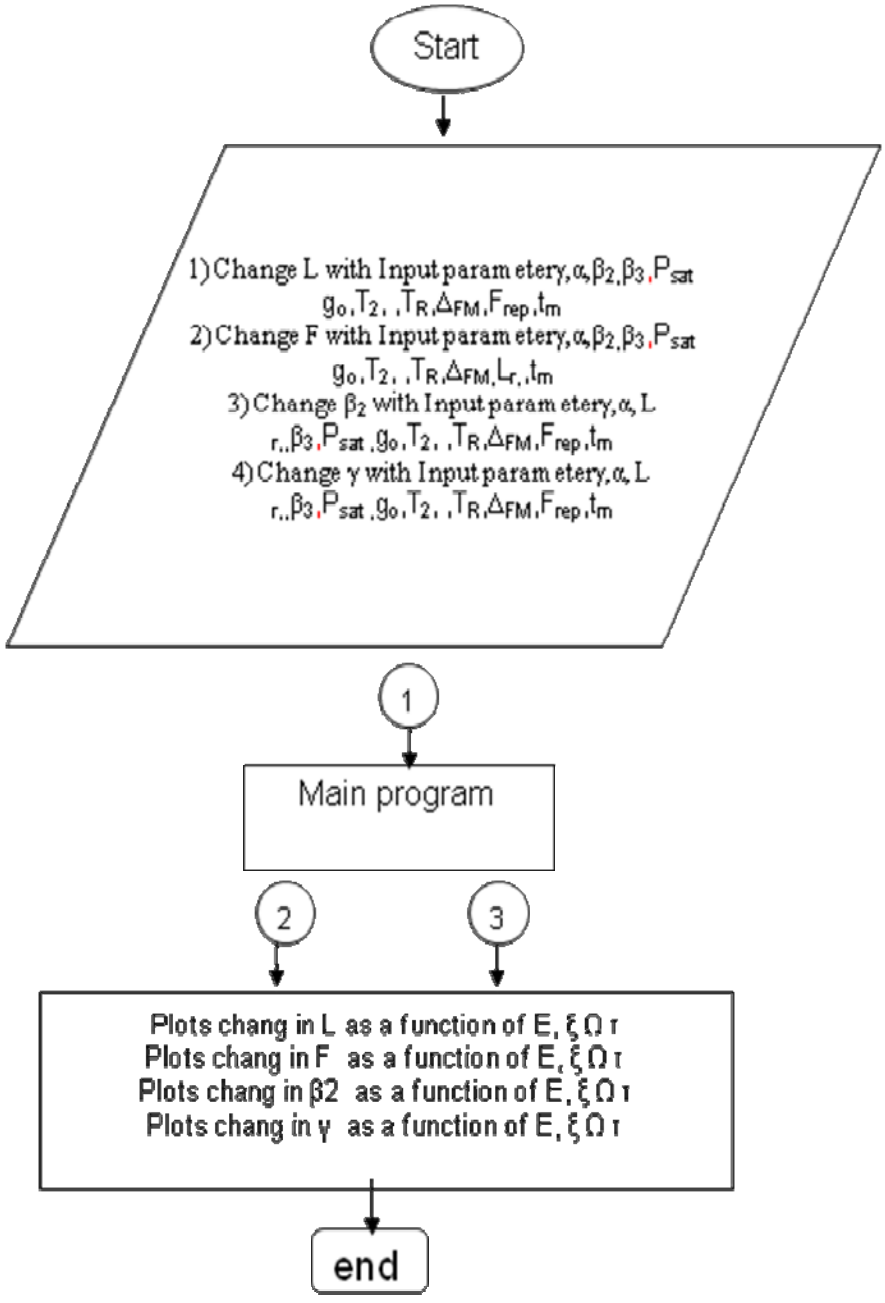

Fig(3-7)Flow chart of the program for study the varying Fr,Lr,γ,β2 for mode-Locking.

3.4.3 Saturable Bragg Reflector Mode Locking

In this work the equations required to obtain the pulse parameters were found with the same assumptions accounted for AM and FM mode locking.

In mode locking using a saturable absorber or saturable Bragg reflector, the optical field experiences a time dependent loss. In this type of mode locking the field is gated by itself. Since no electronics are required, it is referred to as a type of "passive" mode locking.

Common devices that act as saturable absorbers are saturable Bragg reflectors (SBR)[69] semiconductor saturable absorber mirrors) (SESAM) , Nonlinear optical loop mirrors, Nonlinear polarization rotation (NLPR) [58] APM[40], and various (carcinogenic) dyes which possess saturable absorption .Fig(3-8) shows the schematic of a mode locking which includes SBR and gain saturated fiber segment. The SBR can be thought of as intensity and wavelength-dependent mirror constructed using a semiconductor material. The wavelength dependence comes from a Bragg grating that is fabricated in the semiconductor host and acts as a mirror. This grating also includes an SA medium, in the form of quantum well (or quantum dots), so that the SBR exhibits an intensity-dependent reflection. If low-intensity light (at the Bragg wavelength) is incident on such a SBR it will all be absorbed. If light of a high

enough intensity (once again at the Bragg wavelength) is incident on the SBR, however, it will be almost completely reflected. Both of these characteristics are a direct result of the SA located at the front of the Bragg grating. The structure of the SBR is shown in Fig.(3-8) .It consists of a Bragg reflector of alternating quarter-wave layers of GaAs and AlAs with two In GaAs–InP quantum wells grown near the surface of a half-wave strain relief layer. The Bragg reflector has a reflection bandwidth of approximately 150 nm centered about 1550 nm and a (saturated) reflectivity exceeding 99.5%.

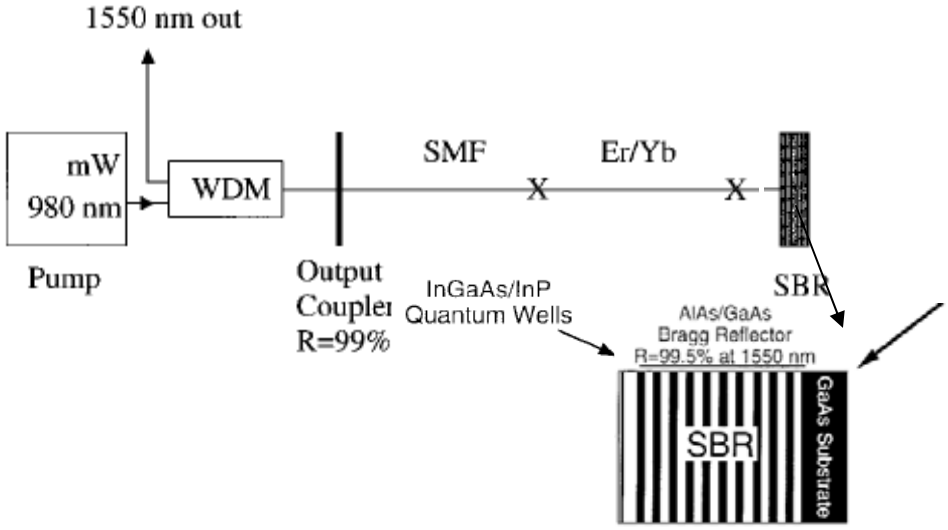

Figure(3-8)Schematic of the fiber laser cavity and structure of the SBR.

Despite the device used, all saturable absorption mode lockers work on the principle that their loss decreases when they are probed with more intense powers. This effect naturally leads to pulse formation in a laser cavity where, for a fixed average power, CW light encounters more loss than a pulse. The

cavity is made of a short section of Yb-doped fiber; a sections of single-mode fiber (SMF), a wavelength division multiplexer (WDM).

Pulses evolve in the single-mode fiber are amplified in the Yb-doped fiber; output at the position of PBS. A pairs of gratings is used to compress the pulse after the PBS in the cavity. The effect of saturable absorption is mathematically represented by[10]

$$M(A,t,T)=\left(\frac{\delta SA}{2}\left[1+\frac{|A|2}{Isat}\right]-1\right)A \quad \ldots\ldots\ldots\ldots\ldots\ldots \quad (3\text{-}46)$$

where:

δ_{SA} : the modulation depth and

I_{sat} : the saturation of the device.

Therefore, pulse propagation in a laser mode locked with a saturable Bragg is modeled by saturable absorption mode-locked lasers almost universally produce "solition" pulses as shown in the following equation which was obtained by substituting(3-46) in (3-13).

$$T_R\frac{\partial A}{\partial T}+\frac{i}{2}\left(\beta_2+i\gamma T_2^2\right)L_R\frac{\partial^2 A}{\partial t^2}-\frac{\beta_3}{6}L_R\frac{\partial^3 A}{\partial t^3}=\gamma L_R|A|^2A+\frac{1}{2}(g-\alpha)L_RA$$

$$+\left[\frac{\delta SA}{2}\left[1+\frac{|A|2}{Isat}\right]-1\right]A \quad \ldots\ldots\ldots\ldots\ldots\ldots\ldots\ldots \quad (3.47)$$

Compared with active mode locking ,the saturable absorption based mode locking allows one to generate femtosecond pulses, since saturable absorbers

saturate on a femtosecond time scale and recover on a picoseconds time scale; ~200 fs pulses at repetition rates ~10 MHz are routinely produced.

Indeed, SESAM's have even been used to produce 10-GHz fundamentally mode-locked solid-state lasers [69,70].

The moment method was applied to the equations governing pulse propagation in all three types of mode-locked lasers. The moment method allows us to develop ordinary differential equations that govern the evolution of the pulse parameters rather than the electric field .Pulse parameters of a saturable-absorption mode-locked laser are obtained by solving the following five rate equations.

$$\frac{T_R}{L_R}\frac{dE}{dT} = (\bar{g} - \bar{\alpha})E - \frac{\bar{g}T_2^2}{2\tau^2}[C_0(1+q^2) + 2\Omega^2\tau^2]E - \frac{\delta_{SA}}{L_R}\frac{2\pi I_{sat}}{\sqrt{1+\frac{2\pi I_{sat}}{E}}}\coth^{-1}\left(\sqrt{1+\frac{2\pi I_{sat}}{E}}\right) \quad \text{..... (3-48)}$$

$$\frac{T_R}{L_R}\frac{d\xi}{dT} = \bar{\beta}_2\Omega - \bar{g}T_2^2 q\Omega + \frac{\bar{\beta}_3}{4\tau^2}[C_0(1+q^2) + 2\Omega^2\tau^2] \quad \text{..... (3-49)}$$

$$\frac{T_R}{L_R}\frac{d\Omega}{dT} = -C_0\frac{\bar{g}T_2^2}{\tau^2}(1+q^2)\Omega \quad \text{..... (3-50)}$$

$$\frac{T_R}{L_R}\frac{dq}{dT}=\frac{\bar{\beta}_2}{\tau^2}[C_0(1+q^2)+2\Omega^2\tau^2]-\frac{\bar{g}T_2^2}{\tau^2}q[C_1(1+q^2)+2\Omega^2\tau^2]$$
$$+C_2\frac{\bar{\gamma}E}{\sqrt{2\pi}\tau}+\frac{\bar{\beta}_3\Omega}{\tau^2}\left[\frac{3}{2C_0}\ (1+q^2)+\Omega^2\tau^2\right]$$
$$+\frac{\delta_{SA}}{L_RE}\frac{2\tau I_{sat}}{\sqrt{1+\frac{2\tau I_{sat}}{E}}}q\cosh^{-1}\left(\sqrt{1+\frac{2\tau I_{sat}}{E}}\right)$$
$$-\frac{\delta_{SA}\tau I_{sat}}{4L_RE}q\left\{\ln^2\left[1+\frac{E}{\tau I_{sat}}\left(1-\sqrt{1+\frac{2\tau I_{sat}}{E}}\right)\right]\right.$$
$$\left.+\ln^2\left[1+\frac{E}{\tau I_{sat}}\left(1+\sqrt{1+\frac{2\tau I_{sat}}{E}}\right)\right]\right\} \quad \text{.....} \quad (3\text{-}51)$$

$$\frac{T_R}{L_R}\frac{d\tau}{dT}=C_3\frac{\bar{\beta}_2}{\tau}q+C_3\frac{\bar{\beta}_3}{\tau}q\Omega+C_0C_3\frac{\bar{g}T_2^2}{2\tau}(C_4-q^2)$$
$$-\frac{3\delta_{SA}\tau^2I_{sat}}{L_RE}\frac{1}{\sqrt{1+\frac{2\tau I_{sat}}{E}}}\coth^{-1}\left(\sqrt{1+\frac{2\tau I_{sat}}{E}}\right)$$
$$-\frac{\delta_{SA}\tau^2I_{sat}}{4\pi^2L_RE}\frac{1}{\sqrt{1+\frac{2\tau I_{sat}}{E}}}\times\left\{\ln^3\left[-\left(\frac{E}{\tau I_{sat}}+1\right)-\frac{E}{\tau I_{sat}}\sqrt{1+\frac{2\tau I_{sat}}{E}}\right]\right.$$
$$\left.-\ln^3\left[-\left(\frac{E}{\tau I_{sat}}+1\right)+\frac{E}{\tau I_{sat}}\sqrt{1+\frac{2\tau I_{sat}}{E}}\right]\right\} \quad \text{.....} \quad (3\text{-}52)$$

where the constants $C0 = 2/3$, $C1 = 1/3$, $C2 = \sqrt{2}\,\pi/3$, $C3 = 6/\pi 2$, and $C4 = 2$.

To illustrate pulse parameters, we solve the five elevation equations numerically for passive type of mode locked ,equations(3.48,49,50,51,52), MATLAB 7.0 program has been written by using fourth order Runge-kutta method which uses the function ODE-45.

MATLAB program used the constants in table 3-2, with the following initial values for pulse parameters.

E(0)=1fJ, $\zeta(0)=0$, $\omega(0)=0$, $q(0)=0$, $\tau(0)=0.5$ ps

Table. 3.2 Input parameter for numerical solution for SBR.

Parameter	Value	Parameter	Value
$\bar{\beta}_2$	$\pm 1.4\times10^{4}$ fs^2/m	$\bar{\beta}_2$	$30\times10^{4} fs^3/m$
$\bar{\gamma}$	$0.012(m\ W)^{-1}$	$\bar{\alpha}$	$0.17m^{-1}$
g	0.55/m	T_2	47 fs/rad
P_{sat}	25mW	L	4m
T_R	40ns	Fr	12.6MHz
$\Delta\delta_{SA}$	0.9	t_m	0
λ	1055 nm	I_{sat}	150mW

The flow chart of the main MATHLAB program used to solve the master equation is shown in Fig(3-9)and the program study the changing the F,β2,γ,Lr and modulation depth $\Delta\delta_{SA}$ shown in fig (3-10).

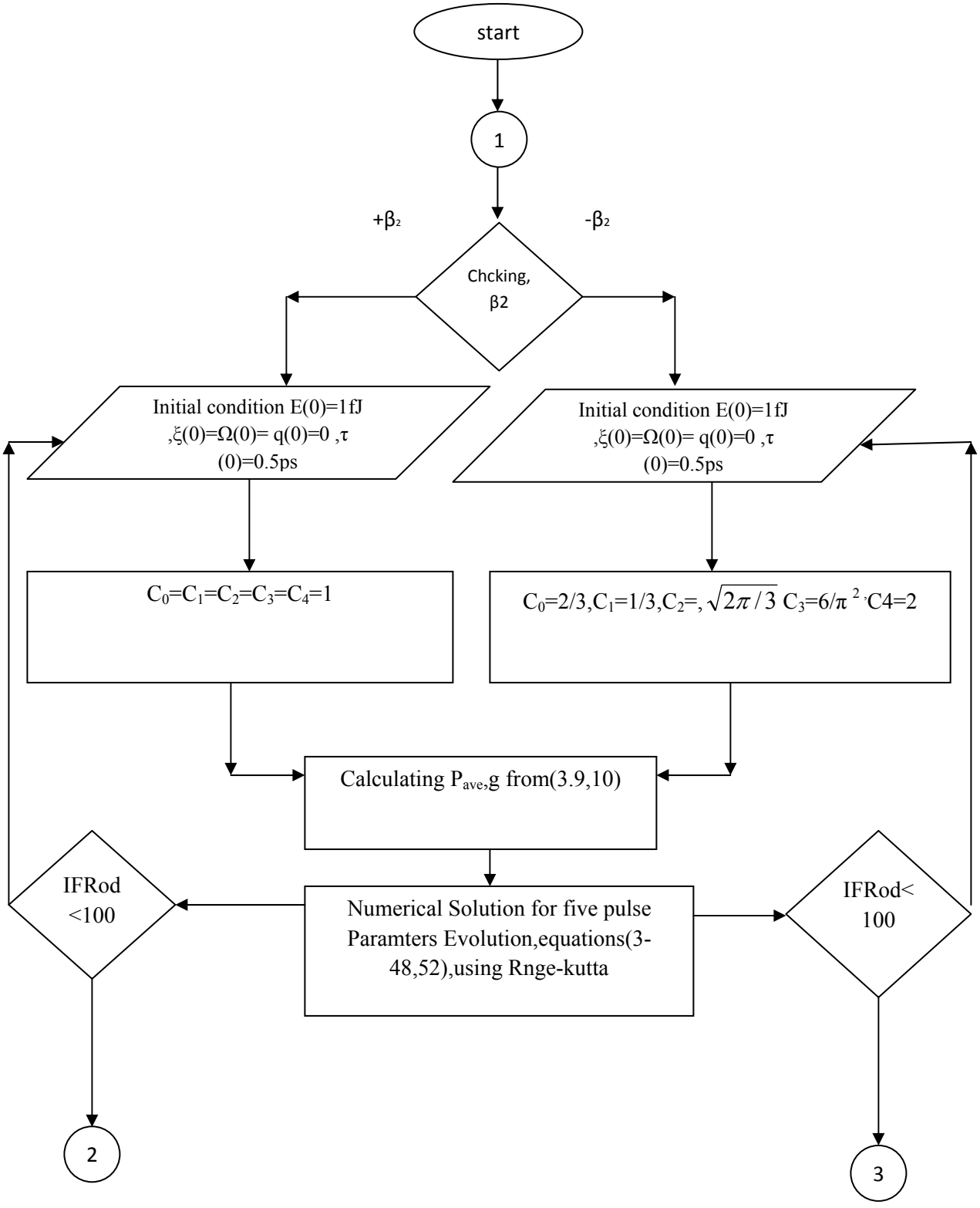

Fig (3-9) Flow chart of the main program for SBR mode Locking.

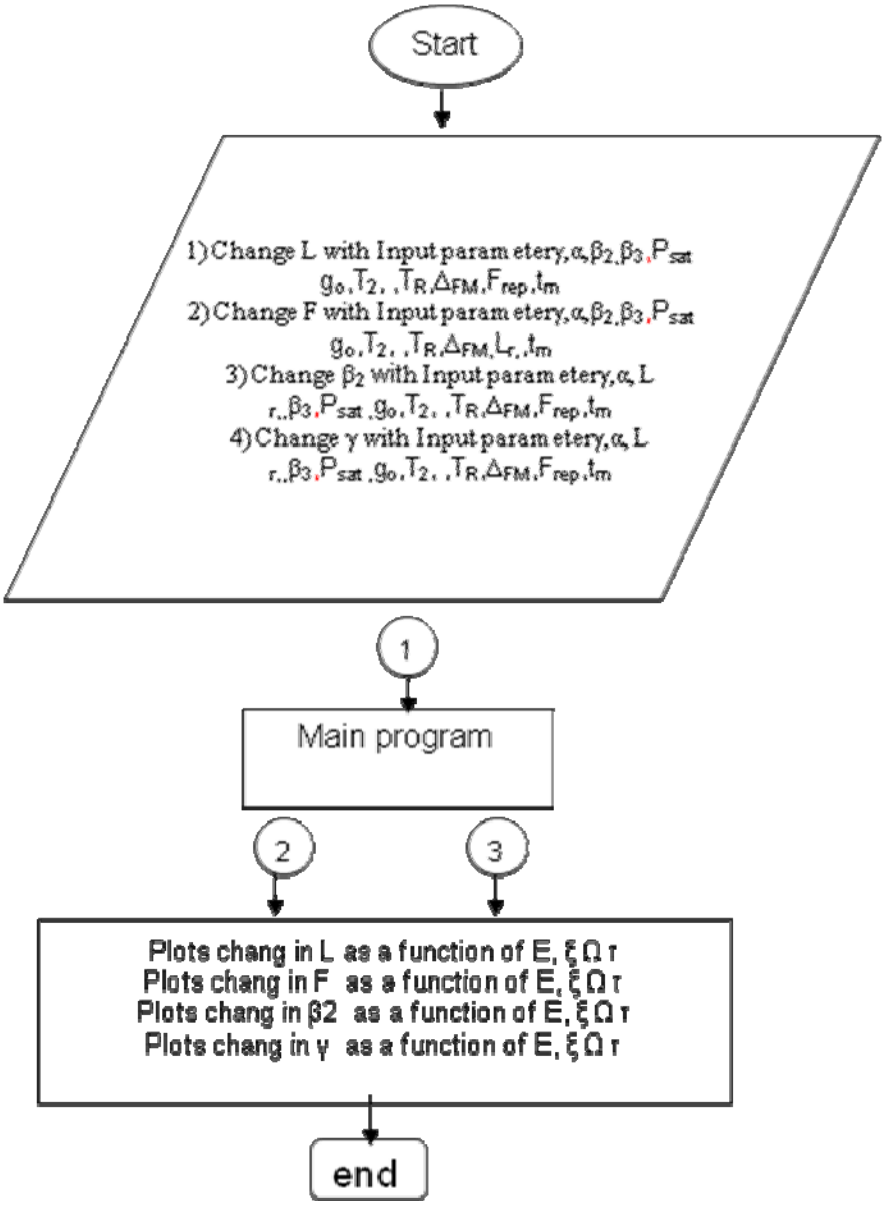

Fig(3-10)Flow chart of the program for study the varying F_r,L_r,γ,β_2 and $\Delta\delta_{SA}$ for mode-Locking.

Chapter Four

Results and Discussions

4.1 Introduction

In the previous chapter, five equations are introduced using moment method which describes pulse parameters evolution at each round trip. To solve these equations numerically we used a Mat-Lab program.

The results that can be shown in this chapter describe the pulse parameter for the three types of mode locking namely AM, FM and SBR.

4.2 FM mode locking

4.2.1 Normal Dispersion Regime

In normal dispersion regime , GVD has positive values i.e. $\beta_2 > 0$ and solution will be done for both cases of TOD $\bar{\beta}_3 = 0$ and $\bar{\beta}_3 = 30 \times 10^{-4}\ fs^3/m$,for studying TOD effect on pulse parameters .Executing the computer program , results for pulse parameters evolution are obtained as plotted in Fig.(4.1) and Fig.(4.2).

As shown in Fig.(4.1) (a and b) , for pulse energy evolution plots , there is no difference in behavior for both cases of TOD ($\bar{\beta}_3 = 0$, $\bar{\beta}_3 \neq 0$).In both cases , E reaches its maximum value 2.795 p J in about 100 roundtrips . Then damping oscillation is going over thousands of roundtrips where $\Delta E = 0.016$ p J (ΔE represents variation between maximum and minimum value) decreasing in magnitude until steady state is achieved. In fact it is obvious that about 4000 roundtrips are needed to achieve steady-state.

The presence of third order dispersion (TOD) has big effect on pulse shape especially for ultra-short pulses of width in range ($\tau < 1$ p s) , so it is necessary to include the β_3 parameter , since it distorts the pulse by broadening it asymmetrically , thus producing a temporal and frequency shift .As shown in Fig.(4.1) (a and b) , in the absence of TOD , no temporal shift ($\zeta = 0$), while in the presence of TOD , a temporal shift is introduced with positive and negative oscillation , not symmetrical around zero axis , $\Delta\xi$=7fs (variation between maximum and minimum) converges to zero .

Eq. (4.1) below, explains the dispersion length due to TOD effect [21] .

$$L_D' = \frac{\tau_0^3}{|\beta_3|} \qquad (4.1)$$

For our case, where pulse width in range $\tau \approx 1$ p s , and using Eq.(4.1) to calculate TOD dispersion length , so $L_D' = 333$ m . Since cavity length L_R =4 m, hence $L_D' \gg L_R$, then TOD effect at the beginning will be weak .Then as number of roundtrips increases as shown in Fig(4.1)(a), TOD effect becomes so strong that affects on the arrival time of the pulse and cause to distorts its shape .Back to Fig. (4.1) (b) for temporal shift plot, it is clear that much more roundtrips are required to achieve steady state, $RT_{ss} \gg 4000$.

The same effect for TOD on pulse frequency shift , when β_3= 0 , no frequency shift is introduced and thus Ω=0, while if β_3 has a value , a negative frequency shift is introduced with negative oscillation, then decreasing with increasing roundtrips, converges to zero steady state .As shown in Fig.(4.1) for frequency shift plot , most frequency shift is negative however , $\Delta\Omega \approx 21.5$ GHz and $\Omega \approx 1$ GHz at $RT = 4000$. While to achieve zero frequency shift, $RT_{ss} \gg 4000$.

As shown in Fig.(4.2)(a) and(b), no effect for TOD on pulse chirp .In fact normal dispersion produces positive pulse chirp , oscillating around zero chirp axis until reaches zero , its steady-state value. Oscillation is symmetrical around zero chirp axes with Δq=22, decreases as roundtrips increase, again $RT_{ss} \gg 4000$

From plots of pulse width evolution as in Fig.(4.2) (a)and (b) , for pulse width plots ,a broadening in pulse width is introduced with maximum width (τ_{max}=11ps) in first 125 roundtrips, then exhibits damped oscillation (Δτ=10ps) over thousands of roundtrips decreasing to steady-state value ($\tau_{ss} \approx 3ps$) ,where large number of roundtrips is needed $RT_{ss} \gg 4000$.From the plots of pulse chirp versus pulse width as in Fig.(4.2), it is clear that steady state is far to achieve unless large number of roundtrips has to be introduced .

4.2.2 Anomalous Dispersion Regime

In anomalous dispersion regime, TOD has two values, $\beta_2 < 0$ and solution will be done for both cases of TOD $\beta_3 = 0$ and $\beta_3 = 30 \times 10^4\ fs^3/m$.

Again, using Table-3.1, the pulse parameters evolution is plotted as in Fig. (4.3) and Fig. (4.4).

As shown in Fig.(4.3) (a) and (b) for pulse energy plots , as in normal regime , there is no difference for pulse energy evolution for both cases of TOD , stating no effect for it on pulse energy evolution . In both cases, E reaches its maximum value $E_{max} \approx 2.794$ p J in about (75) roundtrips as shown in Fig (4.3a) (while in normal regime in about 125 roundtrips).Then damping oscillation isgoing over thousands of roundtrips, where (Δ E= 0.014pJ) but much faster than in

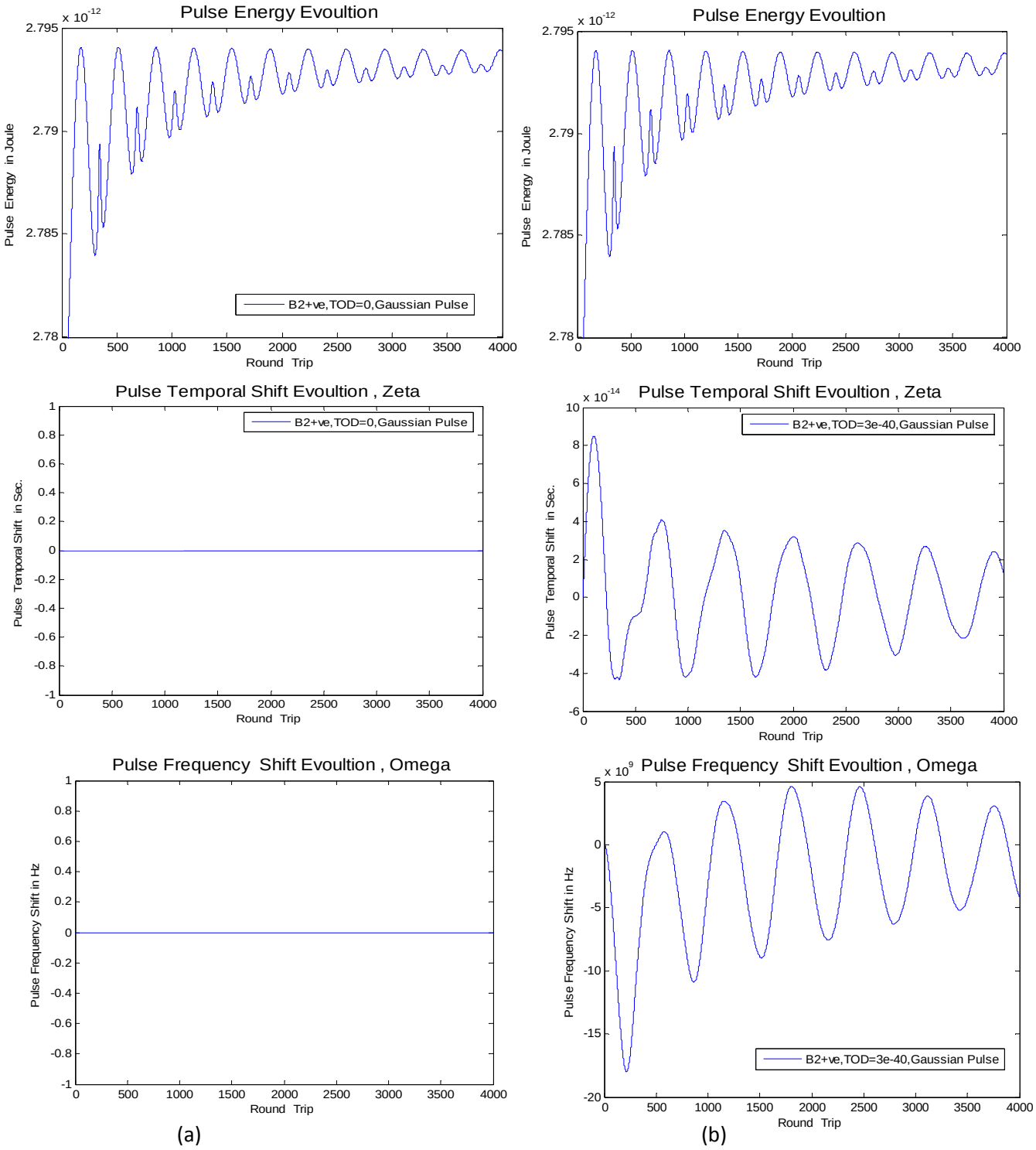

Fig(4.1) Pulse parameters evolution :Energy, Temporal and frequency shift for Normal regime (a)without TOD.(b) with TOD.

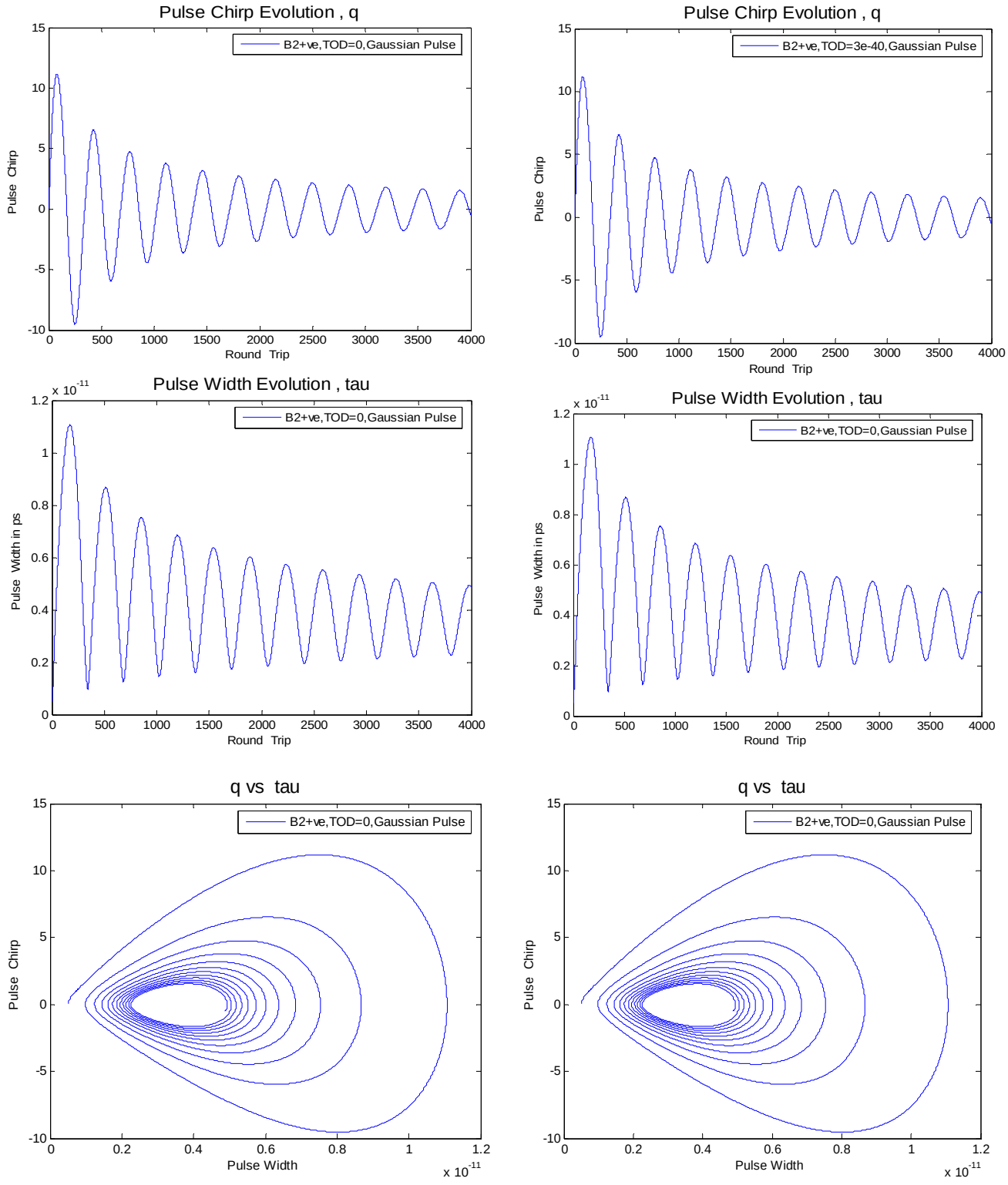

Fig(4.2) Pulse parameters evolution: pulse chirp and width for Normal regime (a)without TOD.(b) with TOD.

normal regime until steady state is achieved .In fact it is obvious that number of roundtrip are needed to achieve steady-state is $RT_{ss} \approx 3500$, while for normal regime $RT_{ss} \approx 4000$.

As mentioned earlier, the presence of (TOD) has great effect on pulse temporal and frequency shift. As shown in Fig.(4.3) , in the absence of TOD, there is no temporal shift (ζ =0), while in the presence of TOD a temporal shift is introduced with positive and negative oscillation ($\Delta\zeta$ =50 f s) .The introduced temporal shift is symmetrical around zero axis, converges to zero value much faster , unlike normal regime where convergence is very slow not symmetrical . Less roundtrips are required to achieve steady state $RT_{ss} \approx 4000$.

The same effect for TOD on pulse frequency shift, when β_3= 0, no frequency shift and thus Ω = 0, while if β_3 has a value, a positive frequency shift is introduced converging to steady state value Ω_{ss} = 5.5 GHz.

Variation is almost symmetrical around steady-state value (unlike normal regime) , with slow damped oscillation ($\Delta\Omega$=5.5GHz) decreasing with increasing roundtrips .Steady state case is achieved faster than in normal regime, where $RT_{ss} \approx 4000$ as shown in Fig. (4.3).

As shown in Fig.(4. 4), anomalous dispersion produces negative pulse chirp whereas the chirp is nearly zero (q=0) this behavior is the consequence of the interplay between dispersion and nonlinearity. In the anomalous regime, the two effects produce chirps with opposite signs, which partially cancel one another, whereas the chirps add in the normal dispersion regime [68] , in normal , a positive chirp is introduced as shown earlier . Damped oscillation is shown around

zero chirp axis until reaches$q_{ss} = 0$, its steady-state value, but much faster than in normal regime. Oscillation is symmetrical around zero chirp axis with Δq≈5 (less than in normal where Δq≈26) decreases rapidly as roundtrips increase .

From plots of pulse width evolution as in Fig.(4.4) , a broadening in pulse width is introduced with maximum width $\tau_{max} = 3ps$ (where in normal Δτ max =11ps) in first (75) roundtrips, then exhibits damped oscillation ($\Delta\tau \approx 2.5\ ps$) over thousands of roundtrips decreasing to steady-state value $\tau_{ss} \approx 0.75\ ps$, (in normal regime Δτ=4ps) where less number of roundtrips than in normal regime is needed $RT_{ss} = 3000$ .While in anomalous regime ,shown the convergence of the pulse width to its steady state value. The large number of round trips necessary before the mode locked pulse converges was expected since the nonlinear and dispersion effects are weak over high round trip .From the plots of pulse chirp with pulse width as in Fig. (4.4), it is clear that steady state is achieved with less number of roundtrips than in normal regime. Table 4.1 summarizes parameters values for both regimes

Table4-1. Pulse Parameters Database for both Dispersion Regimes (Fr=10GHz)FM mode locked

	Normal Regime							Anomalous Regime						
PRAMETER	Max	RT max	Min	RT min	Δ	SS	RT SS	Max	RT max	Min	RT min	Δ	SS	RT_{ss}
E	2.794 p J	100	2.778 p J	200	0.016 p J	2.792 p J	>4000	2.794 pJ	75	2.752 PJ	125	0.042 P J	2.785 p J	4000<
ζ	85 fs	100	-45fs	300	40 fs	0	>4000	+2.5 fs	100	-2.25fs	450	0.25fs	0.25	4000<
Ω	5 GHz	1750	-18 GHz	200	23 GHz	2.51	>4000	+7 GHz	250	1.5 GHz	600	2.5 GHz	5.5 GHz	4000<
q	+2.5	200	-2.5	100	5	0	>4000	+0.9	25	-0.7	100	0.2	0	4000<
τ	11 ps	100	1ps	225	10ps	4ps	>4000	4ps	110	0.5ps	225	3.5ps	0.7ps	4000<

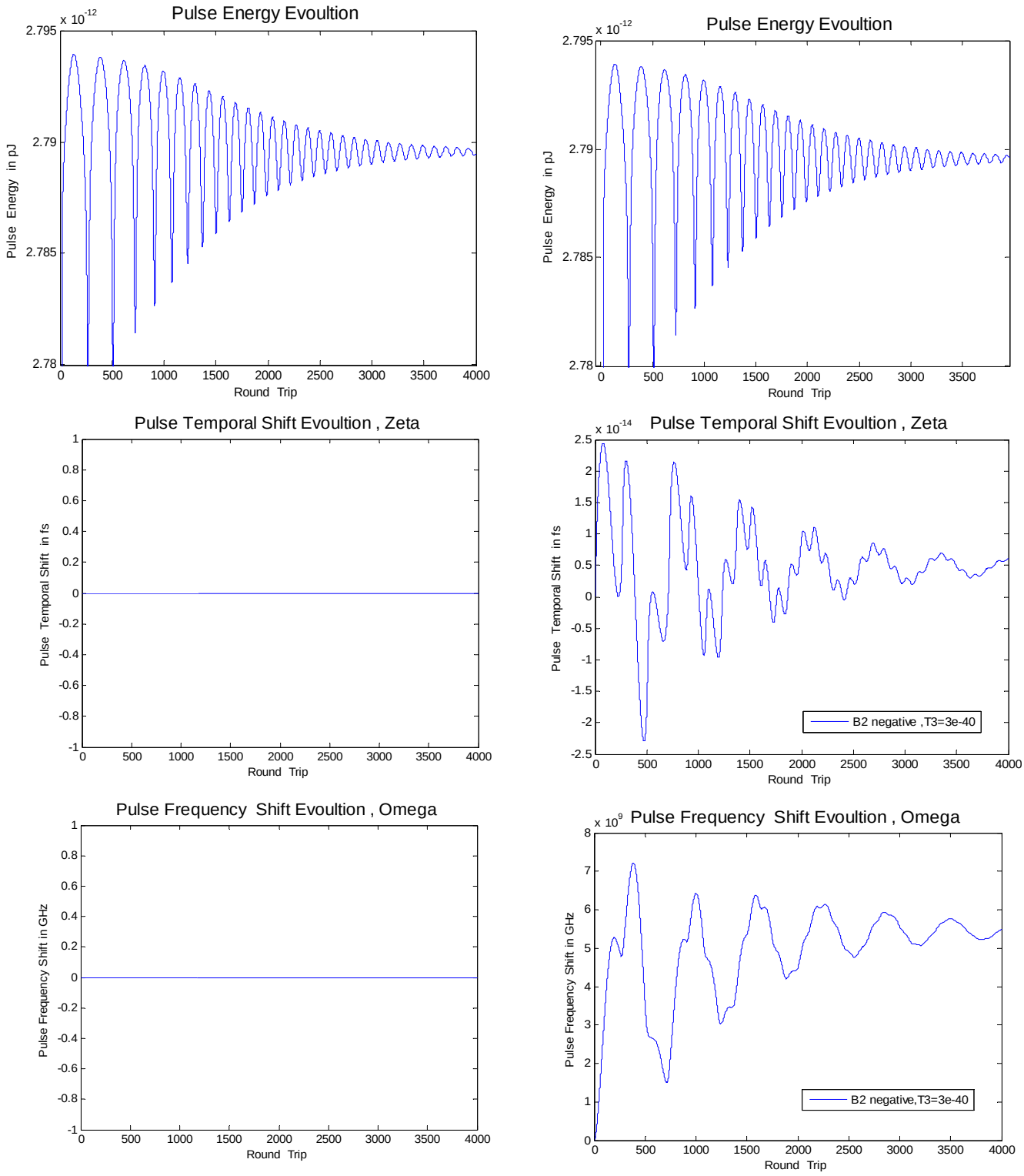

Fig(4.3) pulse parameters evolution :Energy, Temporal and frequency shift for Anomalous regime (a)without TOD.(b) with TOD.

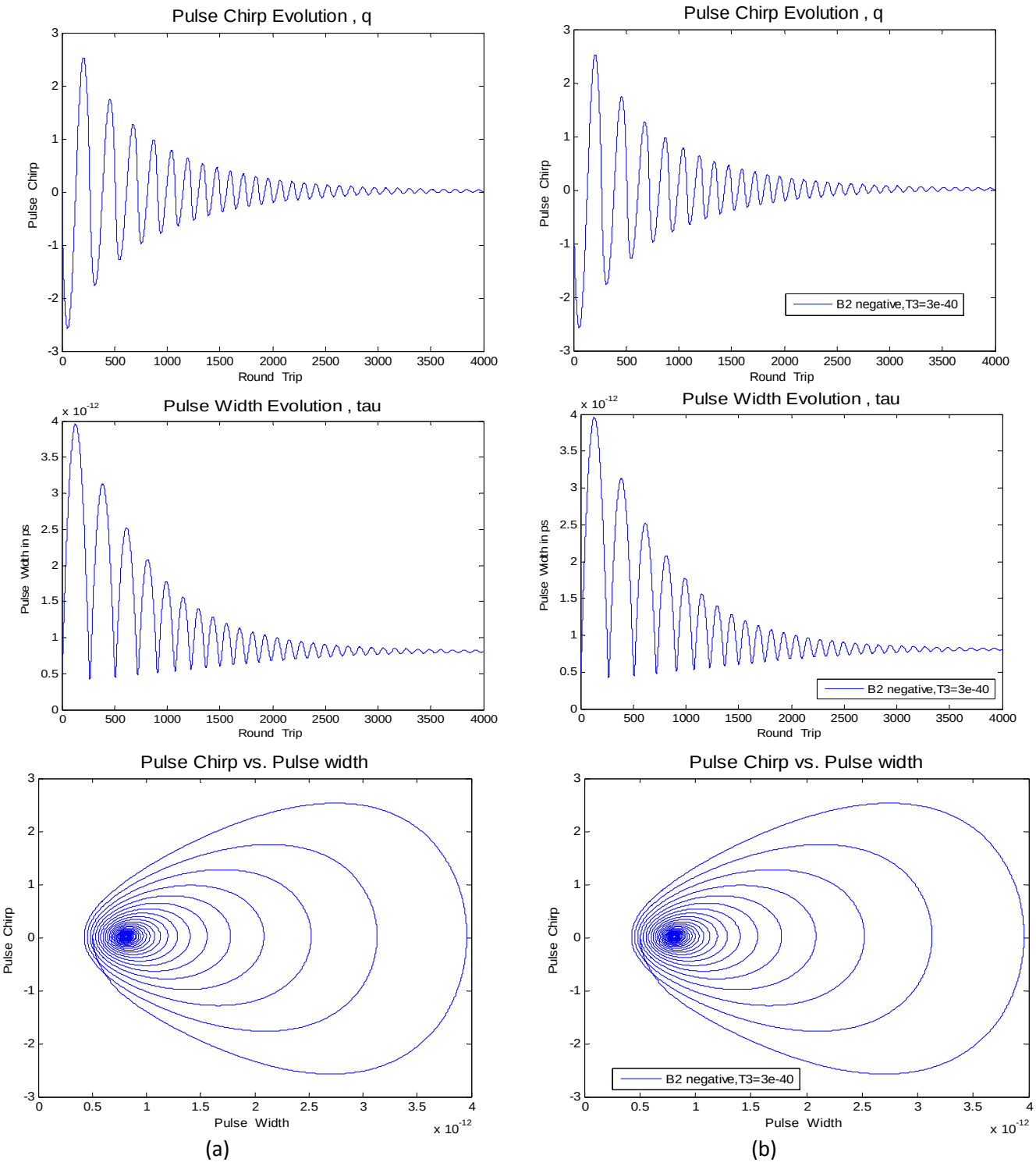

Fig(4.4) pulse parameters evolution: pulse chirp and width for Anomalous regime (a)without TOD.(b) with TOD.

4.2.3 Pulse Parameters versus Modulation Frequency for both Dispersion Regimes

To demonstrate the effect of changing modulation frequency on pulse parameters and make comparison for both dispersion regimes , a plot for each pulse parameter as function of F_r as drawn in Fig.(4.5) for normal and anomalous dispersion regimes .

The two regimes shown in Fig.(4.5) are almost of the same behavior for pulse energy for variable F_r . Energy decreases exponentially as $F_r$increases which is attributed to increase in pulse repetition rate as mentioned earlier , with constant pumping power .Then decreasing rate after certain value of modulation frequency (F_r= 5 GHz) becomes so small for high values and almost constant straight line .But the main difference between both regimes is the stability of E fluctuations . In anomalous regimes roundtrips the required E_{max} is less than in normal regime as shown in Fig (4.1) a and b and Fig. (4. 3)a and b for different F_r.

It is seen that for temporal shift shown in plots Fig.(4.5)(part one),are almost of the same behavior in both regimes . Pulse temporal shift decreases exponentially as $F_r$decreases until certain value (F_r=5 GHz), then a steady state is reached where very small changes in temporal shift withF_r, almost straight line.

The main difference is that : in anomalous regime , converging to steady state value is much faster (less roundtrips are required) . Examples are F_r= 5 GHz , RT_{ss}= 1500 for anomalous , while in normal $RT_{ss} \gg 4000$.

Inspecting plots for pulse frequency shift in Fig.(4.5)(part two) the stability of anomalous regime's clear . For normal regime , the frequency shift suffers from

large oscillation (negative and positive variations) as $F_r$increases , while in anomalous regime , frequency shift decreases in negative values to zero then positive peak value at F_r= 5 GHz , then slight decrease , and after that constant positive values almost straight line with increasing F_r. For F_r= 5 and 7.5 GHz, in anomalous regime, steady state is achieved in $RT_{ss} \approx 1500$ and 3000 respectively, which is much faster than normal, where $RT_{ss} \gg 4000$ are required.

As shown in Fig. (4.5)(part two) ,the induced frequency chirp increases with modulated frequency , the pulse chirp in normal regime suffers from oscillation for variable $F_r$that is decreasing with increasing of F_r until reaches its zero steady state value .In anomalous regime , the negative produced chirp decreases exponentially with increasing $F_r$approaching to zero steady state value at F_r= 5 GHz much faster than normal regime . For $F_r > 5$ GHz, almost flattened relation with almost constant zero chirp. An important case for F_r= 5 GHz , is the case where very low and fast oscillation damped rapidly to zero steady state chirp with $RT_{ss} \ll 1500$ compared with same case in normal regime where $RT_{ss} \gg 4000$.

The fiber dispersion and nonlinear effects inside the fiber may also introduce a chirp to the output pulse. Thus the total chirp is the sum of the induced chirps by unbalanced phase modulators, by fiber dispersion and nonlinear effects.

Modulation frequency has great effect on pulse width since it is responsible for mode-locking mechanism and producing pulses train. As shown in Fig.(4.5), pulse width decreases exponentially with $F_r$increases , but for anomalous regime is much faster in magnitude and in less $F_r$values compared with normal

regime .Almost , for anomalous regime, the minimum pulse width is obtained when F_r= 5 GHz and much faster ($RT_{ss} \approx 1500$) .

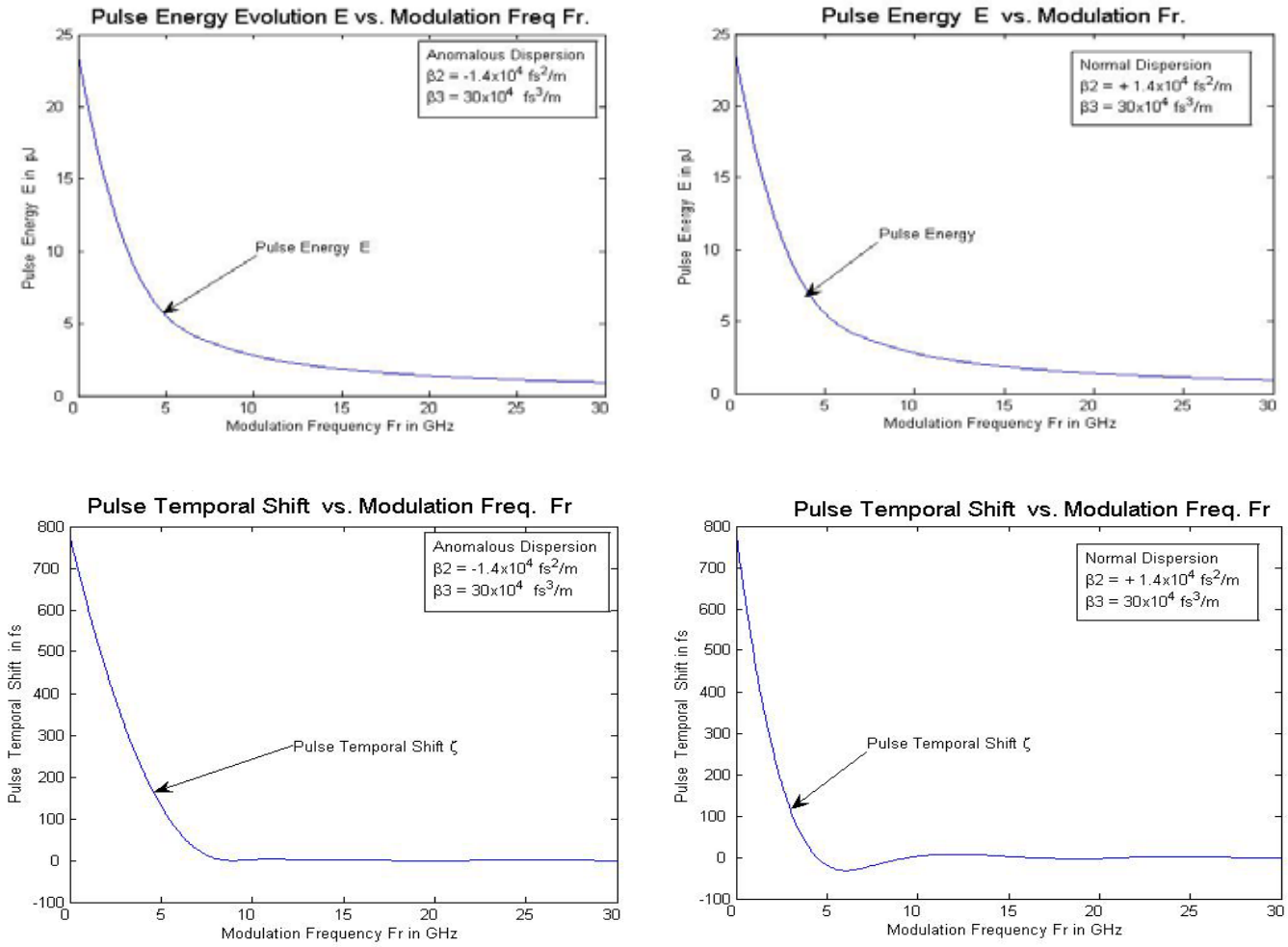

(a) (b)

Fig(4-5) (part one) Pulse energy, temporal shift versus modulation frequency(a) Anomalous and (b) Normal dispersion .

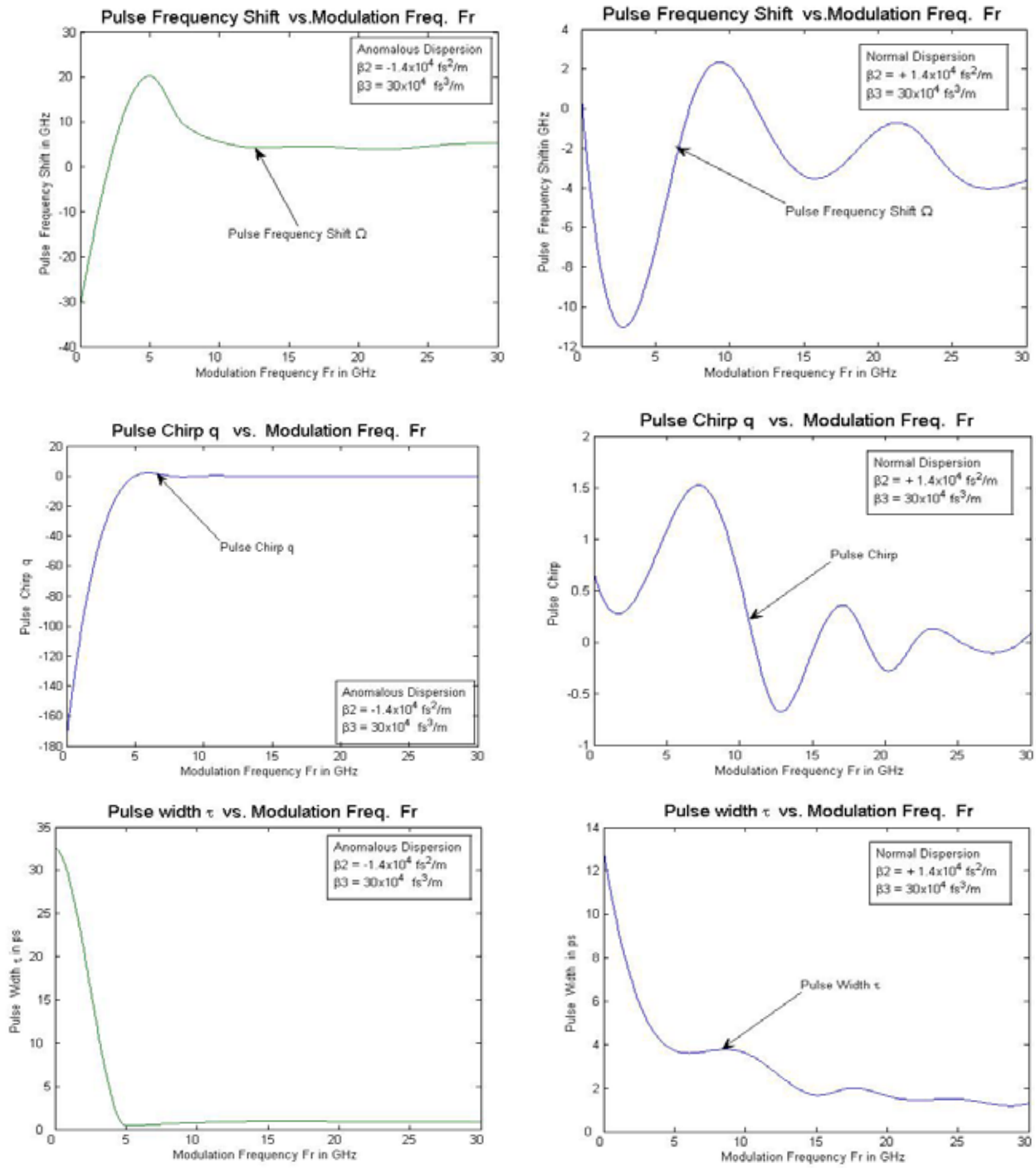

(a) (b)

Fig.(4.5)(part two) Frequency shift, chirp and width versus modulation frequency in(a) Anomalous and (b) Normal dispersion .

4.2.4 Pulse Parameters versus Cavity Length for both Dispersion Regimes

To demonstrate the effect of changing cavity length on pulse parameters and make comparison for both dispersion regime , a plot for each pulse parameter as L_r function is drawn in Fig.(4.6) for normal and anomalous dispersion regimes .

As shown in Fig.(4. 6)(part one) almost same behavior for pulse energy is seen for variable L_r. Energy decreases exponentially as L_r increases .Then decreasing rate after certain value of cavity length (L_r = 5 m) and becomes so small for high values and almost constant straight line .

Temporal shift plots in Fig.(4.6) (part one)for both regimes, are shown almost the same behavior in both regimes . Pulse temporal shift is increases linearly as L_r increases. The main difference is that : in anomalous regime , the temporal shift is greater than normal regime by five times.

Inspecting plots for pulse frequency shift in Fig.(4.6)(part two) the linear relation in anomalous and normal regime is seen. For normal regime , the frequency shift decrease linearly with L_r increases , while in anomalous regime , frequency shift increases with increase L_r .

For pulse chirp as function of cavity length, as shown in Fig. (4.6)(part two) , the pulse chirp in normal regime suffers from positive linear relation for variable L_r increasing with increasing of L_r .In anomalous regime , the negative linear relation chirp decreases with increasing L_r .This linear chirp enables us to compare the pulse outside the laser cavity without deforms in an anomalous dispersion regime until free chirp pulse is introduce[13].

Cavity Length has great effect on pulse width since it is responsible for mode-locking mechanism and producing pulses train . As shown in Fig.(4.6), pulse width increases exponentially with the increase of Lr , but for anomalous regime it is much faster increasing in magnitude and less in Lr values as compared with normal regime .Almost , for anomalous regime, the minimum pulse width is obtained .

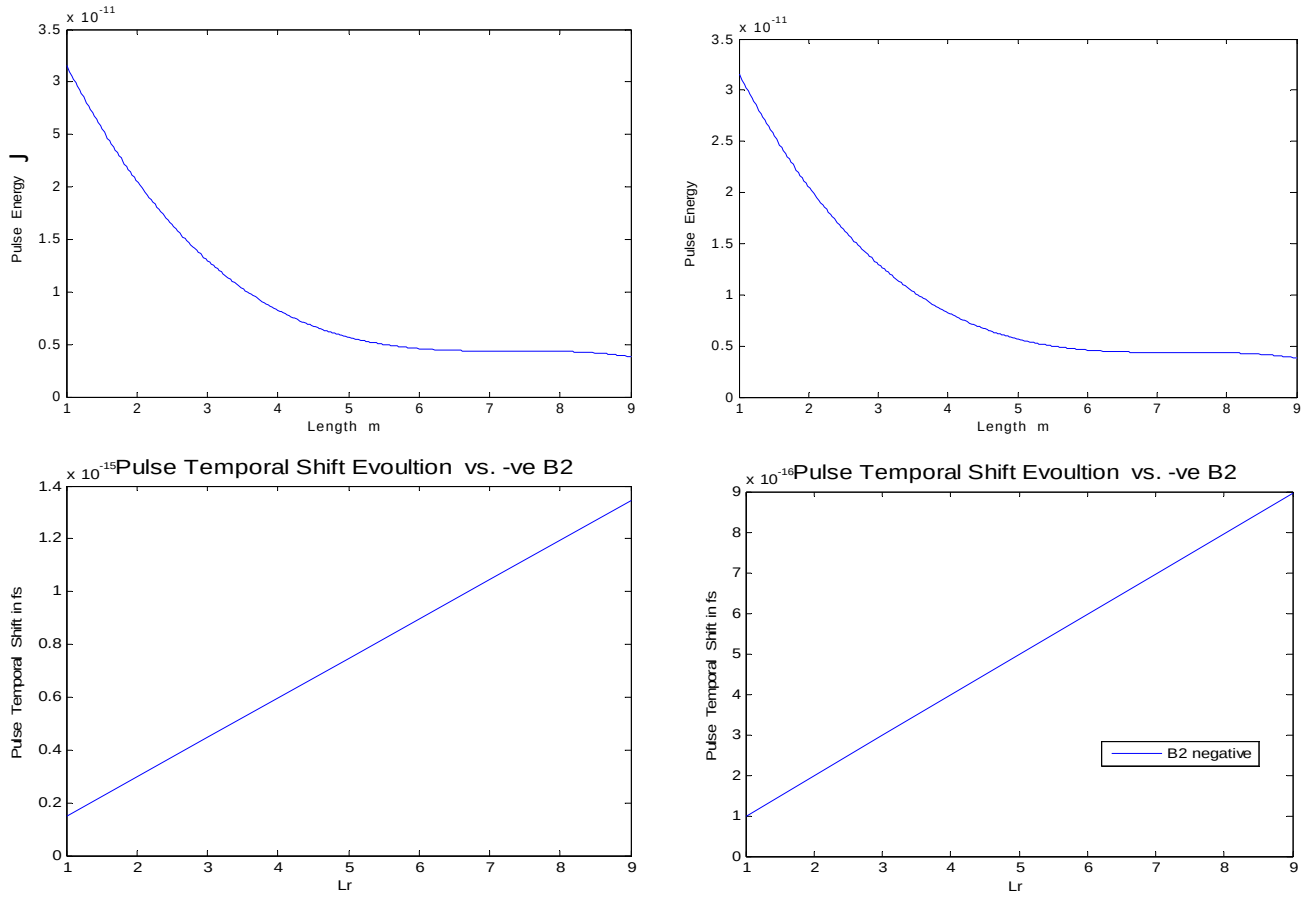

(a) (b)

Fig.(4. 6) (part one): Pulse energy, temporal shift versus cavity length in(a) Normal and(b) Anomalous dispersion .

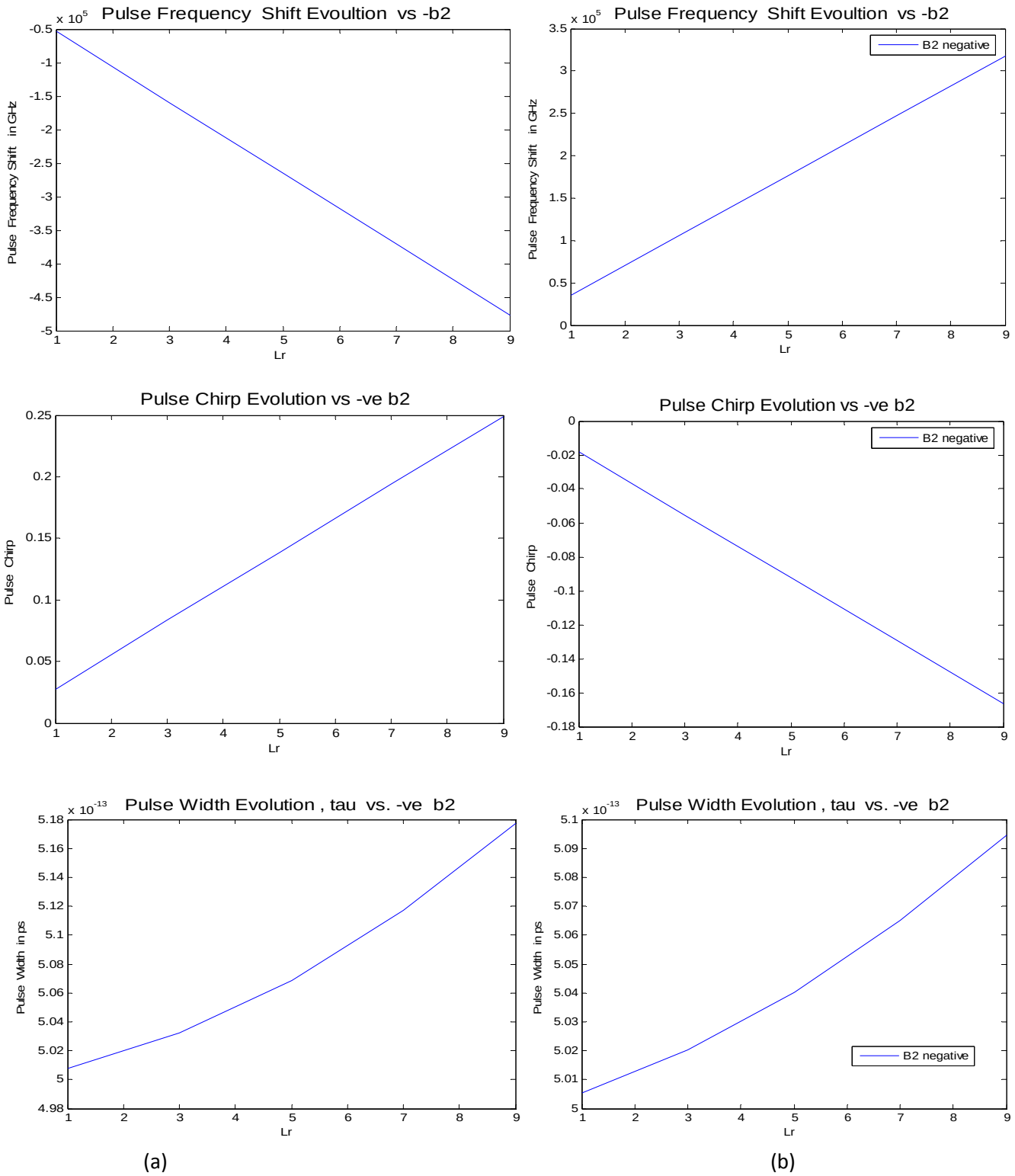

Fig.(4. 6)(part two) : Frequency shift, chirp and width versus cavity length in(a) Normal and(b) Anomalous dispersion .

4.2.4 Pulse Parameters versus Nonlinearity for both Dispersion Regimes

To demonstrate the effect of changing nonlinear coefficient on pulse parameters and make comparison for both dispersion regime , a plot for each pulse parameter as function of γ is drawn as in Fig.(4.7)) for normal and anomalous dispersion regimes respectively .The pulse characteristics are affected by increasing nonlinearity in away similar to situation when fiber length increasing.

Energy increases linearly as γ increases in anomalous dispersion but in normal dispersion decreasing with increase γ that is shown in Fig.(4.7) (part one) .

For temporal shift plots in Fig.(4.7)(part one) the relation is a linear behavior in both regimes . Pulse temporal shift increases linearly as γ increases in normal regime, but in anomalous regime the temporal shift decreased with the increase of γ.

Inspecting plots for pulse frequency shift in Fig.(4.7)(part two) it is clear that both anomalous and normal regimes have the negative linear relation . For normal regime, the frequency shift suffers from inversely linear relations with increasing γ, while in anomalous regime, frequency shift increases with increase γ.

For pulse chirp as function of Nonlinearity, as shown in Fig. (4.7)(part two) the pulse chirp in normal regime suffers from positive linear relation for variable γ that increases with increasing of γ .In anomalous regime , the negative linear relation chirp increases with increasing γ .

Nonlinearity has great effect on pulse width since it is responsible for mode-locking mechanism and producing short pulses. As shown in Fig.(4.7)(part two) pulse width increases linearly with γ increases in normal case , but for anomalous

regime the pulse width is shorted with the increase of γ values compared with normal regime .Almost , for anomalous regime the minimum pulse width is obtained .

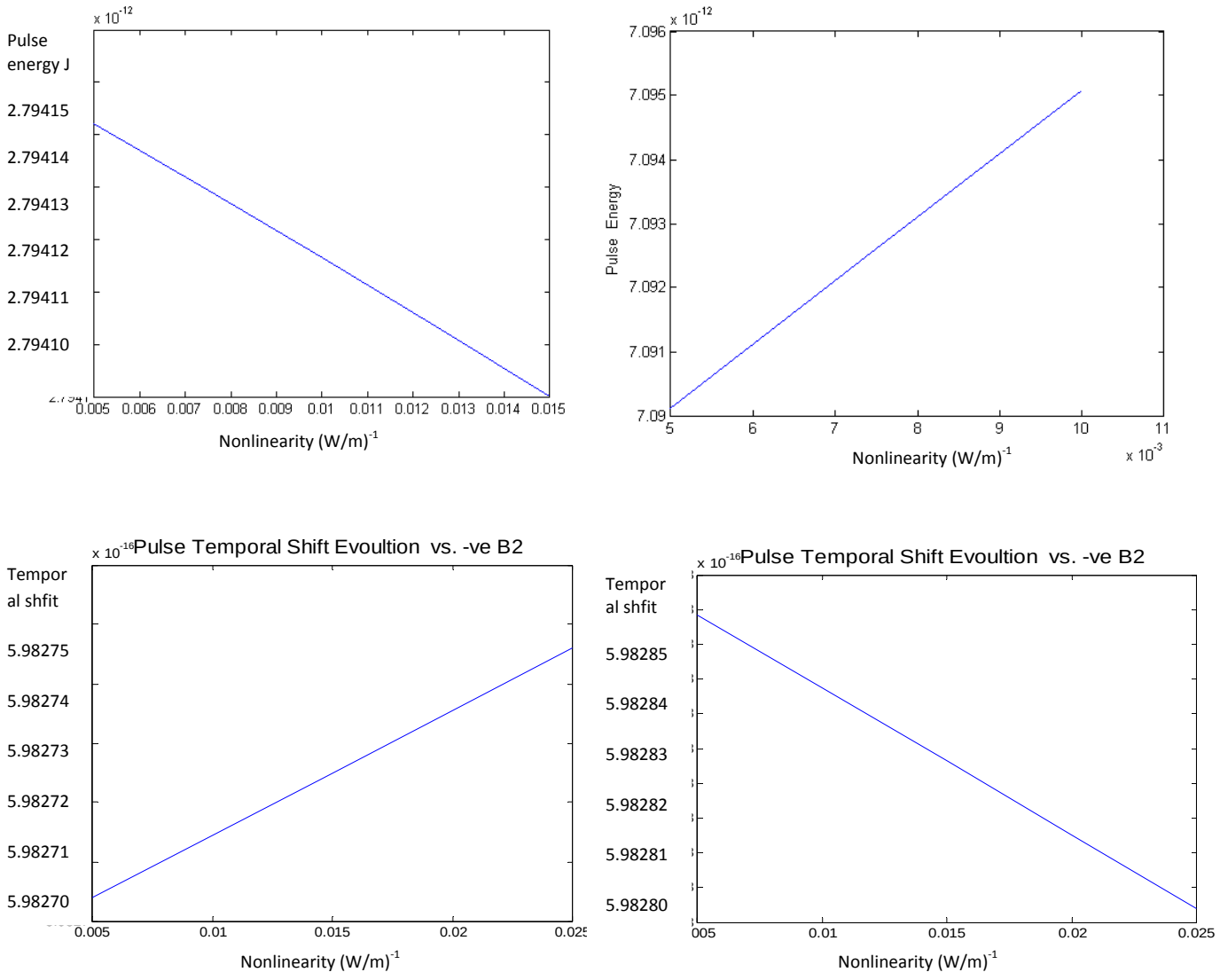

(a) (b)

Fig.(4.7) (part one): Pulse energy, temporal shift versus nonlinearity in(a) Normal and (b) Anomalous dispersion.

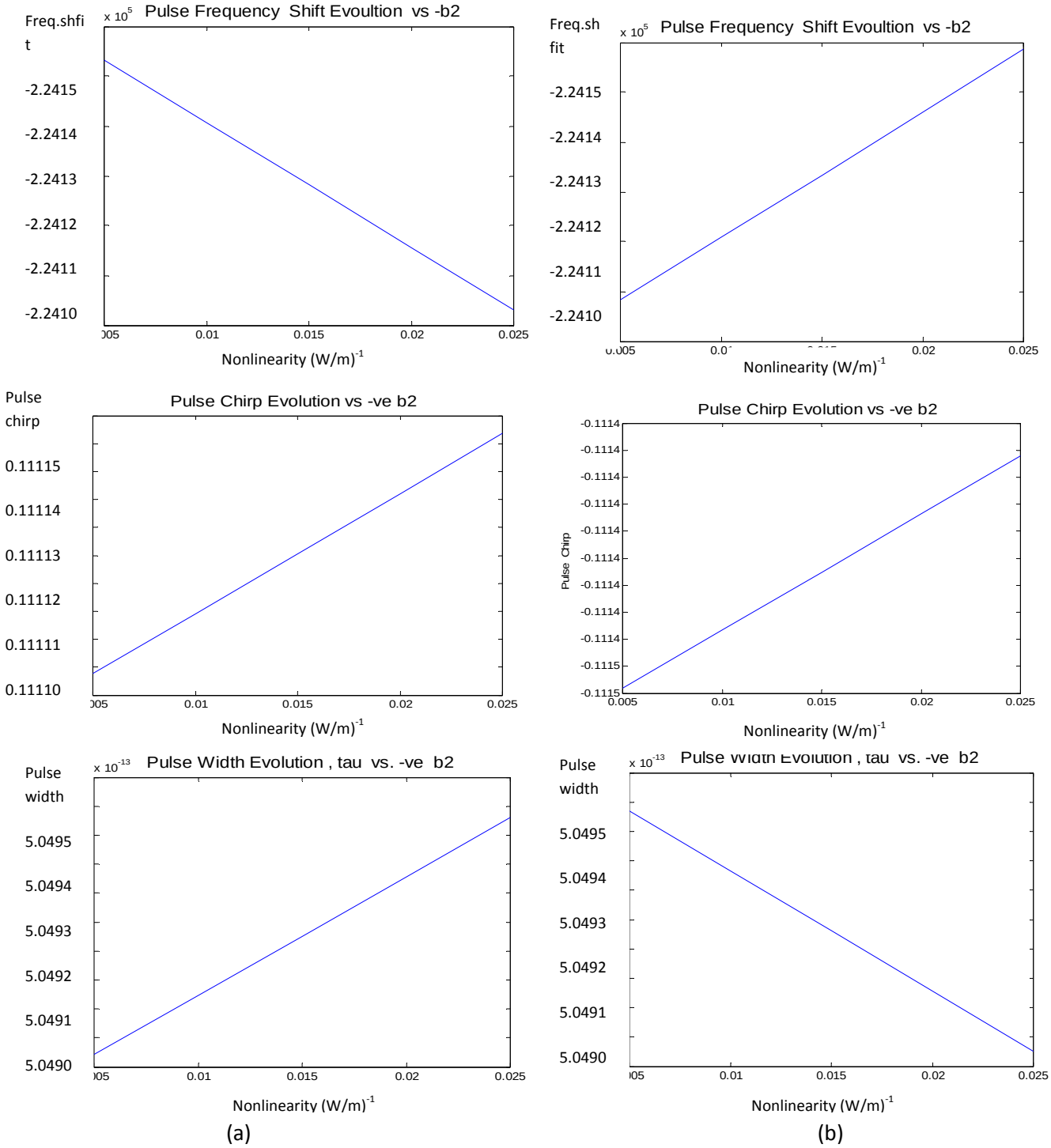

Fig.(4.7)(part two) : Frequency shift, Chirp and Pulse width versus nonlinearity in(a)Normal dispersion(b) Anomalous dispersion.

4.2.5 Pulse Parameters versus second order dispersion for both Dispersion Regimes

To demonstrate the effect of changing second order dispersion on pulse parameters and make comparison for both dispersion regime , a plot for each pulse parameter as if function β_2 is drawn as in Fig.(4.8) for normal and anomalous dispersion regimes .

As shown in Fig.(4.8)(part one) the behavior of normal regime for variable β_2. The energy is increasing rapidly until reach the maximum value(2.7927pJ) at β_2=2.5fs^2/m .In anomalous regime energy oscillate around the value (2.79pJ)as β_2 increases until reach maximum value(2.792 pJ) at β= -1fs^2/m than decrease rapidly .

For temporal shift plots in Fig.(4.8)(part two) ,almost the behavior of normal regime temporal shift decreases exponentially with the increase of β_2 until certain value(β_2=3ps^2/m) ,then it will reach the steady state value then to a very small changes in temporal shift with β_2, almost straight line. In anomalous regime decreasing temporally shift with increasing β_2 until reach $\xi\approx 0$ at the period (β_2= -1.5 to -1fs^2/m), then decrease to ξ =-8e-13s at β_2=0.5ps^2/m.

Inspecting plots for pulse frequency shift in Fig.(4.8)(part two) it is clear that in the normal regime the frequency shift Ω suffers from exponential decrease with the increase of Ω (positive value) as β_2 increases until it reaches steady state at β_2 =2.5e-26s^2/m (Ω =0.25e9Hz). In anomalous regime, frequency shift equals to zero until it reaches β_2=-1.5e-26 s^2/m then increases in positive

values to maximum (Ω=5GHz) at β_2=-1e-26 s^2/m then decreases rabidly in negative value with increase β_2 .

For pulse chirp as function of second order dispersion, as shown in Fig. (4. 8) (part two) , the pulse chirp in normal regime suffers from linear relation increase in **q** with increase of β_2 **.**In anomalous regime ,the produced chirp increases approximately exponentially with increasing β_2 approaching to zero steady state value at β_2= -0.5e-26 s^2/m.

Second order dispersion has great effect on pulse width since it is responsible for mode-locking mechanism and producing pulses train . As shown in Fig.(4.8)(part two)(part two), pulse width increases linearly with β_2 increases , but for anomalous regime is of much faster decrease **τ** in magnitude and reach minimum value **τ** at β_2= -0.75e-26s^2/m than increasing rapidly after β_2= - 0.5e-26 s^2/m.

Almost , for anomalous regime, the minimum pulse width is obtained than normal regime.

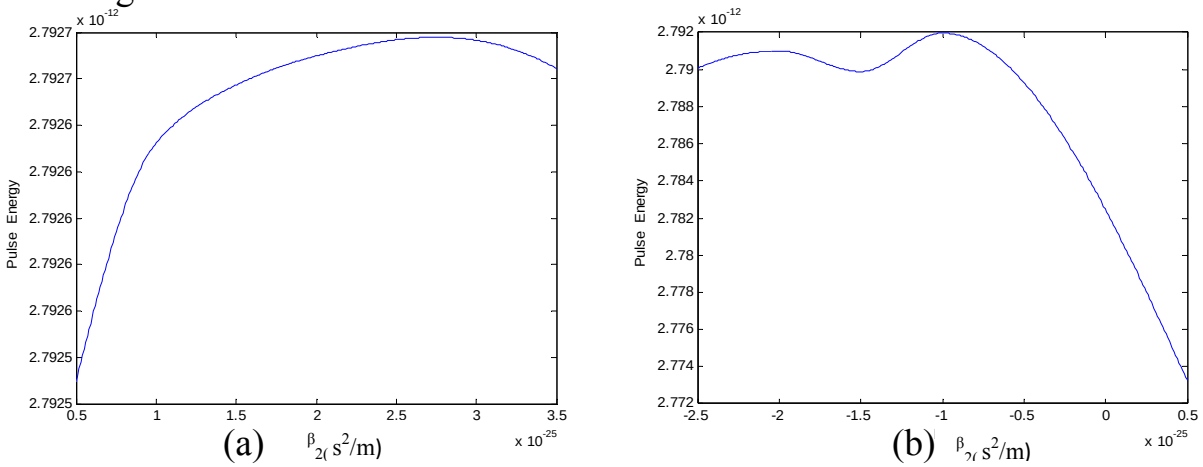

Fig.(4.8) (part one) : Pulse energy versus second order dispersion in (a)Normal,(b)Anomalous dispersion.

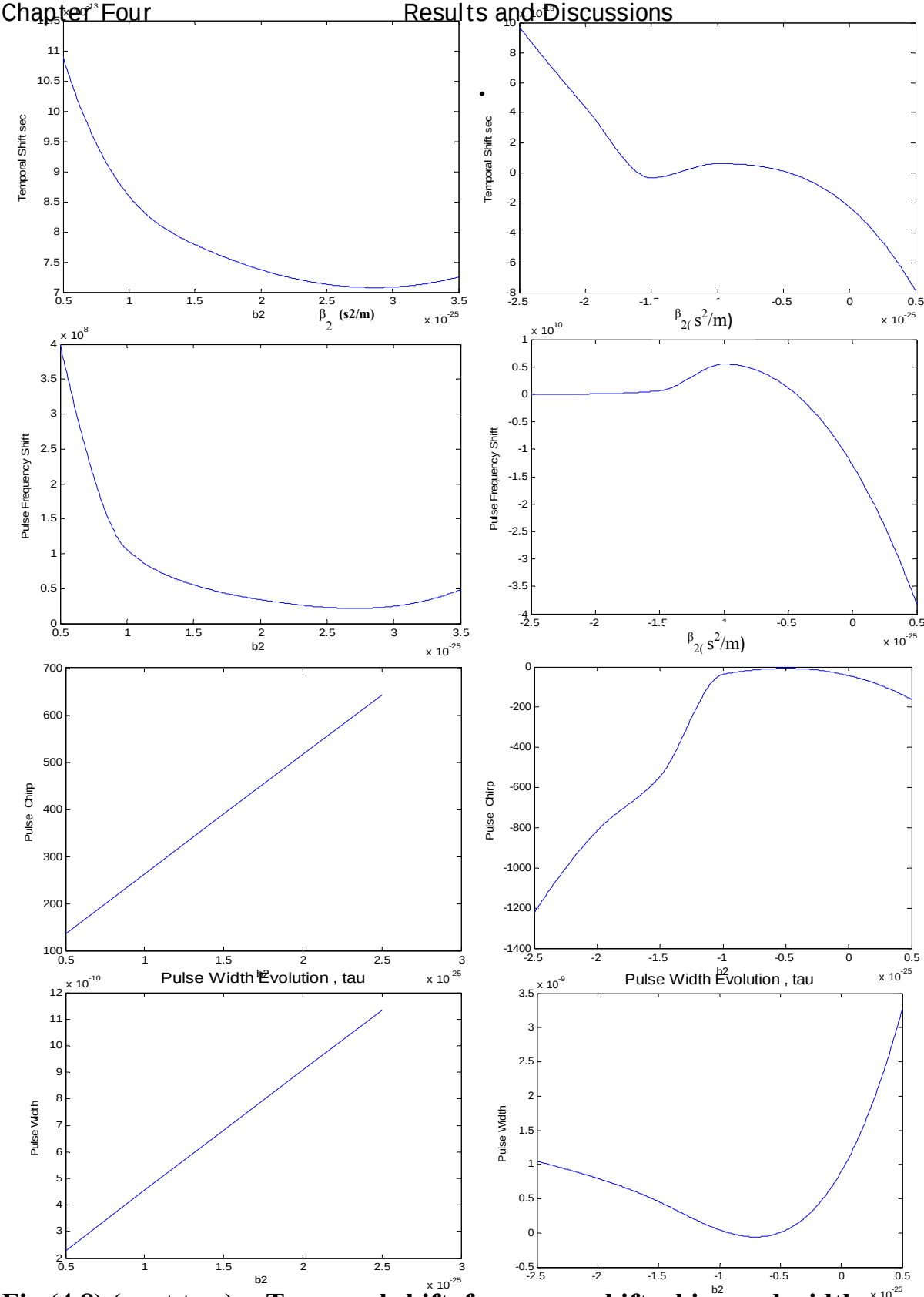

Fig.(4.8) (part two) : Temporal shift, frequency shift, chirp and width versus second order dispersion in (a)Normal,(b)Anomalous dispersion.

4.3 AM mode locking

4.3.1 Normal Dispersion Regime

In normal dispersion regime , GVD has positive values i.e. $\beta_2 > 0$ and solution will be done for both cases of TOD : $\bar{\beta}_3 = 0$ and $\bar{\beta}_3 = 30 \times 10^4\ fs^3/m$,to study TOD effect on pulse parameters .Executing the computer program , results are pulse parameters evolution as plotted in Fig.(4.9) and Fig.(4.10).

For pulse energy evolution plots , there is no difference in behavior for both cases of TOD ($\bar{\beta}_3 = 0$, $\bar{\beta}_3 \neq 0$) as shown in Fig.(4.9) (a and b).In both cases , E reaches its maximum value $E_{max} \approx 3.5$ p J in about 200 roundtrips as shown in Fig (4.9) (a). Then short damping oscillation is going to few hundred of roundtrips where $\Delta E = 2.5$ pJ (ΔE represents variation between maximum and minimum value) decreasing in magnitude until steady state is achieved. In fact it is obvious that about 400 roundtrips are needed to achieve steady-state.

In Fig.(4.9), in the absence of TOD , no temporal shift is introduced ($\zeta = 0$), while in the presence of TOD , a temporal shift is introduced with positive value oscillation, $\Delta\xi = 11$ps (variation between maximum and minimum) converges to 10ps .

The same effect for TOD on pulse frequency shift is shown, when $\beta_3 = 0$, no frequency shift is introduced and thus $\Omega = 0$, while if β_3 has a value , a positive and negative frequency shift is introduced with negative oscillation, then increasing with increasing roundtrips, converges to steady state axis ,as shown in Fig.(4.10) for frequency shift plot $\Delta\Omega \approx 1$MHz and $\Omega \approx 65$ MHz at RT=400.

Also no effect for TOD on pulse chirp is seen as shown in Fig.(4.10)(a) and(b) .In fact normal dispersion produces positive pulse chirp , oscillating around

chirp axis until reaches steady-state value. with Δq=90, decreases as roundtrips increase, to q=64 at RTss=400 .

From plots of pulse width evolution as in Fig.(4.10) (a) and (b) , for pulse width plots ,a broadening in pulse width is introduced with maximum width (τ_{max} =6 ps) in first 75 roundtrips, then exhibits damped oscillation ($\Delta\tau\approx$4.5 ps) over hundred of roundtrips increasing to steady-state value ($\tau_{ss}\approx$2.9 ps),where the number of roundtrips is needed RTss≈400 .From the plots of pulse chirp versus pulse width as in Fig.(4.10), it is clear that steady state is achieved by hundred number of roundtrips.

4.3.2Anomalous Dispersion Regime

In anomalous dispersion regime, TOD has negative values, $\beta_2 < 0$ and solution will be done for both cases of TOD β_2= 0 and β_2= 30 x 10^4 fs^3/m Again, using Table-3.1, the pulse parameters evolution is plotted as in Fig. (4.11) and Fig. (4.12).

As shown in Fig.(4.11) (a) and (b) for pulse energy plots , as in normal regime , there is no difference for pulse energy evolution for both cases of TOD , stating no effect for it on pulse energy evolution . In both cases, E reaches its maximum value $E_{max} \approx$ 5 p J in about (150) roundtrips as shown in Fig (4.11)(a) (while in normal regime in about 200 roundtrips).Then damping oscillation is going over handred of roundtrips, where (Δ E= 4.75pJ) but much faster than in normal regime until steady state is achieved .In fact it is obvious that number of roundtrip are needed to achieve steady-state that is RTss=350, while for normal regime RTss=400 .

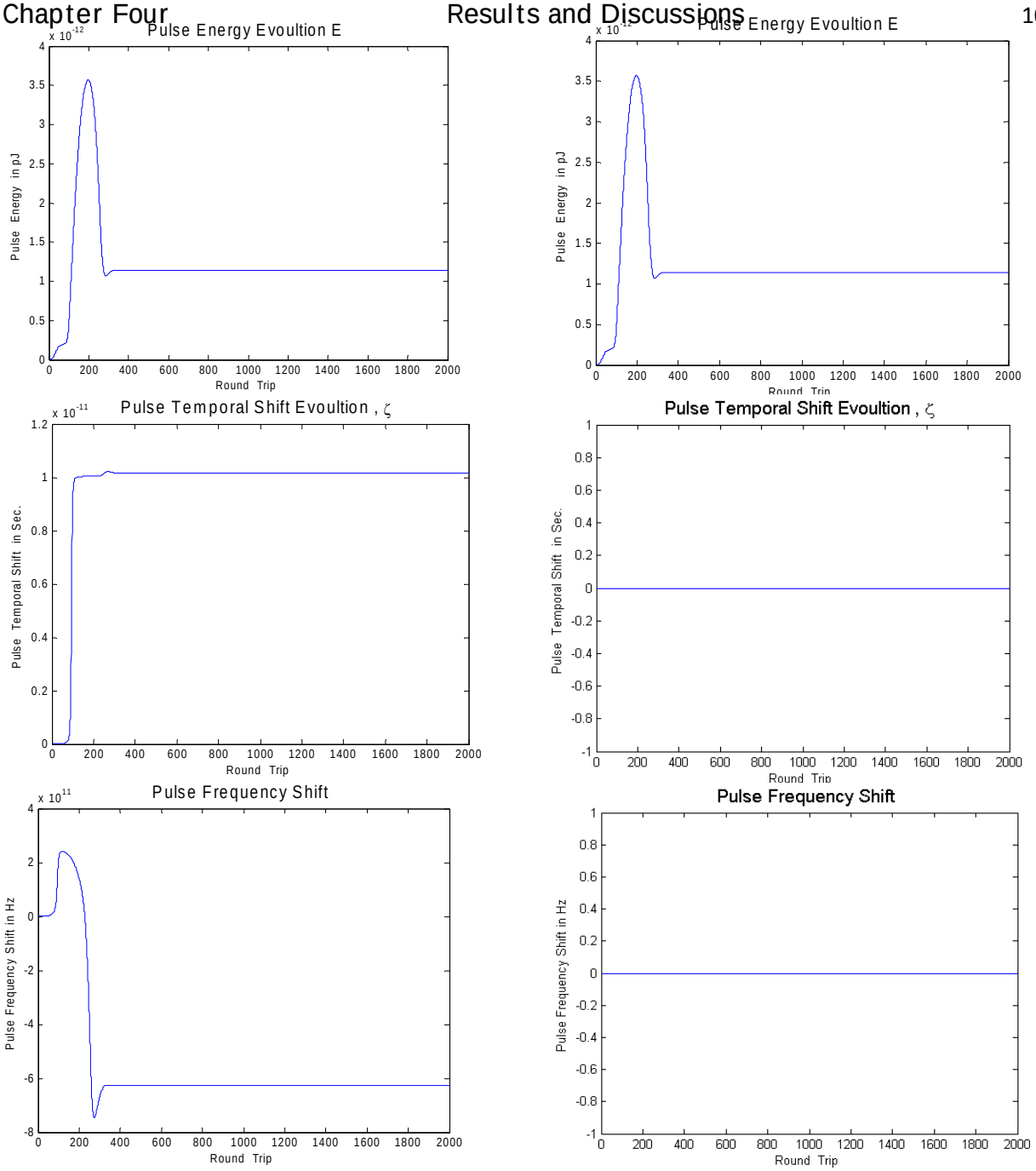

(a) (b)

Fig(4.9) pulse parameters evolution: Energy, Temporal and frequency shift for Normal regime (a)without TOD.(b) with TOD.

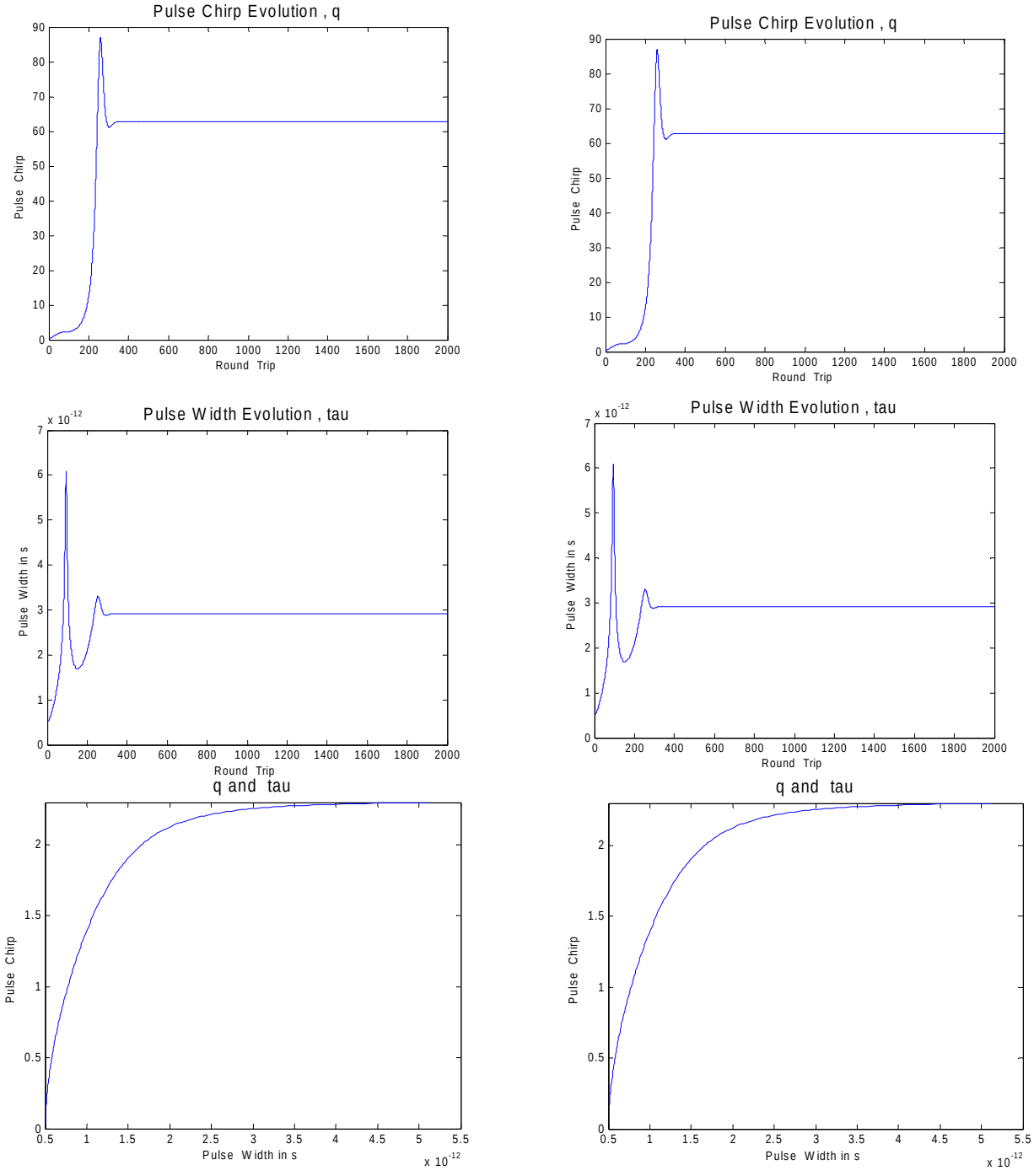

Fig(4.10) Pulse parameters evolution: pulse chirp and width for Normal regime (a)without TOD.(b) with TOD.

As mentioned earlier, the presence of (TOD) has great effect on pulse temporal and frequency shift. As shown in Fig.(4.11) , in the absence of TOD, there is no temporal shift (ζ =0), while in the presence of TOD a temporal shift is introduced with positive and negative oscillation ($\Delta\zeta$ =350 f s) .

The introduced temporal shift is symmetrical around a temporal axis, converges to steady state value .

The same effect for TOD on pulse frequency shift, when β_3= 0, no frequency shift is present and thus Ω = 0, while if β_3 has a value, a positive frequency shift is introduced converging to steady state value Ω_{ss} = 58MHz.

Variation is almost symmetrical around steady-state value (unlike normal regime) , with slow damped oscillation ($\Delta\Omega$=7Mhz) decreasing with increasing roundtrips . Steady state case is achieved faster than in normal regime, where RTss =300 as shown in Fig. (4.11).

As shown in Fig.(4.12), anomalous dispersion produces negative pulse chirp, while in normal , a positive chirp is introduced as shown earlier . Damped oscillation is shown around chirp axis until reaches q_{ss}=-59, its steady-state value, but much faster than in normal regime. Oscillation is symmetrical around chirp axis with Δq=-120 (less than in normal where Δq=+50) decreases rapidly as roundtrips increase, RTss =400.

From plots of pulse width evolution as in Fig.(4.12) , a broadening in pulse width is introduced with maximum width τ_{max} =2.75ps (where in normal τ_{max} =6ps) in first (200) roundtrips, then exhibits damped oscillation ($\Delta\tau\approx$1.15ps)

over handered of roundtrips decreasing to steady-state value $\tau_{ss} \approx 1.75$, (in normal regime $\tau_{ss} \approx 2.9$ps) where less number of roundtrips than in normal regime is needed RTss =300 . From the plots of pulse chirp with pulse width as in Fig. (4.11), it is clear that steady state achieves less number of roundtrips than in normal regime.

From the figures especially to anomalous and normal regime the approach to steady state in both normal and anomalous dispersion regimes can be shown. It severed that the pulse converges quickly in anomalous dispersion regime but takes >400 round trip before converging in normal dispersion regime.

Table 4.2 summarizes parameters values for both regimes.

Table 4.2 Pulse Parameters Database for both Dispersion Regimes (Fr=10GHz)AM mode locked

	Normal Regime							Anomalous Regime						
PRAMETER	Max	RT max	Min	RT min	Δ	SS	RT SS	Max	RT max	Min	RT min	Δ	SS	RT_{ss}
E	3.5 p J	200	1 p J	300	2.5 p J	1.2 p J	400	5 pJ	150	0.25 PJ	225	4.75 P J	0.49 p J	400 <
ζ	10.2 pJ	300	10pss	100	0.2p s	10.2ps	400	86ps0.	210	0.4p s	250	0.34p s	4.5p s	400 <
Ω	2 MH z	100	-7.5MH z	200	10 MHz	-65MH z	400	135MH z	205	0.58 MHz	300	0.77 MHz	0.58 MHz	400 <
q	+90	250	160	300	05	62	400	-170	200	-50	250	-120	-59	400 <
τ	6ps	75	1.5ps	175	4.5ps	2.9 ps	400	2.75ps	200	1.6p s	225	1.15	1.75	400 <

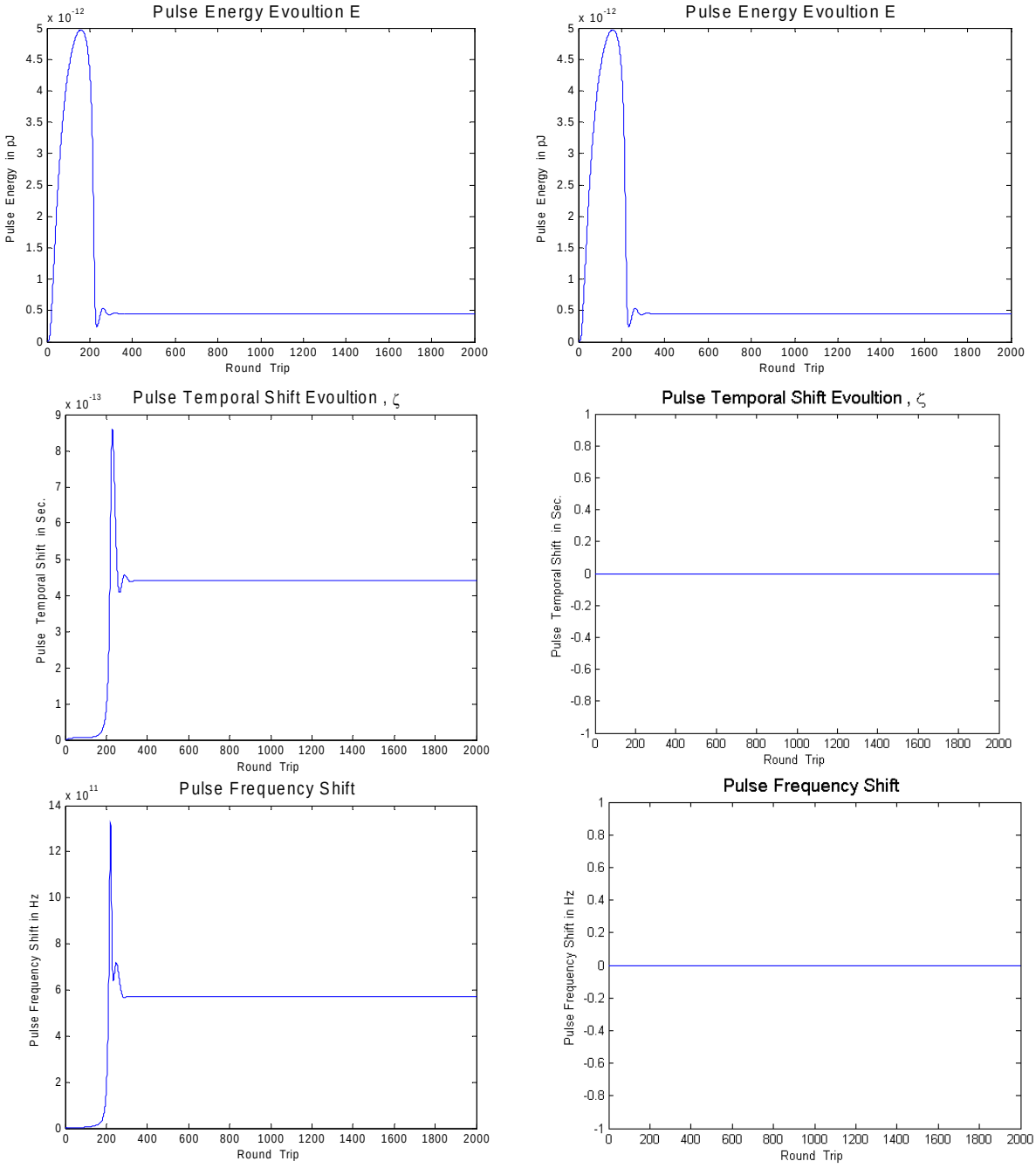

(a) (b)

Fig(4.11) pulse parameters evolution :Energy, Temporal and frequency shift for Anomalous regime (a). with TOD (b) without TOD.

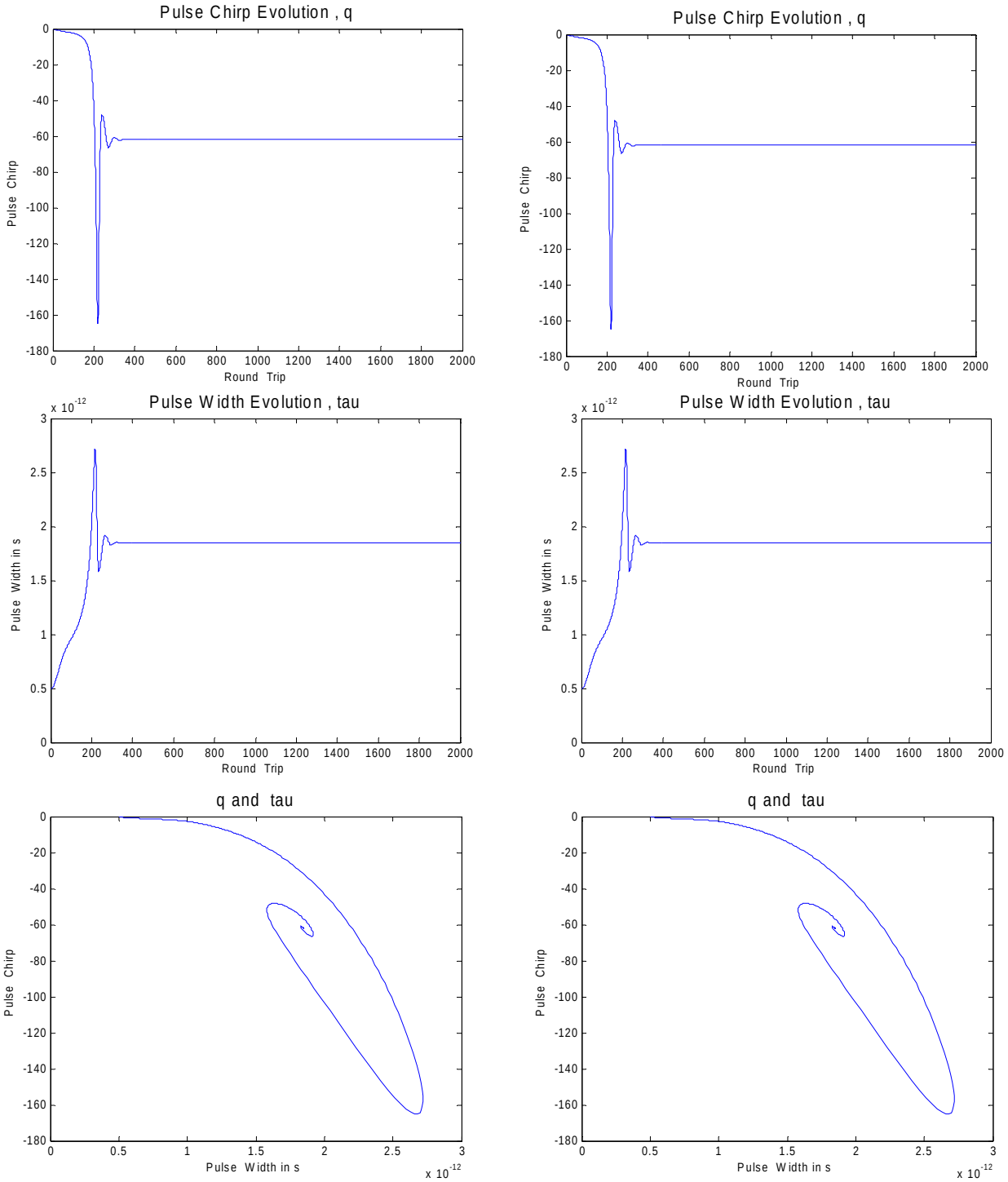

(a) (b)

Fig(4.12) pulse parameters evolution: pulse chirp and width for Anomalous regime (a)without TOD.(b) with TOD.

4.3.3 Pulse Parameters versus Modulation Frequency for both Dispersion Regimes

To demonstrate the effect of changing modulation frequency on pulse parameters and make comparison for both dispersion regime , a plot for each pulse parameter as F_r function is drawn as in Fig.(4.13) for normal and anomalous dispersion regimes .

As shown in Fig.(4.13)(part one) plots have same behavior for pulse energy for variable F_r . Energy decreases exponentially as $F_r$increases which is attributed to the increase in the pulse repetition rate as mentioned earlier , with constant pumping power .Then decreasing the rate after certain value of modulation frequency (F_r=1. 5 GHz in normal regime , F_r=2. 5 GHz in anomalous regime) becomes so small for high values and almost constant straight line .

But the main difference between both regimes is the stability of E fluctuations . In anomalous regimes roundtrips are required for E_{max}which is less than in normal regime.

For temporal shift plots in Fig.(4.13) (part two) for both regimes, almost the same behavior in both regimes is seen .Pulse temporal shift decreases exponentially as $F_r$decreases until is reaches a steady state value(in normal regime ζ =1.8e-13s,in anomalous regime ζ =0.4ps)where very small changes in temporal shift withF_r, almost straight line is shown. The main difference is that : in anomalous regime , converging to steady state value is much faster (less roundtrips are required)

Inspecting plots for pulse frequency shift in Fig.(4.13) (part two) it is clear that the stability of anomalous regime is introduced. For normal regime, the

frequency shift suffers from exponential decrease (negative variations) as $F_r$increases, while in anomalous regime , frequency shift is exponentially increased in positive values to positive steady state value at F_r= 40 GHz with increasing F_r.

For pulse chirp as function of modulation frequency, as shown in Fig. (4.13) (part two), the pulse chirp in normal regime suffers from inversely positive exponential for the variable F_r decreasing with increasing F_r until reaches its q=70 at(Fr=40GHz) steady state value .In anomalous regime , the exponential relation for variable F_r produced negative chirp increases with increasing $F_r$approaching to steady state value at F_r= 40 GHz, much faster than normal regime .

Modulation frequency has great effect on pulse width. As shown in Fig.(4.13) (part two),in normal regime the pulse width decreases exponentially with increases of F_r until it reaches steady state value at Fr=40GHz(τ =4ps). In anomalous regime pulse width increases exponentially with $F_r$increases until it reaches steady state value at Fr=40GHz(τ =2.5ps) which is a shorter pulse than normal. We show when Fr is below 15GHz the pulse width equals negative value that means no laser.

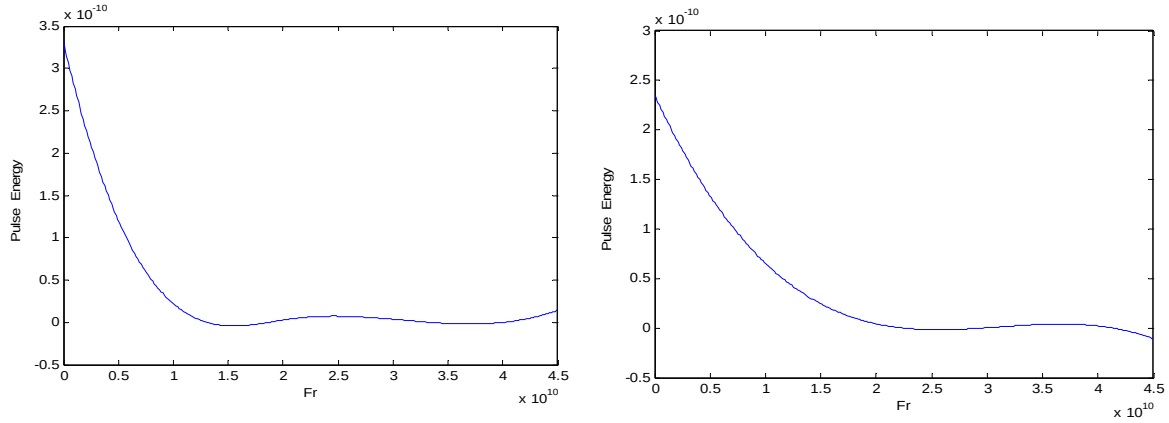

Fig.(4.13)(part one): Pulse energy versus modulation frequency in (a)Normal ,(b) Anomalous dispersion .

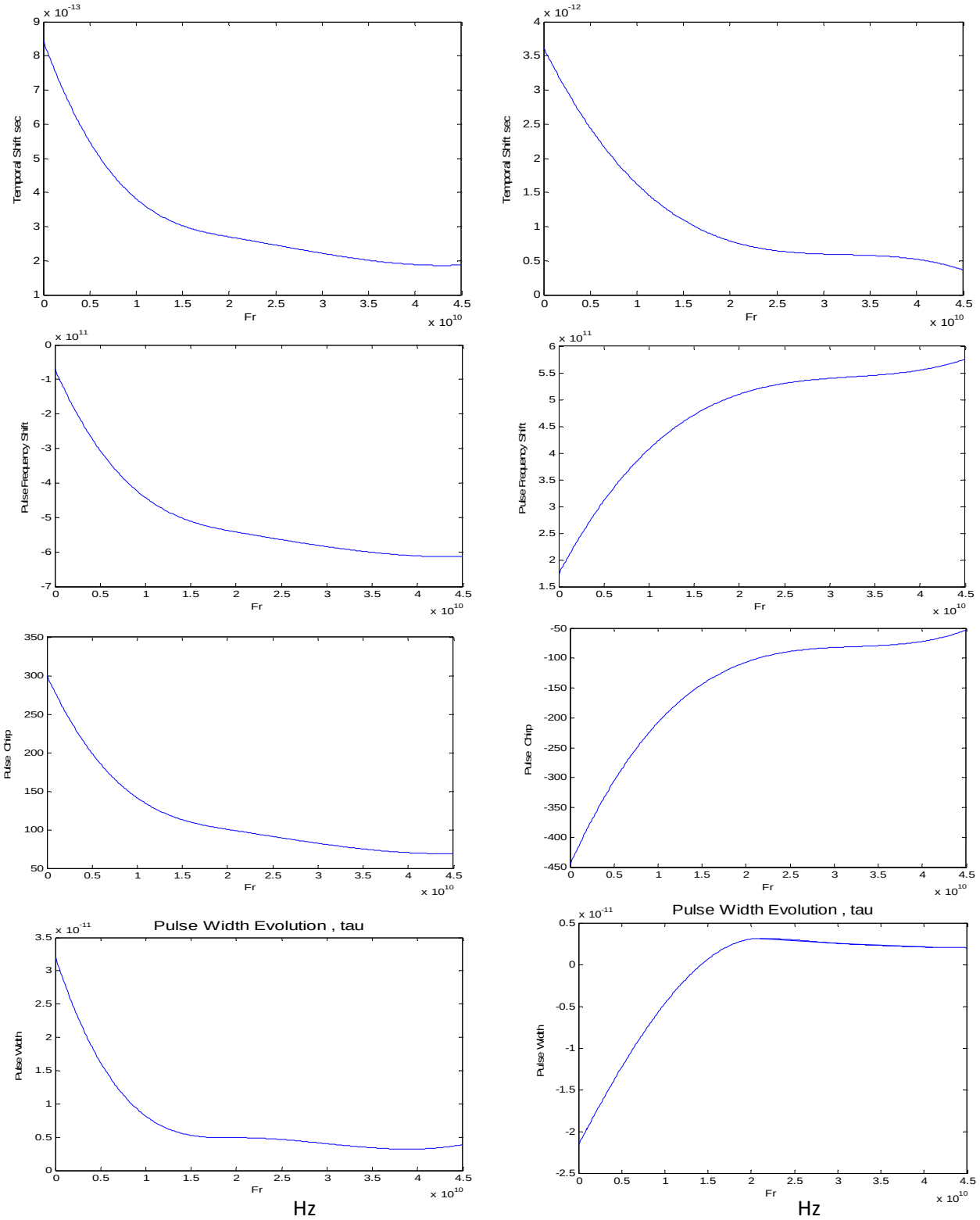

Fig.(4.13)(part two): Frequency shift, chirp and width versus modulation frequency in (a)Normal ,(b) Anomalous dispersion .

4.3.4 Pulse Parameters versus Nonlinearity(γ) for both Dispersion Regimes

To demonstrate the effect of changing nonlinear coefficient (**γ**) on pulse parameters and make comparison for both dispersion regime, a plot for each pulse parameter as(**γ**)function is drawn as in Fig.(4.14) for normal and anomalous dispersion regimes .

In normal regime the behavior of the relation between pulse energy and nonlinearity is decreases linearly with increases **γ** ,as shown in Fig.(4. 14) (part one). In anomalous regime increasing with increase **γ** until reach maximum value(7.376pJ) at **γ** =0.01 than decrease with increase **γ.**

For temporal shift plots in Fig.(4.14) (part two),in normal regime the relation is a linear behavior Pulse temporal shift ζ increases linearly as **γ** increases, but in anomalous regime the temporal shift ζ decreases with the increase **of γ** until it reaches minimum value(ζ=1.49ps)at **γ**=0.01 than the increasing of ζ with increase of γ.

Inspecting plots for pulse frequency shift in Fig.(4.14) (part two) it is clear that the frequency shift suffers from inversely linear relations with the **γ** increases in normal regime. For anomalous regime frequency shift increases with the increase of **γ** until reaches maximum value(Ω=4.5763e-11s)at **γ** =0.01 than it decreases rapidly with the increase of **γ**.

For pulse chirp as function of Nonlinearity, as shown in Fig. (4.14) (part two) , the pulse chirp in normal regime suffers from positive linear relation for variable **γ** that it is increasing with the increasing of **γ .**In anomalous regime , the

negative relation chirp decreases with the increasing of **γ** until(q=-153.545) **γ** =0.01 than the increasing with the increase of **γ** .

Nonlinearity has great effect on pulse width since it is responsible for mode-locking mechanism and producing short pulses. As shown in Fig.(4.14) (part two), pulse width decreases linearly with **γ** increases in normal case , but for anomalous regime the **τ** increases until reaches **γ** =0.009(τ=5ps)they decreases the **τ** with the increase of **γ** .We see important note at **γ** =0.0135 where the pulse width equals minus value that means no laser is produced at this value. Almost , for anomalous regime, the minimum pulse width is obtained .

In the normal dispersion regime the nonlinear effects add to the dispersion and broaden the pulse width (τ)to τ=5ps,they reducing its peak power and the role played by nonlinearity. In the anomalous dispersion regime the interplay between dispersion and nonlinearity prolongs the convergence.

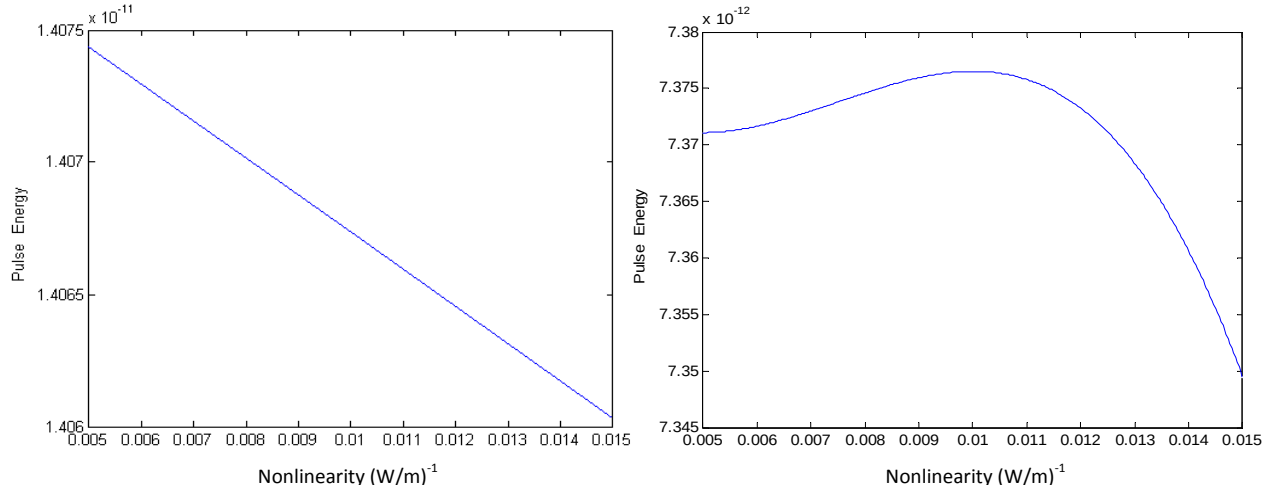

(a) (b)

Fig(4. 14)(part one): Pulse energy versus Nonlinearity in (a)Normal(b)Anomalous dispersion .

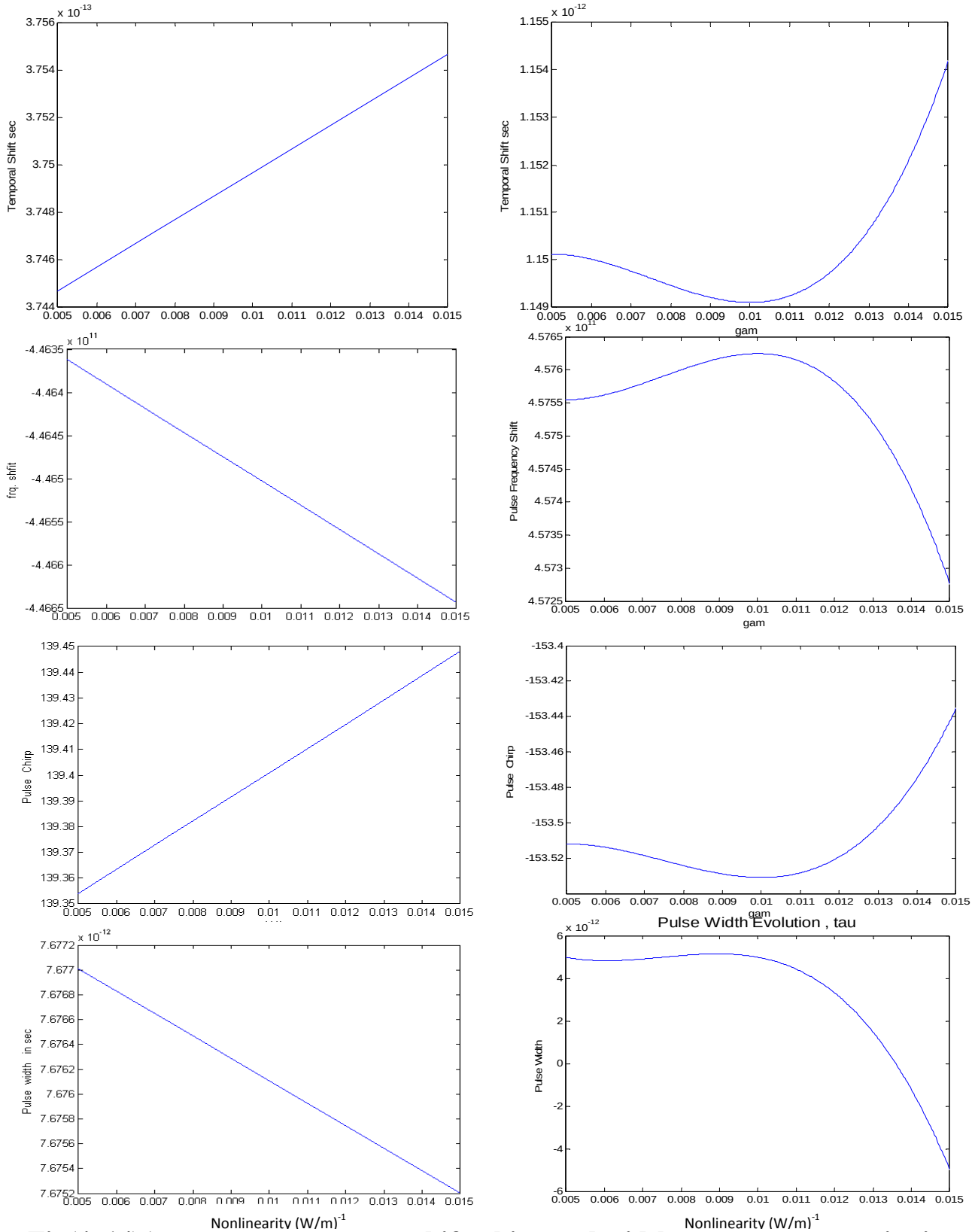

Fig(4. 14)(part two): Frequency shift, chirp and width versus Nonlinearity in (a)Normal(b)Anomalous dispersion .

4.3.5 Pulse Parameters versus second order dispersion(β_2) for both Dispersion Regimes

To demonstrate the effect of changing second order dispersion on pulse parameters and make comparison for both dispersion regime , a plot for each pulse parameter as β_2 function is drawn as in Fig.(4.15) for normal and anomalous dispersion regimes respectively .

The behavior of normal regime for variable β_2 energy is decreasing exponentially until reach the steady state value (1.79pJ) at β_2=3.2fs^2/m is shown in Fig.(4.15) (part one) . In anomalous regime energy increases exponentially as β_2 increases until reach the value(1.05 pJ) at β_2= 0.5e-25s^2/m .

In normal regime temporal shift decreases exponentially with the increase of β_2 until reach the steady state value is shown in Fig.(4.15) (part one). In the anomalous regime the temporally shift is increasing exponentially with increasing β_2 until it reaches $\xi \approx 1.7$ps at (β_2=0.5ps^2/m).

Inspecting plots for pulse frequency shift in Fig.(4.15) (part two) it is clear that in the normal regime the frequency shift Ω suffers from negative exponential increase with the increase of Ω (negative value) as β_2 increases until reached steady state at β_2 =2.5e-26s^2/m (Ω =-0.3e11Hz), while in anomalous regime , frequency shift increase exponentially with the increase of β_2 .

For pulse chirp as function of second order dispersion, as shown in Fig. (4.15) (part two) , the pulse chirp in normal regime suffers from approximate exponential relation that increases **q** with increase of β_2 (positive values)**.**In

anomalous regime , produced chirp increases approximately exponentially with the increasing of β_2(negative value).

Second order dispersion has great effect on pulse width since it is responsible for mode-locking mechanism and producing pulses train . As shown in Fig.(4.15), pulse width increases approximately exponentially with the increases of β_2, but for anomalous regime τ is decrease much faster in magnitude and reaches minimum value τ=0.01ps at β_2=0.5e-26s^2/m.

Almost , for anomalous regime, the minimum pulse width is obtained than normal regime.

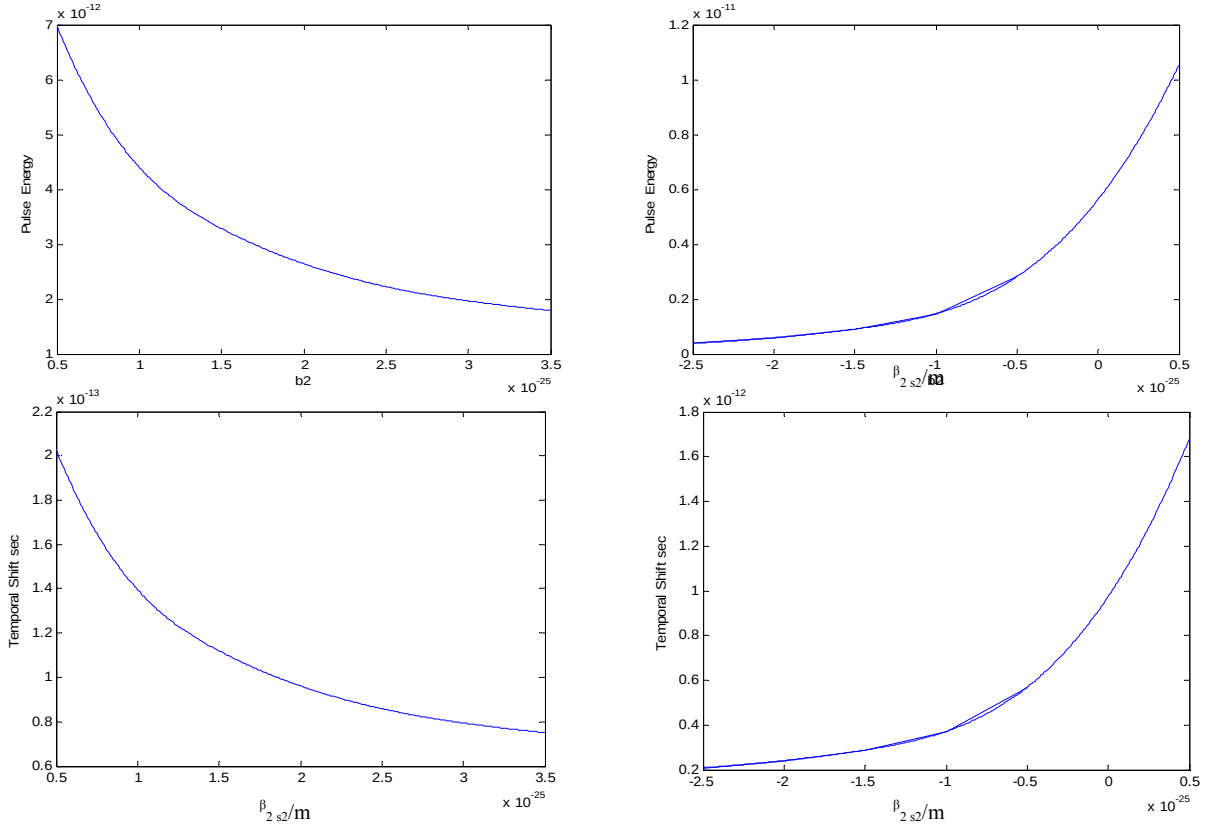

Fig.(4. 15)(part one): Pulse energy, Temporal shift versus second order dispersion in (a)Normal(b) Anomalous dispersion .

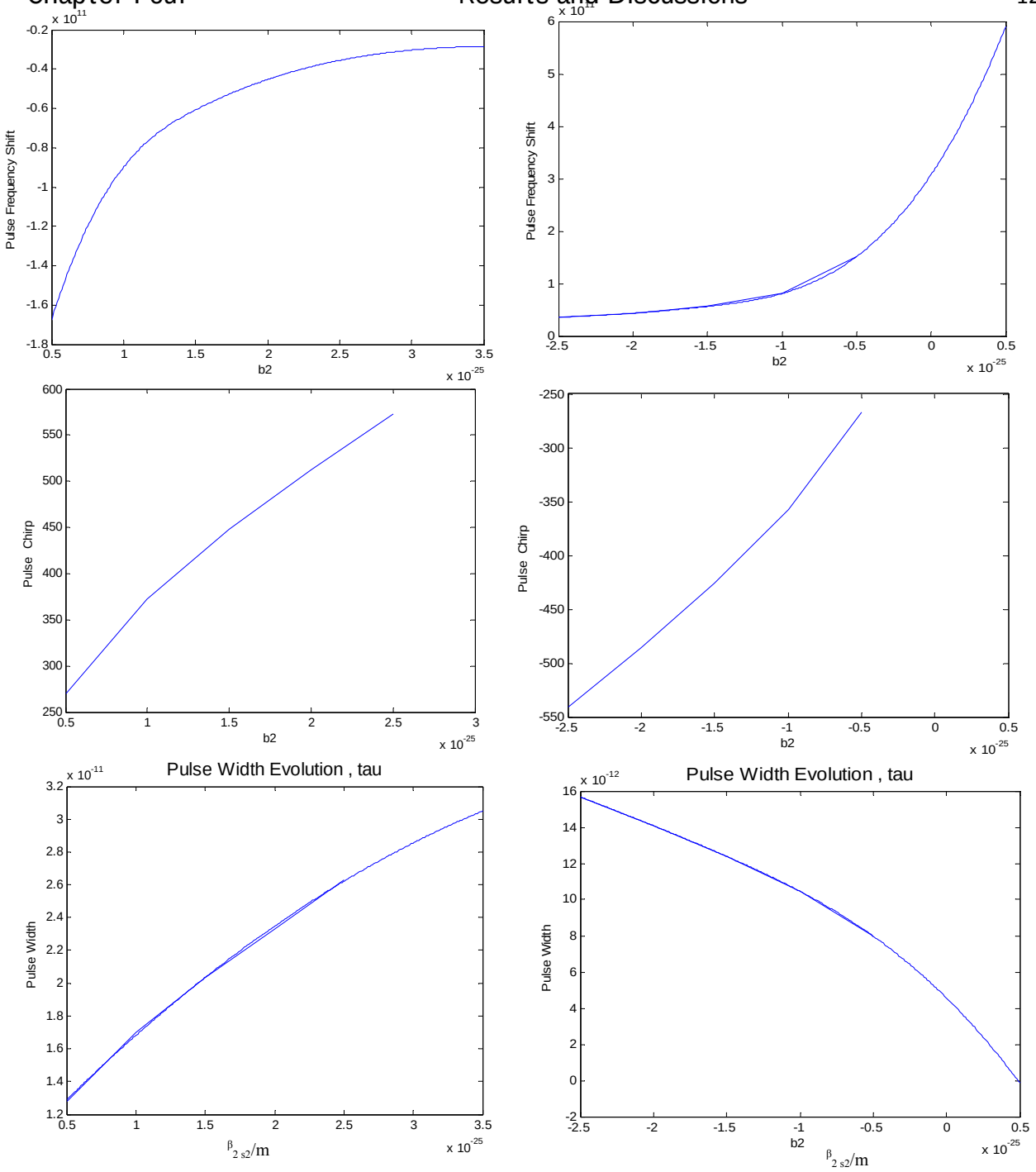

(a) (b)

Fig.(4. 15)(part two) Frequency shift, Chirp and Pulse width versus second order dispersion in (a)Normal(b) Anomalous dispersion .

4.3.6 Pulse Parameters versus Cavity Length for both Dispersion Regimes

Naturally, the length of the Yt-doped fiber makes an important impact not only on pulse characterization but also on output pulse stability as will be explained in the all case.

To demonstrate the effect of changing cavity length on pulse parameters and make comparison for both dispersion regime, a plot for each pulse parameter as L_r function is drawn as in Fig (4.16) for normal and anomalous dispersion regimes.

The behavior of pulse energy for variable Lr is shown in Fig.(4. 16) (part one). Energy decreases exponentially as L_r increases .Then is reaching to the steady state value at the cavity length L_r = 5 m in anomalous regimes and Lr=6m in normal regimes.But the main difference between both regimes is the stability of E fluctuations . In anomalous regimes Lr required to reaches steady state is less than in normal regime .

For temporal shift plots in Fig.(4.16) (part two) for both regimes, almost the same behavior in both regimes is obtained. Pulse temporal shift decreases exponentially as L_r increases. The main difference is that : in anomalous regime , the temporal shift is greater than normal regime and reaches to the steady state value by shorter length.

Inspecting plots for pulse frequency shift in Fig.(4.16) (part two), for normal regime , the frequency shift decreases exponentially as L_r increases(positive value)until reaches steady state value. While in anomalous regime, frequency shift is exponentially increased (negative value) until reaches zero steady state value with the increase of L_r .

The function of Chanchiang cavity length for pulse chirp is shown in Fig. (4. 16).The pulse chirp in normal regime suffers from exponentially increased (negative value) with increasing L_r**.** The anomalous regime exponentially decreases(positive value) with increasing of L_r.

Laser cavity has great effect on pulse width since it is responsible for mode-locking mechanism and producing pulses train . As shown in Fig.(4. 16) (part onetwo), for normal regime pulse width increases exponentially with the increases L_r until reaches steady state value($\tau \approx 10$ps) at $L_r \approx 4$ m below that τ is a negative value , but for anomalous regime pulse width decreases exponentially with increased L_r until reaches pulse width minima value($\tau \approx 1.9$ps) at $L_r = 4$m ,then τ increasing with the increase of Lr. Almost , for anomalous regime, the minimum pulse width is obtained .

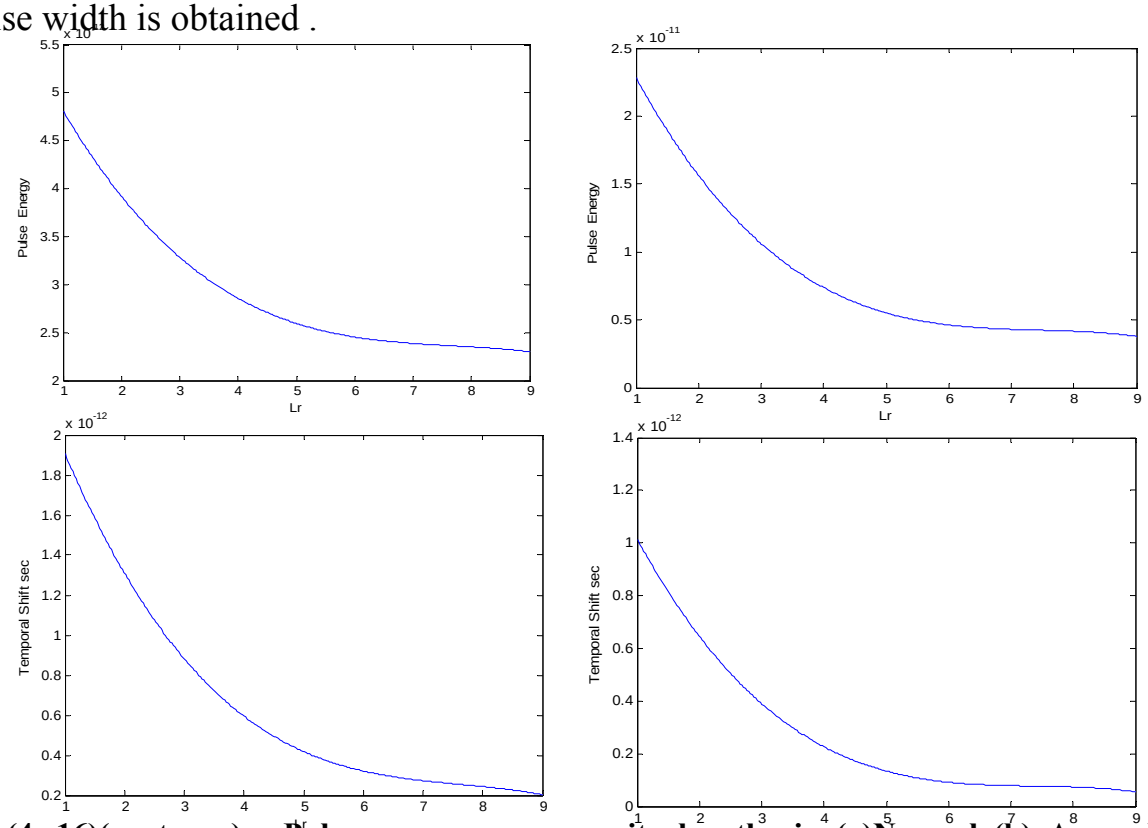

Fig.(4. 16)(part one) : Pulse energy versus cavity length in (a)Normal (b) Anomalous dispersion .

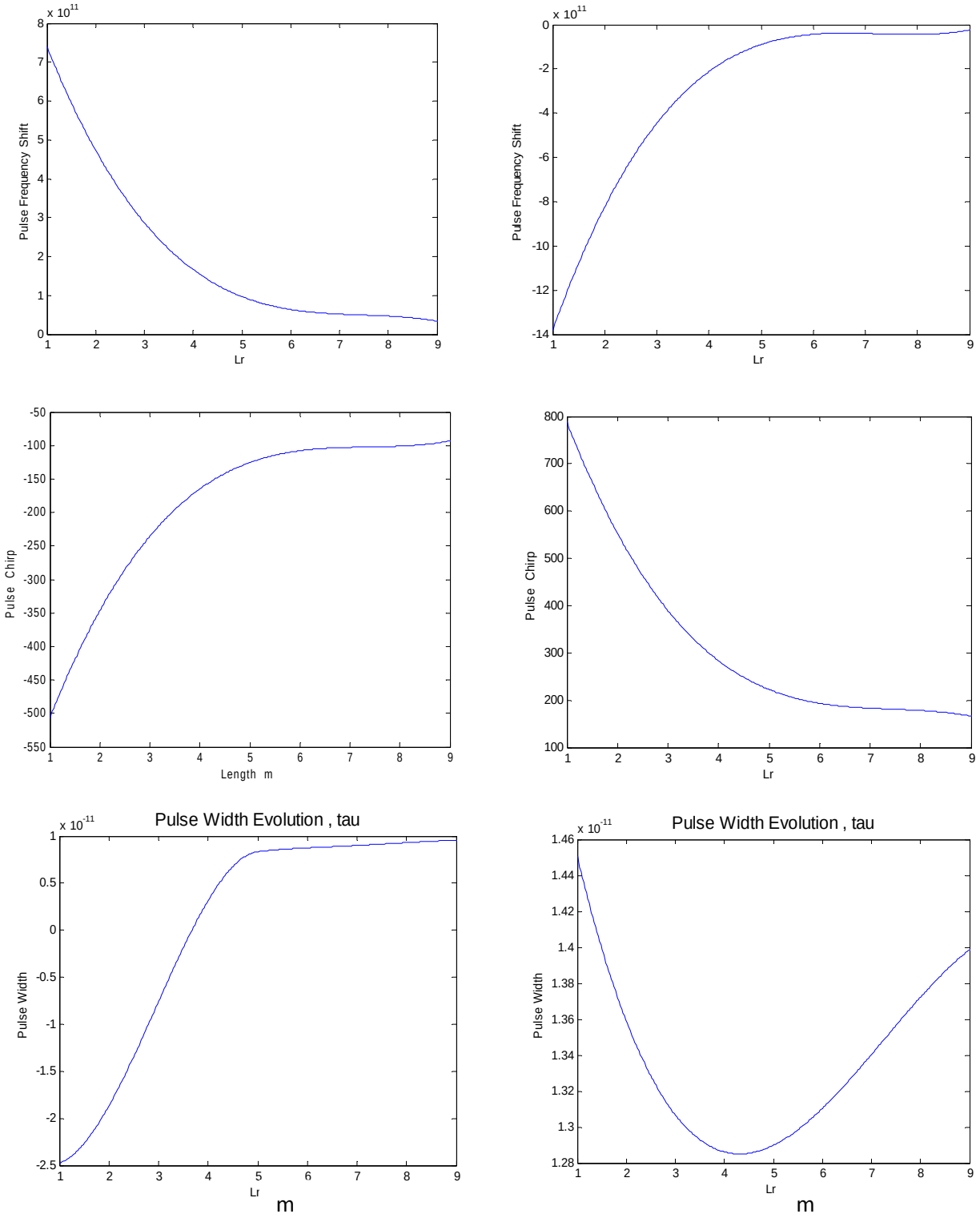

Fig.(4. 16)(part two) : Temporally shift, frequency shift, Chirp and pulse width versus cavity length in (a)Normal (b) Anomalous dispersion .

4.4 Passive mode locking (SBR)

4.4.1 Normal Dispersion Regime

In normal dispersion regime , $\beta_2 > 0$ and solution will be done for both cases of TOD : $\bar{\beta}_3 = 0$ and $\bar{\beta}_3 = 30 \times 10^4\ fs^3/m$,for studying TOD effect on pulse parameters .Executing the computer program , results for the pulse parameters evolution are obtained are obtained as in Fig.(4.17) and Fig.(4.18).

As shown in Fig.(4.17) (a and b) , for pulse energy evolution plots , there is no difference in behavior for both cases of TOD ($\bar{\beta}_3 = 0$, $\bar{\beta}_3 \neq 0$).In both cases , E reaches its maximum value $E_{max} \approx 0.12$ p J in about fifteen roundtrips as shown in Fig (4.17)(a). Then small damping oscillation is going over tenth of roundtrips where $\Delta E = 0.15$ p J In fact it is obvious that about one hundred roundtrips are needed to achieve steady-state.

The presence of third order dispersion (TOD) has big effect on pulse shape, so it is necessary to include the β_3 parameter , since it is distorts the pulse by broadening it , thus producing a temporal shift .

As shown in Fig.(4.17) (a and b) , in the absence of TOD , no temporal shift ($\zeta = 0$), while in the presence of TOD , a temporal shift is introduced with positive oscillation , a symmetrical around temporal axis ,$\Delta\ \zeta \approx 2$ms (variation between maximum and minimum) converges to steady state .

Pulse frequency shift is equals zero when $\beta_3 = 0$ or $\beta_3 \neq 0$. It is seen that for frequency shift in fig (3-17).

As shown in Fig.(4.18)(a and b), no effect for TOD on pulse chirp . Normal dispersion produces positive pulse chirp, small oscillating around chirp

axis until reaches steady-state value, with Δq=0.6e4, decreases as roundtrips increase, RTss>100 .

From plots of pulse width evolution as in Fig.(4.18) (a and b) , for pulse width plots ,a broadening in pulse width is introduced with maximum width (τ_{max} =0.502fs) in first 45 roundtrips, then exhibits small damped oscillation (Δτ≈0.03fs) over tenth of roundtrips decreasing to steady-state value (τ_{ss}≈0.50 fs),where the number of roundtrips is needed RTss>70 .From the plots of pulse chirp versus pulse width as in Fig.(4.18), the steady state is achieved unless by tenth number of roundtrips.

4.4.2 Anomalous Dispersion Regime

In anomalous dispersion regime, TOD has negative values, $\beta_2 < 0$ and solution will be done for both cases of β_2= 0 and β_2= 30 x 10^4 fs^3/m Again, using Table-3.2, the pulse parameters evolution is as in Fig. (4.19) and Fig. (4.20).

As shown in Fig.(4.19) (a) and (b) for pulse energy plots , as in normal regime , there is no difference for pulse energy evolution for both cases of TOD , stating no effect for it on pulse energy evolution . In both cases, E reaches its maximum value $E_{max} \approx$ 0.01 p J in about (35) roundtrips as shown in Fig (4. 19)(a) (while in normal regime in about 50 roundtrips).Then small damping oscillation is going over tenth of roundtrips, where (Δ E= 0.01pJ) but much faster than in normal regime until steady state is achieved .In fact it is obvious that number of roundtrip are needed to achieve steady-state is RTss=40, while for normal regime RTss=50 .

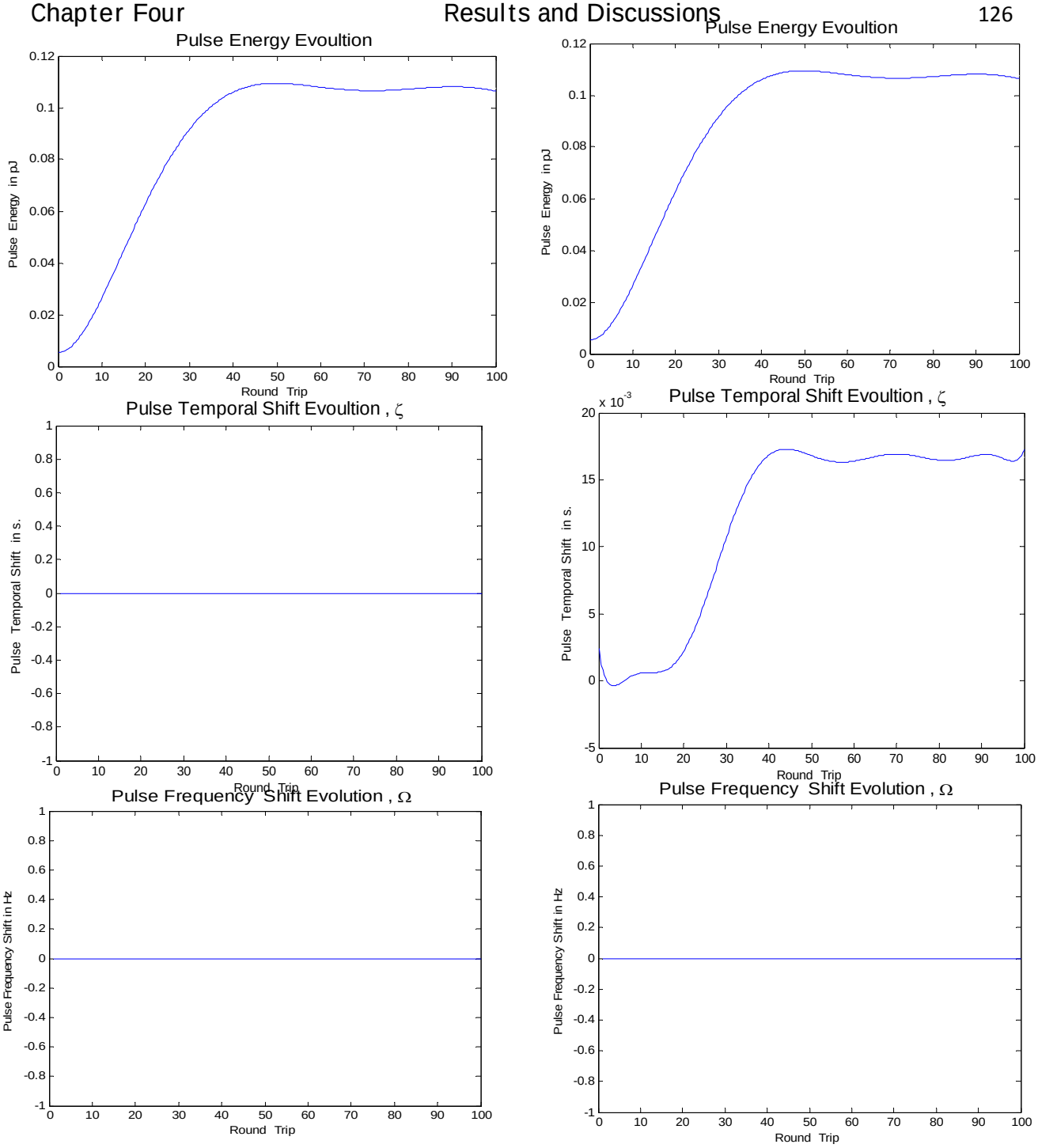

Fig(4.17) pulse parameters evolution: Energy, Temporal and frequency shift for Normal regime (a)without TOD.(b) with TOD.

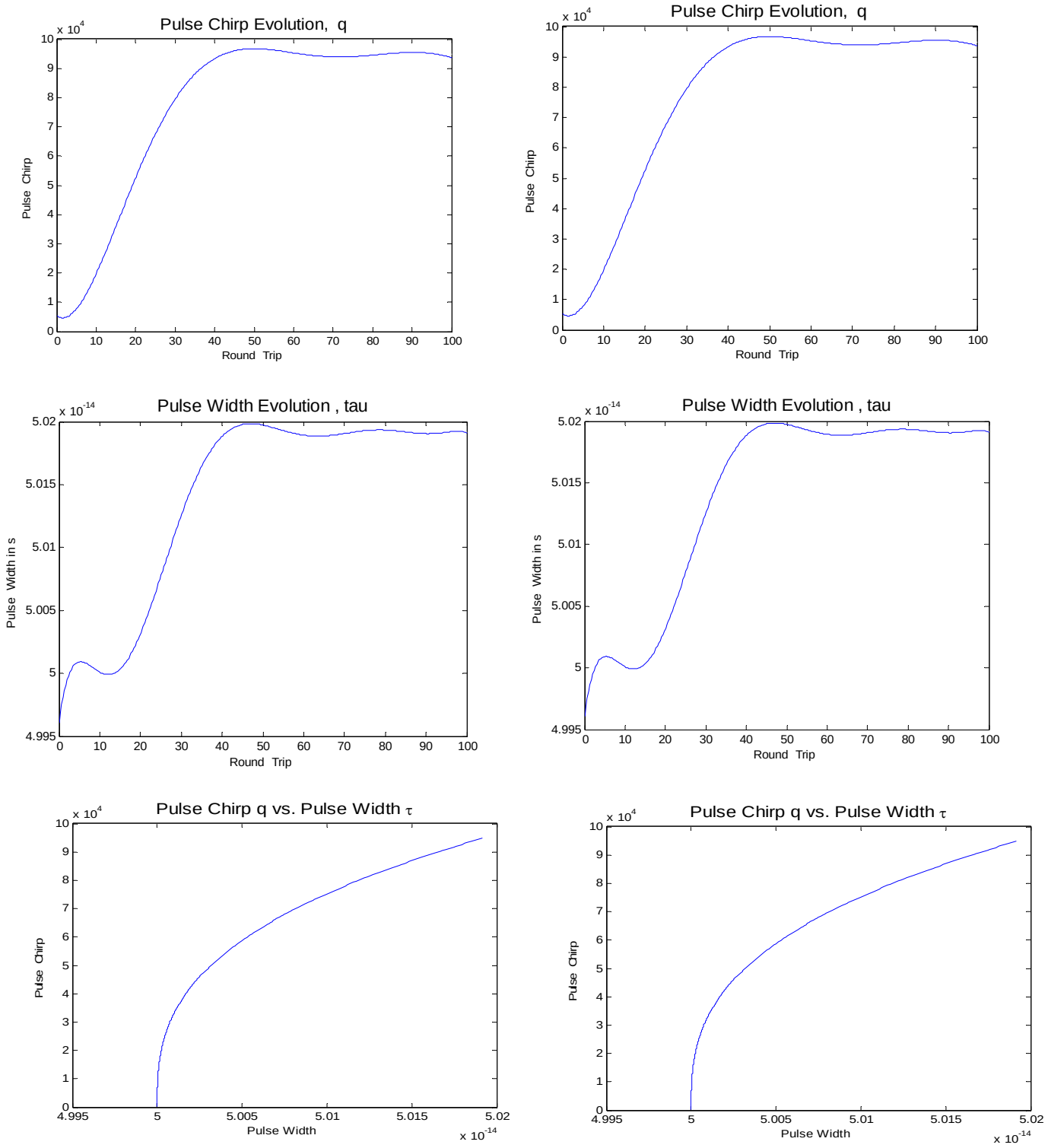

Fig(4-18) pulse parameters evolution: chirp and pulse width, for Normal regime (a)without TOD.(b) with TOD.

The presence of (TOD) has great effect on pulse temporal and frequency shift. As shown in Fig.(4.19) , in the absence of TOD, there is no temporal shift (ζ =0), while in the presence of TOD a temporal shift is introduced with positive oscillation ($\Delta\zeta$ =1m s) .The introduced temporal shift is symmetrical around a temporal axis, converges to steady state value.

There is no effects with or without β_3= 0, no frequency shift .

In anomalous regime produces positive pulse chirp , while in normal , a positive chirp as shown in Fig.(4.20), is introduced as shown earlier . Damped oscillation is shown around chirp axis until reaches qss=9, its steady-state value, but faster than in normal regime. Oscillation is symmetrical around chirp axis with $\Delta q \approx 0.5e4$ (less than in normal where$\Delta q \approx 0.7e4$) decreases rapidly as roundtrips increase,$RT_{ss} \approx 50$.

From plots of pulse width evolution as in Fig.(4.20) , a broadening in pulse width is introduced with maximum width τmax=048.8fs(where in normal τmax=50fs) in first (15) roundtrips, then exhibits damped oscillation ($\Delta\tau \approx 0.498$fs) over tenth of roundtrips decreasing to steady-state value $\tau_{ss} \approx 48.8$fs, (in normal regime $\tau_{ss} \approx 50.1$fs) where less number of roundtrips than in normal regime is needed RTss=100 . Table 4.3 summarizes parameters values for both regimes.

Table 4-3. Pulse Parameters Database for both Dispersion Regimes (Fr=10GHz)SBR mode locked														
	Normal Regime							Anomalous Regime						
PRAMETER	Max	RT max	Min	RT min	Δ	SS	RT SS	Max	RT max	Min	RT min	Δ	SS	RT_{ss}
E	0.12pJ	50	0.01 p J	5	0.11 p J	0.105 p J	>100	0.11	35	0.10	750	0.01 P J	0.105 p J	70
ζ	17ms	40	-0.5ms	5	16.5 ms	16ms	>100	13 ms	40	11.8m s	50	1.2ms	12.5ms	70
Ω	0	_	0	_	0	0	_	0	_	0	_	0	0	_
q	9.5e4	45	0.5e4	5	9e4	9.25e4	>100	10e4	35	9e4	60	1e4	9.1e4	70
τ	50.2fs	45	25fs	3	0.25	50.1	>100	50fs	15	48.8f	45	0.003fs	48.88fs	70

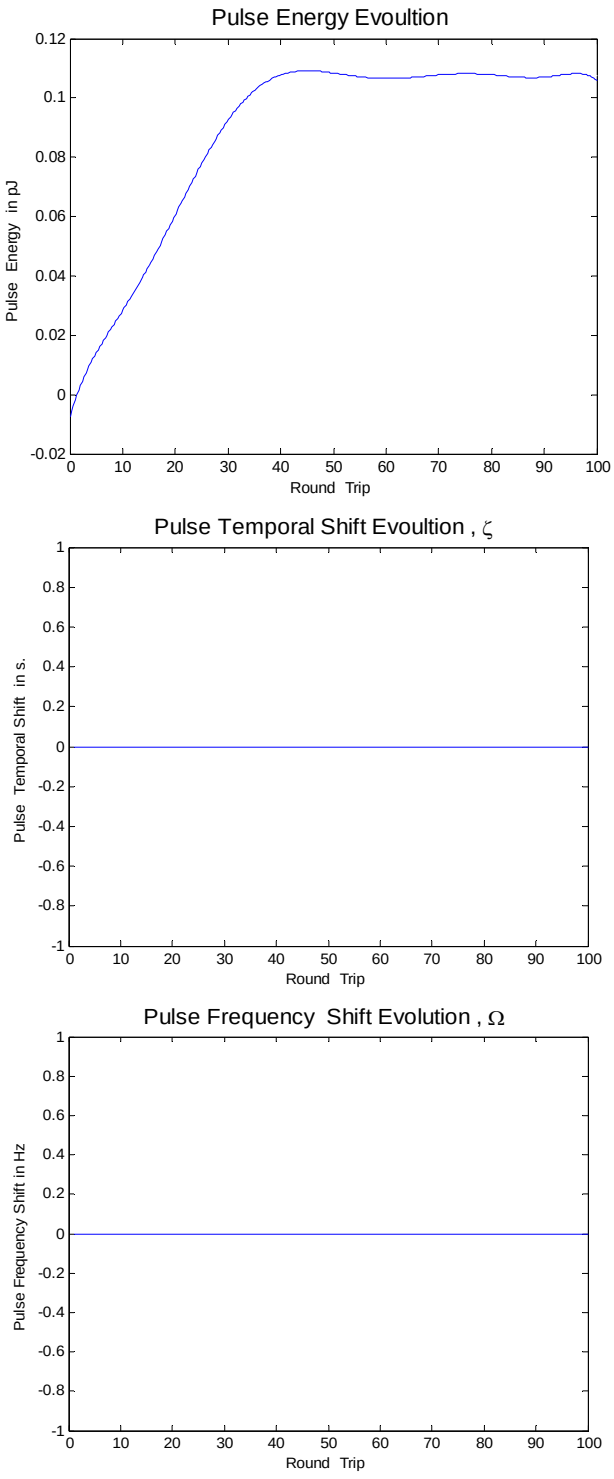

(a)

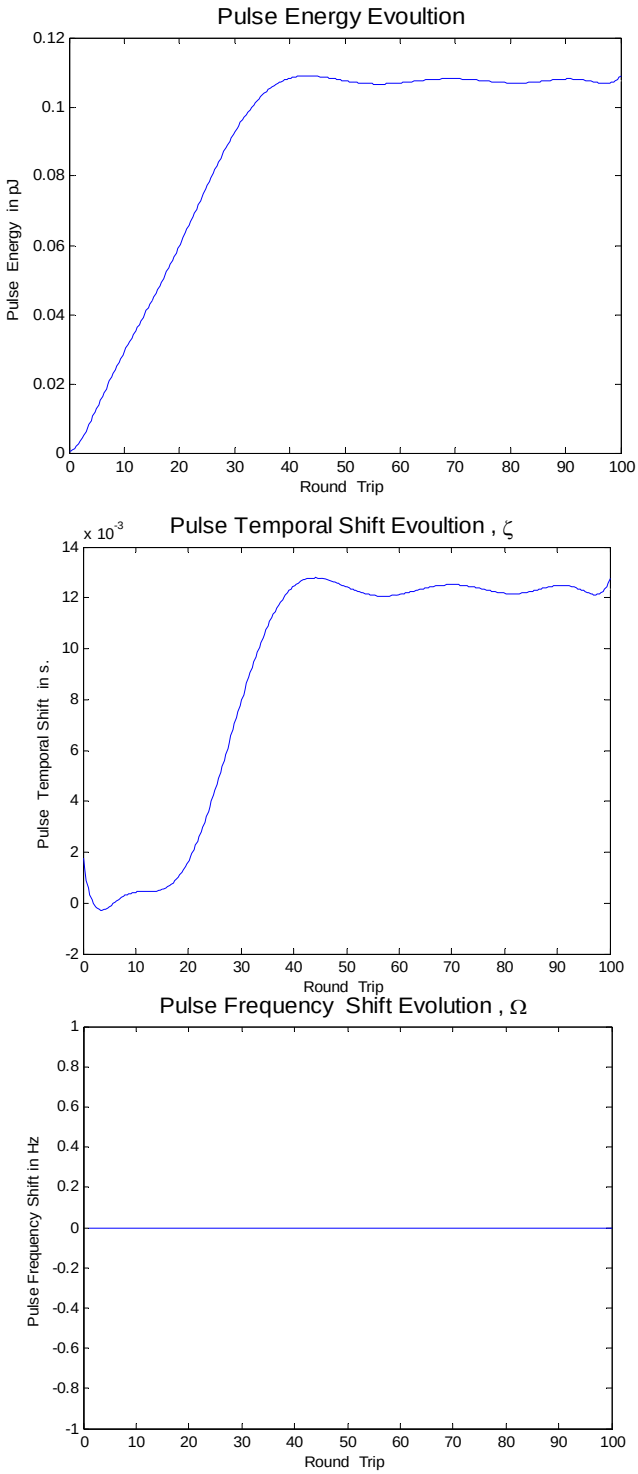

(b)

Fig(4.19) pulse parameters evolution: Energy, Temporal and frequency shift for Anomalous regime (a)without TOD.(b) with TOD.

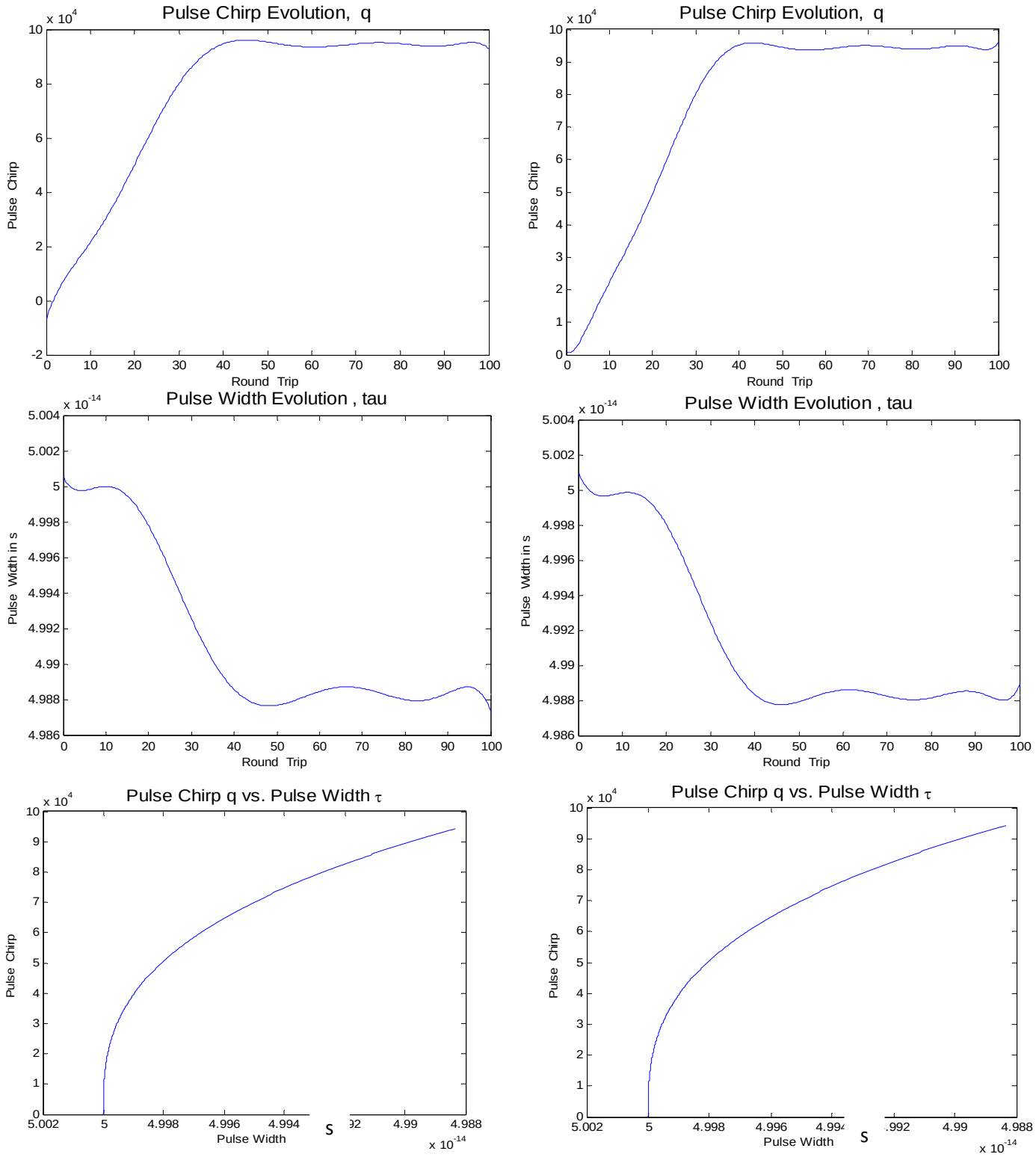

Fig(4.20) Pulse parameters evolution: Chirp and Pulse width, for Anomalous regime (a)without TOD.(b) with TOD.

4.4.3 Pulse Parameters versus Cavity Length for both Dispersion Regimes

To demonstrate the effect of changing cavity length on pulse parameters and make comparison for both dispersion regime , a plot for each pulse parameter as Lr. function is drawn in Fig.(4.21) for normal and anomalous dispersion regimes .

As shown in Fig.(4. 21) (part one) is almost same behavior for pulse energy for variable Lr in both normal and anomalous regimes. Energy is consistent value(E=0.3pJ) without any change with variable Lr(in anomalous regimes and normal regimes).

Temporal shift plots as in Fig.(4.21) (part one), almost the same behavior in both regimes. Pulse temporal shift increases exponentially as Lr increases. The main difference is that : in anomalous regime , the temporal shift(ζ =7.5ms) less than normal regime(ζ=6.5ms).

The plots for pulse frequency shift in Fig.(4.21) (part two). For normal regime and anomalous regime the frequency shift equal zero with variable Lr.

For pulse chirp as function and of cavity length, as shown in Fig. (4.21) (part two) , the pulse chirp in normal regime and anomalous regime suffers from linear increases with increasing of Lr .

Laser cavity length has great effect on pulse width since it is responsible for mode-locking mechanism and producing pulses train . In normal regime pulse width decreases exponentially with increases of Lr until reach steady state value($\tau\approx$500.42fs) at Lr=8 m , the same behavior for anomalous regime pulse width decreases exponentially with increases of Lr until reach pulse width minim

value. In anomalous regime, the minimum pulse width is obtainable as a function of total cavity length. The length of the residual fiber into cavity(i.e Yt doped fiber amplifier was ≈500 fs with 5m fiber section) . Fig (4-21) (part two) summarizes the pulse width depended on total cavity lengths for the two regimes

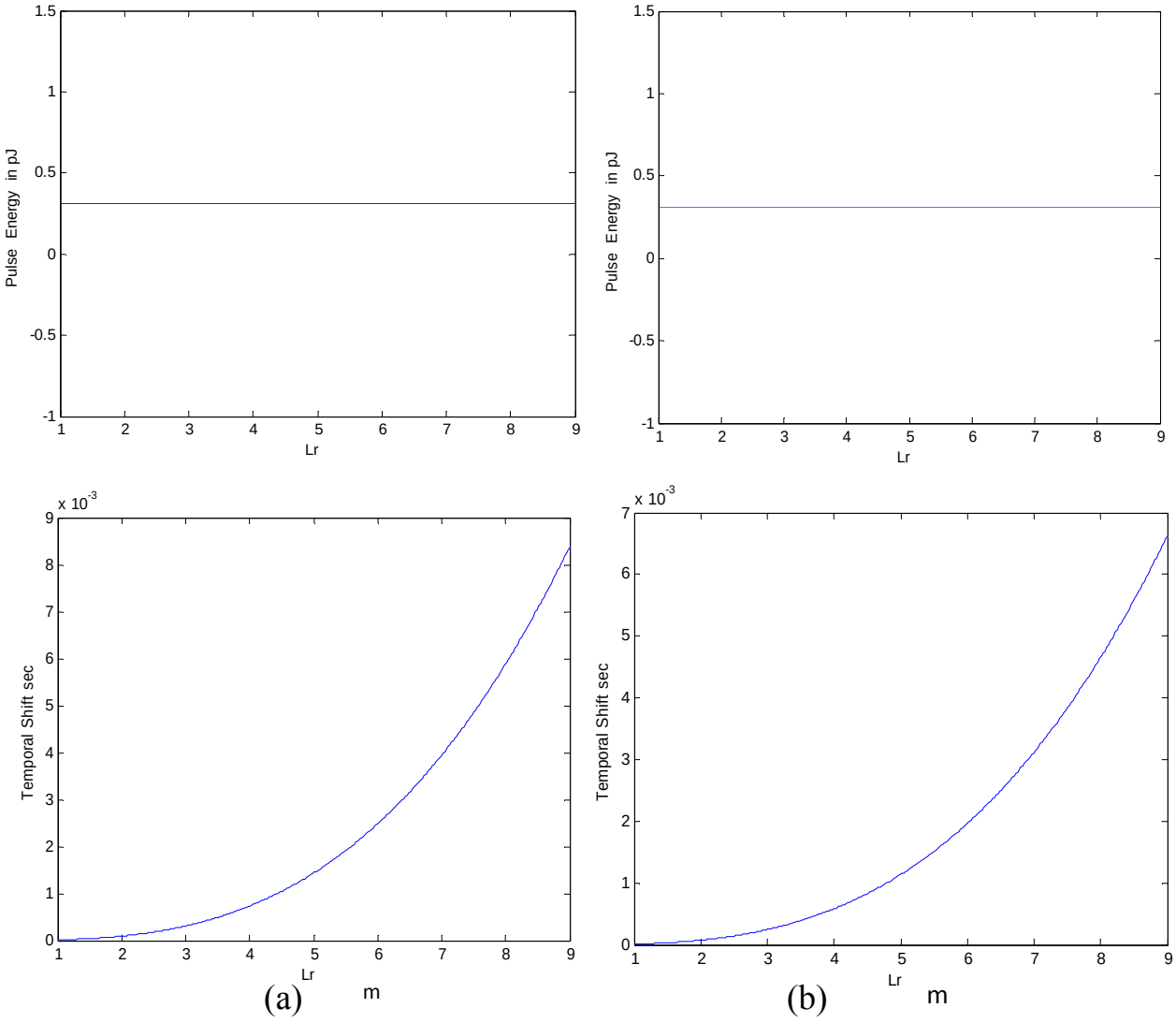

Fig.(4.21)(part one) : Pulse energy, temporal shift versus Lr fiber length in(a) Normal (b) Anomalous dispersion .

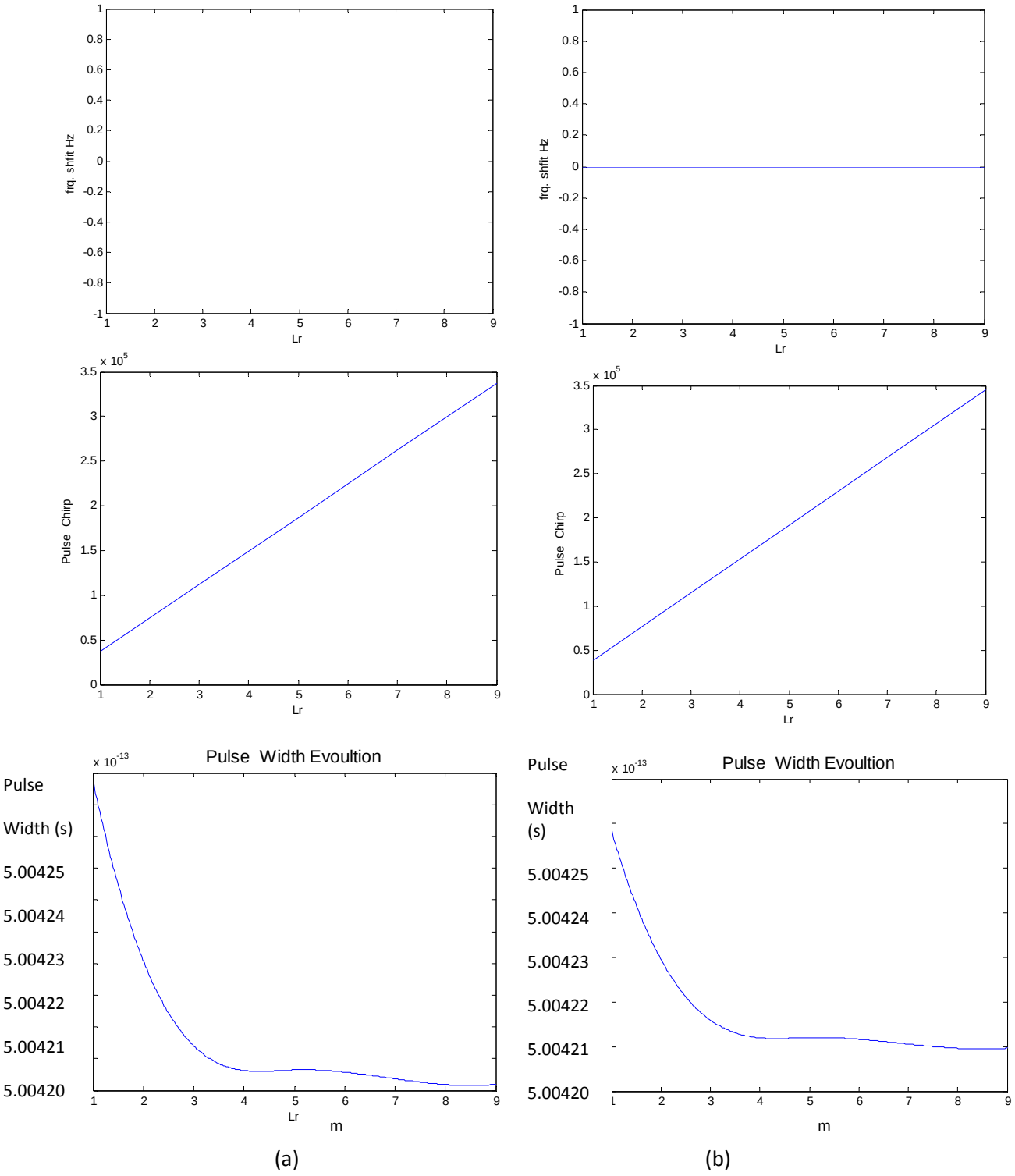

Fig.(4.21) (part two) : Frequency shift, chirp and width versus Lr Cavity length in(a) Normal (b) Anomalous dispersion .

4.4.4 Pulse Parameters versus Modulation Frequency for both Dispersion Regimes

To demonstrate the effect of changing modulation frequency on pulse parameters and make comparison for both dispersion regime , a plot for each pulse parameter as function of F_r as drawn in Fig.(4.22) for normal and anomalous dispersion regimes .

As shown in Fig.(4.22) (part one) is almost same behavior for pulse energy with variable F_r . Energy don't change with increases of F_r which is constant straight line (E=0.3pJ) for both regimes.

Pulse temporal shift increases exponentially as increases of F_r until reach a steady state value (in normal regime ζ =3.159e-3s, in anomalous regime ζ =2.498e-3s). The main difference is that: in anomalous regime, converging to steady state value is much faster than normal regime (less roundtrip are required) as shown in fig (4-22) (part one).

There is no frequency shift in both regimes with variable Fr as shown in fig (4-22) (part two).

For pulse chirp as function of modulation frequency, as shown in Fig. (4.22) (part two) , the pulse chirp in normal regime suffers from positive exponential for variable increasing of F_r until reaches its q=2.4336e5 at(Fr=15MHz) steady state value .In anomalous regime , the exponentially relation for variable F_r produced positive chirp increases with increasing $F_r$approaching to steady state value(q=2.498e5) at F_r= 15MHz greater than normal regime .

Modulation frequency has great effect on pulse width. As shown in Fig.(4.22) (part two),in normal regime pulse width increases exponentially with

increases of F_r until reach steady state value at Fr=12MHz(τ =5.004e-13s).In anomalous regime pulse width increases exponentially with increases of F_r until reach steady state value at Fr=10MHz(τ =4.997e-13s) is shorter pulse than normal.

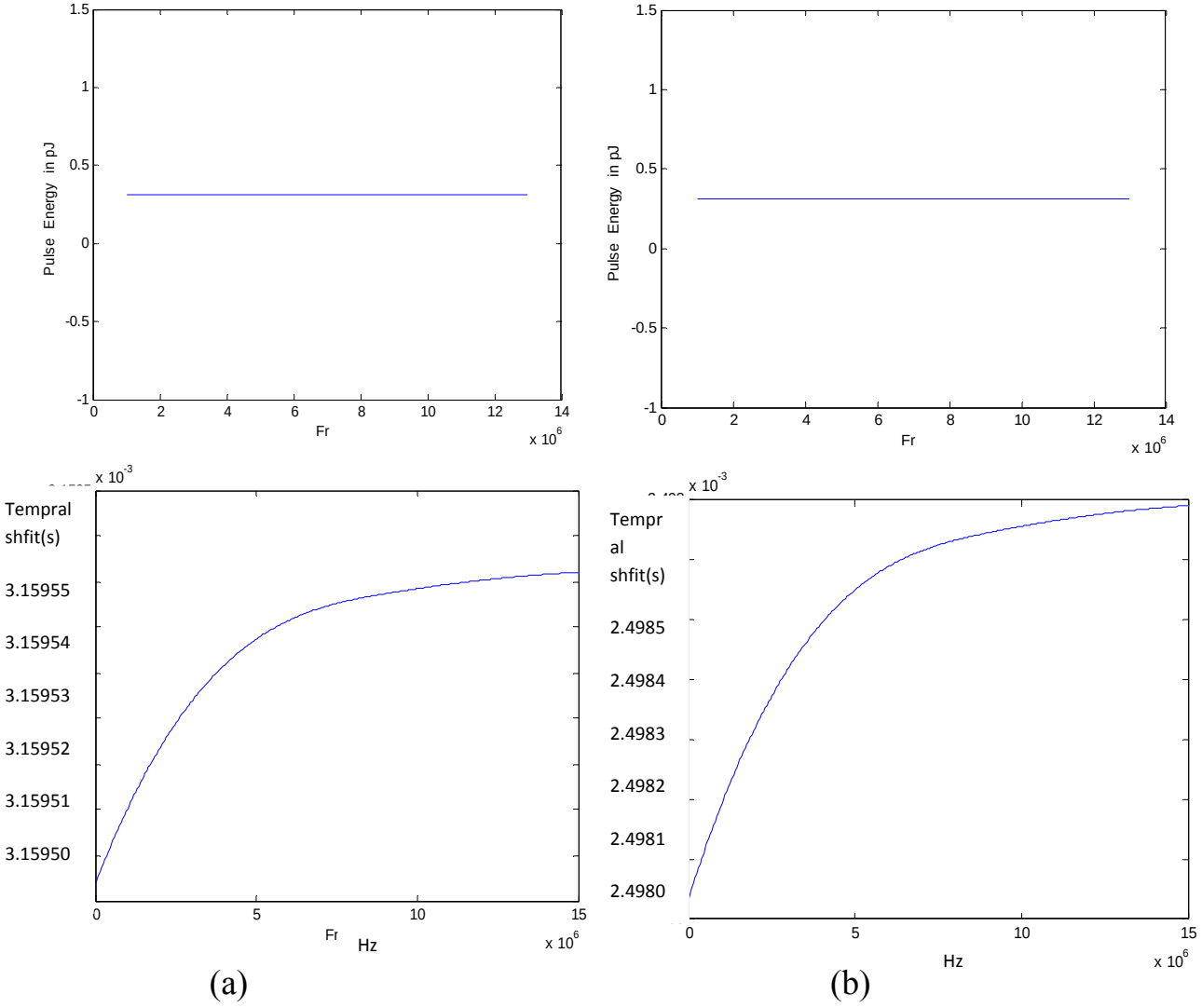

Fig.(4. 22) (part one) :Pulse energy, temporal shift versus Fr Frequency modulation in (a)Normal (b) Anomalous regimes.

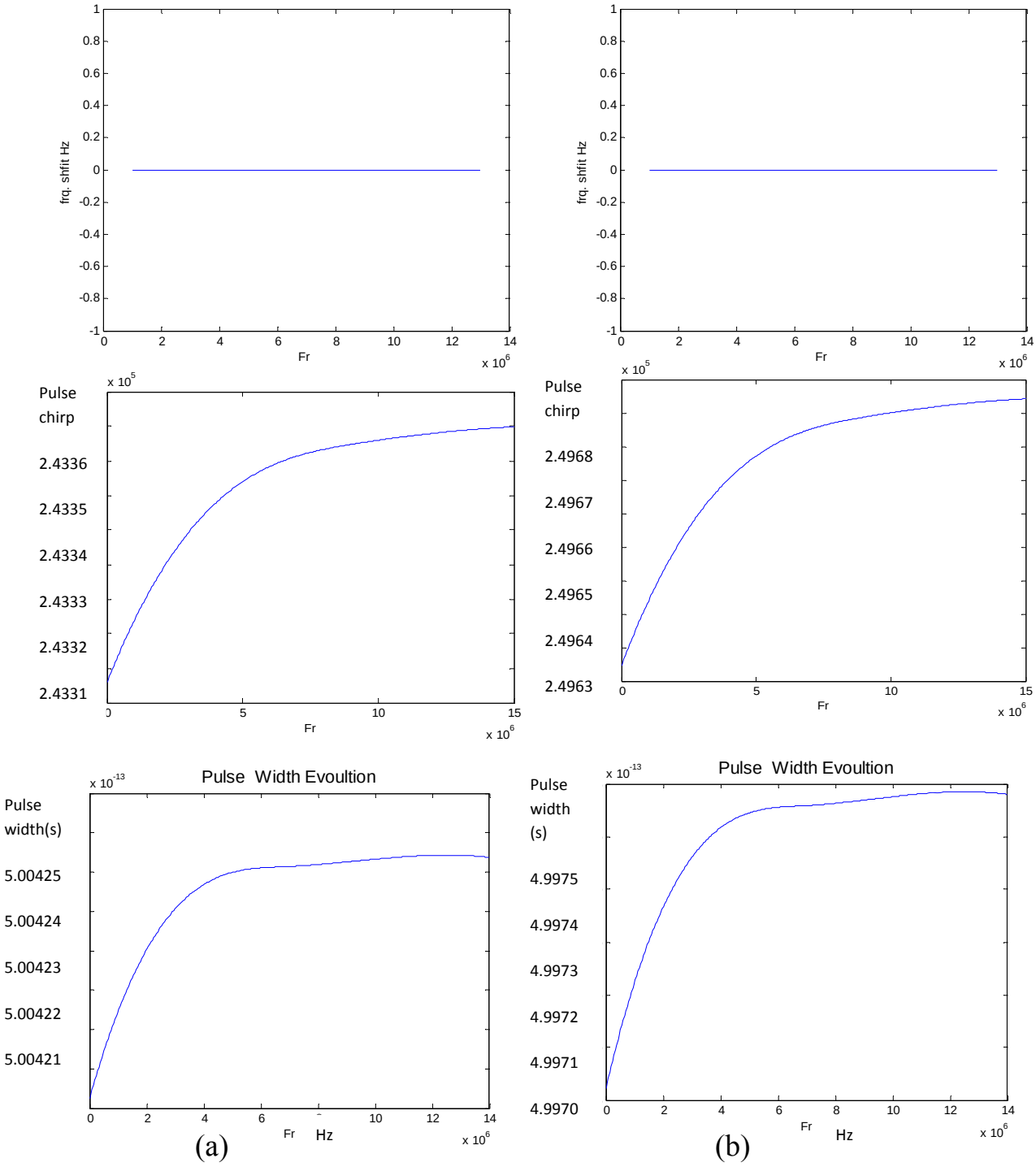

Fig.(4. 22) (part two) Frequency shift, chirp and width versus Fr Frequency modulation in (a)Normal (b) Anomalous regimes.

4.4.5 Pulse Parameters versus Nonlinearity for both Dispersion Regimes

To demonstrate the effect of changing nonlinear coefficient on pulse parameters and make comparison for both dispersion regime , a plot for each pulse parameter as γ function is drawn as in Fig.(4.23) for normal and anomalous dispersion regimes .

As shown in Fig.(4. 23) is almost the behavior of pulse energy for variable γ in normal regime and anomalous dispersion are constant value(E=0.3pJ) as increases γ.

For temporal shift plots in Fig.(4.23),in normal regime and anomalous regime the relation are a linear behavior Pulse temporal shift ζ increases linearly as increases γ.

Inspecting plots for pulse frequency shift in Fig.(4.23) it is clear the frequency shift(Ω=0) don't effect with increase the γ.

For pulse chirp as function of Nonlinearity, as shown in Fig. (4.23), the pulse chirp in normal regime and anomalous regime suffer from positive linear relation for increasing of chirp with the increasing of γ .

Nonlinearity has great effect on pulse width since it is responsible for mode-locking mechanism and producing short pulses. As shown in Fig.(4.23), pulse width increases linearly with increases of γ in normal case and for anomalous regime. Almost, for anomalous regime, the minimum pulse width is obtained(in normal τ=50.42e-13s,in anomalous τ=50.06e-13s).

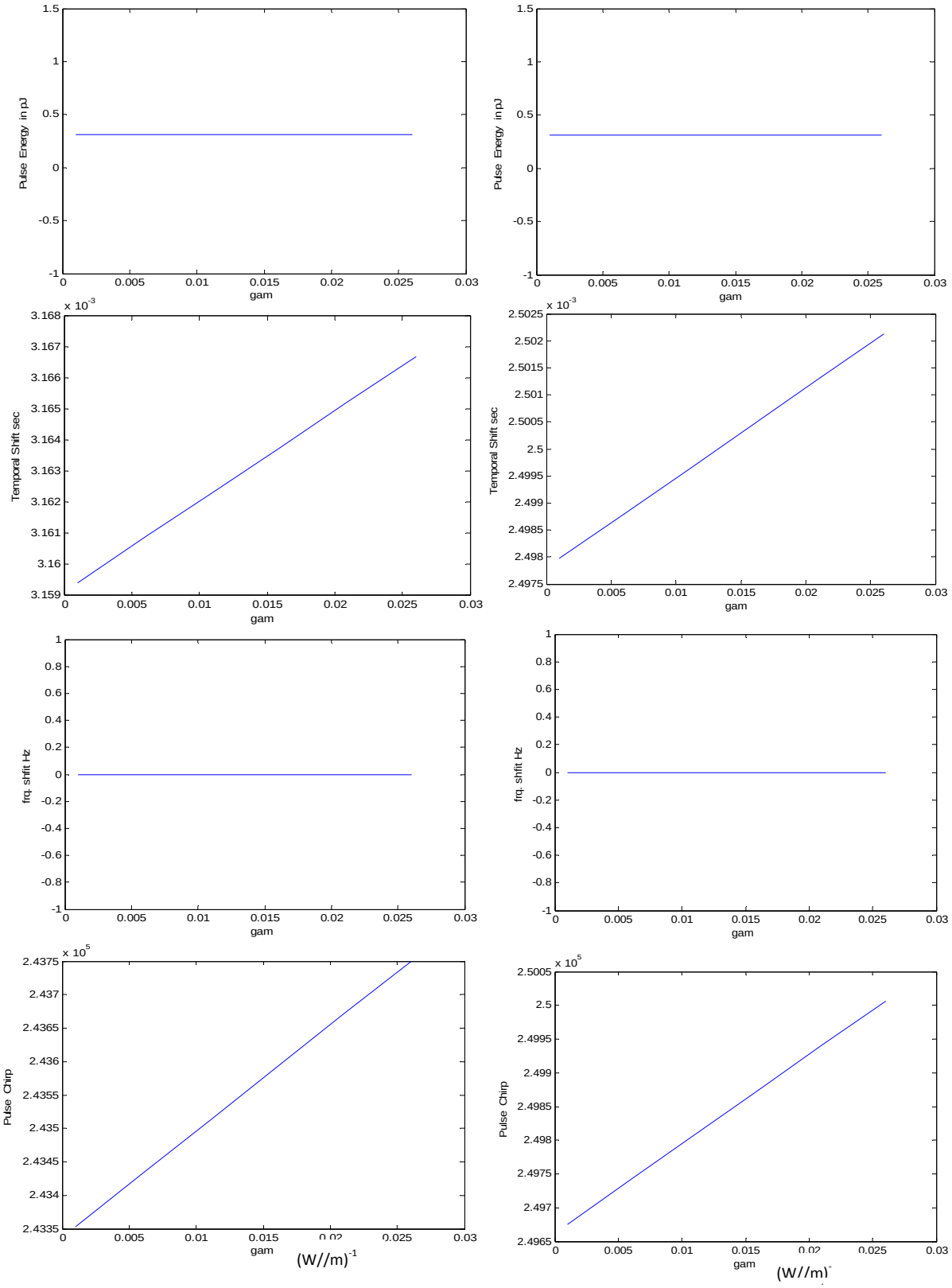

Fig.(4. 23 (part one) : Pulse energy, temporal shift, frequency shift and chirp versus nonlinearity in(a) Normal(b)Anomalous dispersion .

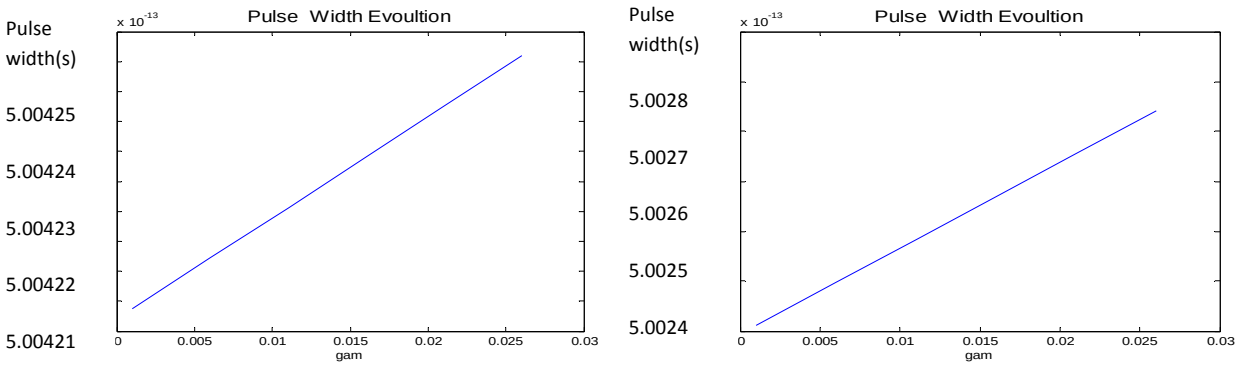

Fig.(4. 23)(part two) : Pulse width versus nonlinearity in(a) Normal(b)Anomalous dispersion .

4.4.6 Pulse Parameters versus second order dispersion for both Dispersion Regimes

To demonstrate the effect of changing second order dispersion on pulse parameters and make comparison for both dispersion regime , a plot for each pulse parameter as function of β_2 is drawn as in Fig.(4.24) for normal and anomalous dispersion regimes .

The behavior of normal regime and anomalous regime for variable β_2 as shown in Fig.(4.24) (part one).The energy doesn't effect .It is consist value (E=0.03pJ).

For temporal shift plots in Fig.(4.24) (part one), the behavior of temporal shift in normal regime decrease rapidly with increase β_2 until certain value(β_2=0.5e-25s2/m) ,than reach the steady state value (ξ=3.15e-3s). In anomalous regime temporally shift increasing linearly with increasing β_2 until reach $\xi\approx$1.7ps at (β_2=0.5ps/m).

Inspecting plots for pulse frequency shift in Fig.(4. 24) (part two) it is clear that in the normal regime and anomalous regime the frequency shift Ω not effect with increase $\beta_2(\Omega=0)$.

For pulse chirp as function of second order dispersion, as shown in Fig. (4.24) (part two) , the pulse chirp in normal regime suffers from linear relation increase **q** with increase β_2 (positive values).In anomalous regime The chirp decreases linearly with increasing β_2.

Second order dispersion has great effect on pulse width. As shown in Fig.(4.24) (part two) , pulse width increases linearly with increases β_2 , but for anomalous regime decrease τ linearly with increases β_2 .

Almost , for anomalous regime, the minimum pulse width is obtained than normal regime.

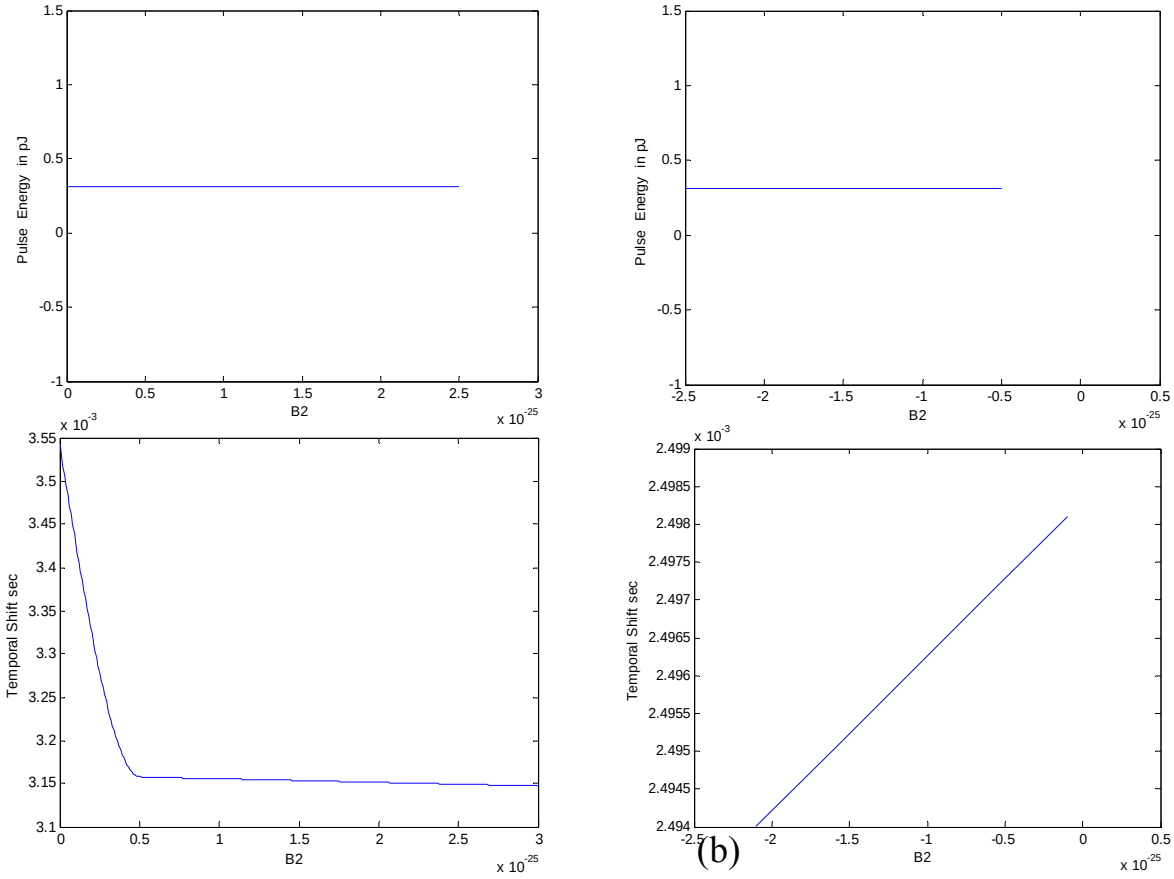

Fig.(4. 24)(part one) : Pulse energy, temporal shift versus second order dispersion in (a)Normal (b)Anomalous dispersion.

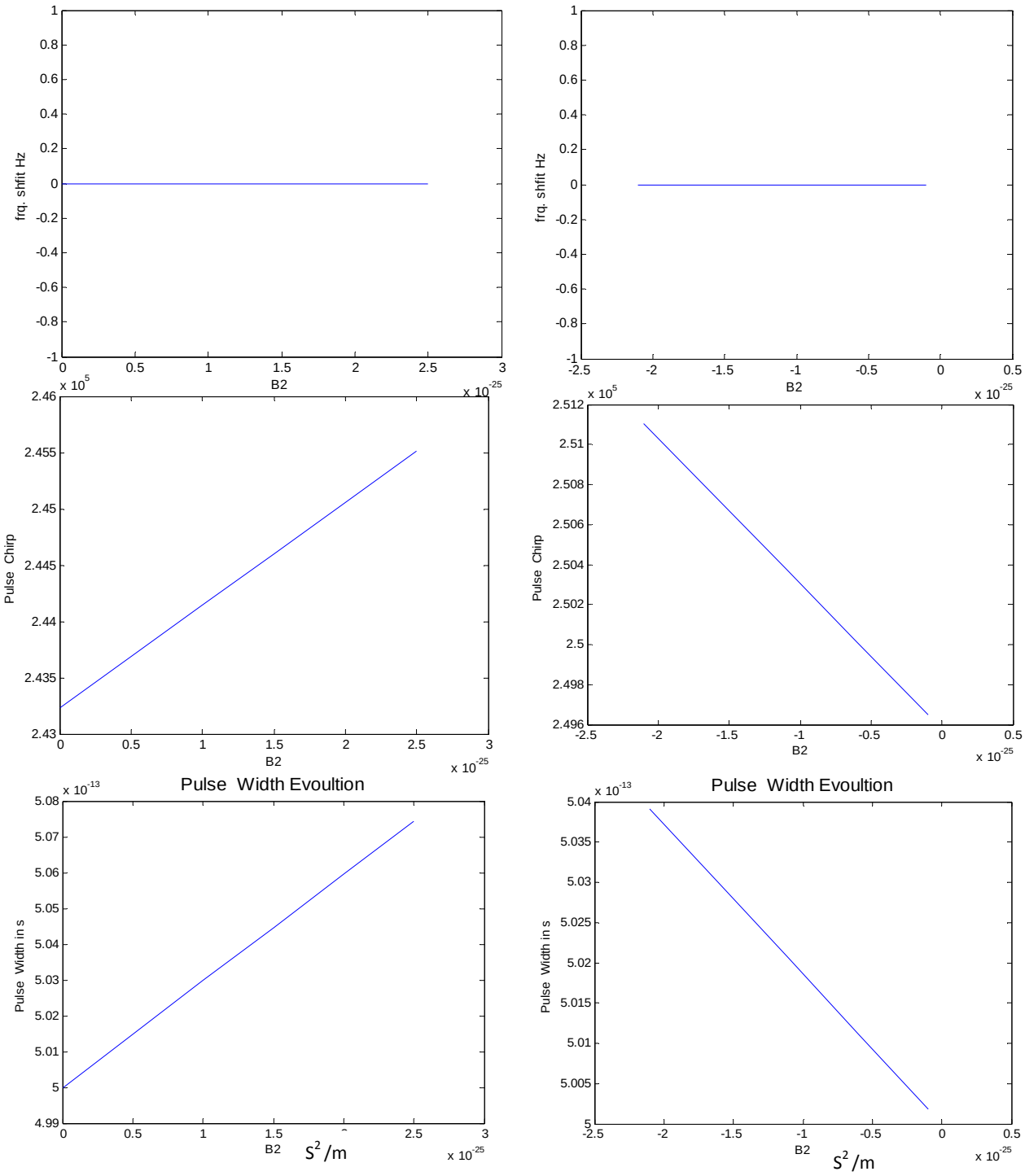

(a) (b)

Fig.(4. 24) (part two): Frequency shift, chirp and width versus second order dispersion in (a)Normal (b)Anomalous dispersion.

4.4.7 Pulse Parameters versus Modulation depth for both Dispersion Regimes

To demonstrate the effect of changing second order dispersion on pulse parameters and make comparison for both dispersion regime , a plot for each pulse parameter as Δ_{SA} function is drawn as in Fig.(4.25) for normal and anomalous dispersion regimes .

As shown in Fig.(4.25) (part one) is almost the behavior of normal regime and anomalous regime for variable Δ_{SA} are linear relation. Energy is decrease with increase modulation depth in normal regime. In anomalous regimes energy is increase with increase modulation depth.

For temporal shift plots in Fig.(4.25) (part one), almost the behavior of normal regime temporal shift decreases approximately exponential with the increase of Δ_{SA}. In anomalous regime temporally shift is increasing exponentially with the increasing of Δ_{SA}.

Inspecting plots for pulse frequency shift in Fig.(4.25) (part two) it is clear in the normal regime and anomalous regime the frequency shift Ω doesn't affect with the increase of Δ_{SA} (Ω=0) .

Modulation depth has great effect on pulse width. As shown in Fig.(4.25), pulse width decreases linearly with the increases of Δ_{SA} , but for anomalous regime τ increases linearly with the increases of Δ_{SA} .

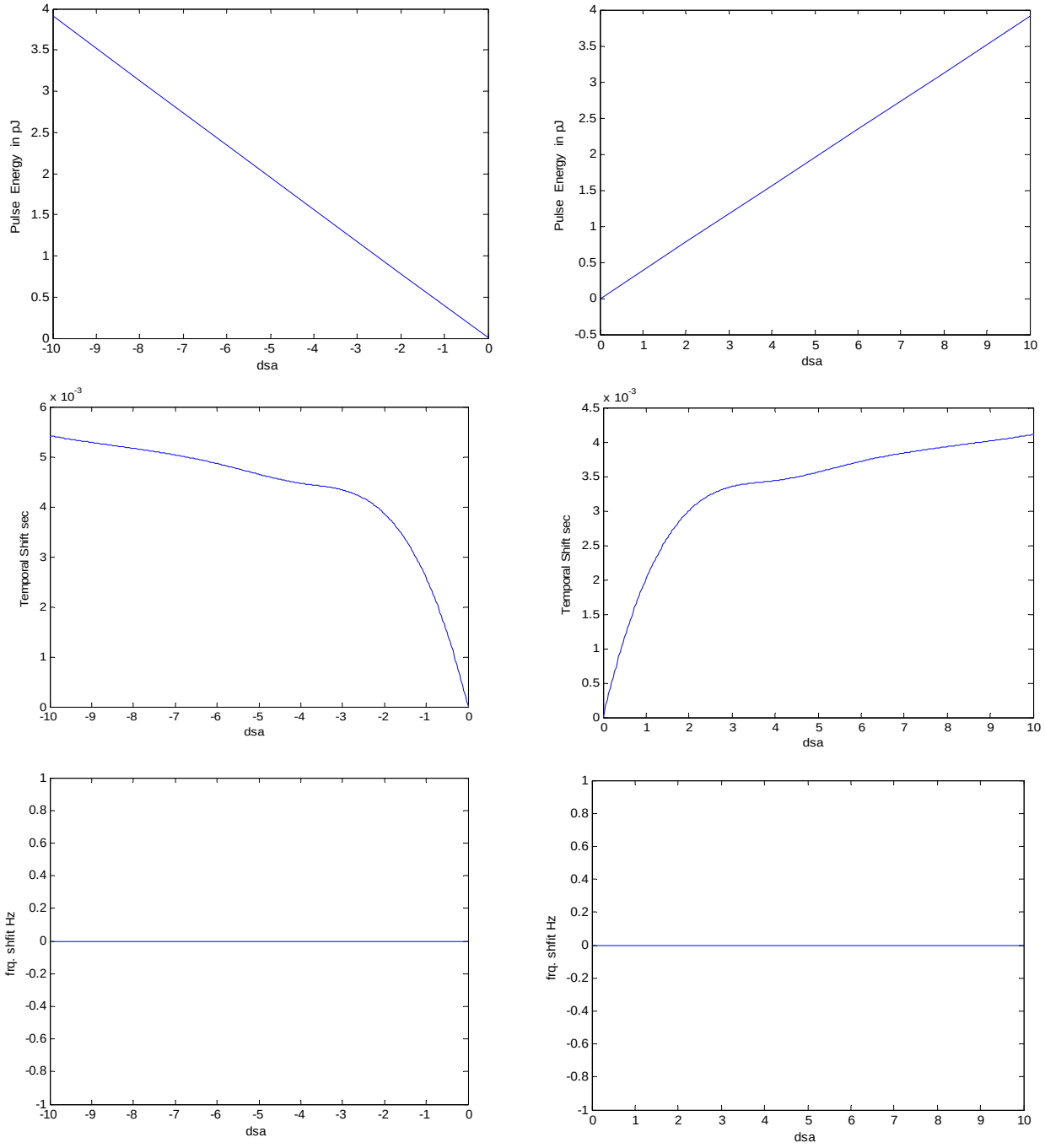

(a) (b)

Fig.(4.25)(part one) : Pulse energy, temporal shift, frequency shift versus Modulation depth in(a) Normal (b)Anomalous dispersion .

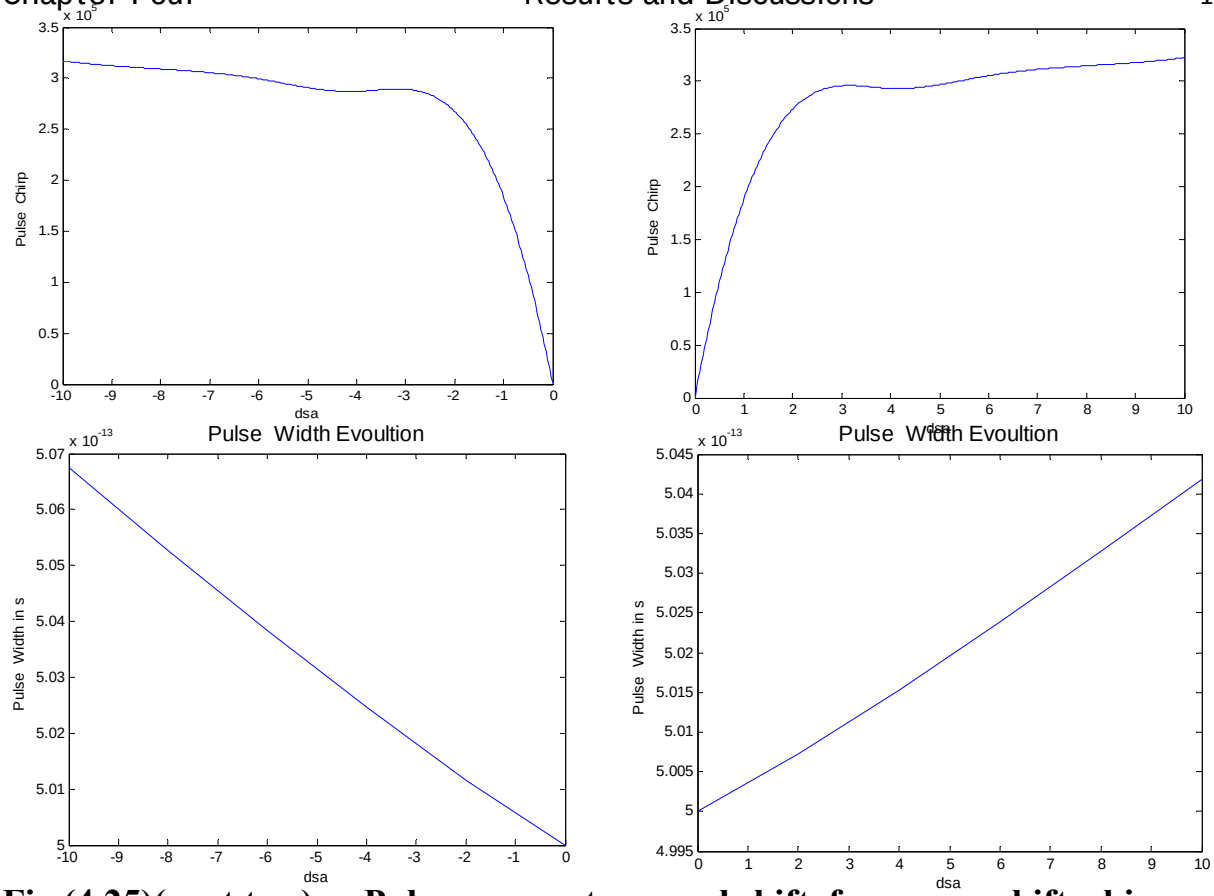

Fig.(4.25)(part two) : Pulse energy, temporal shift, frequency shift, chirp and width versus Modulation depth in(a) Normal (b)Anomalous dispersion.

Table(4-3). ***Pulse Parameters Database for three types mode-locked and both Dispersion Regimes***

	AM		**FM**		**SBR**	
	Normal	Anomalous	Normal	Anomalous	Normal	Anomalous
Energy	1.2 p J	0.49 p J	2.792 p J	2.785 p J	0.105 p J	0.105 p J
Temporally Shift	10.2ps	4.5ps	0	0.25	16ms	12.5ms
Frequency Shift	-65MHz	0.58 MHz	2.51 GHz	5.5 GHz	0	0
Chirp	62	-59	0	0	9.25e4	9.1e4
Pulse width	2.9ps	1.75ps	4ps	0.7ps	50.1 fs	49.88 fs

Form the result shown in table (4-3) the shortest pulse width produced from APM mode- locked in anomalous regime , Zero chirp produced from FM mode-locked, and maximum Energy from FM mode-locked are concluded

The result in this work is great with other results as shown in table below:

References	Types of mode-locked	Pulse width(τ)
[37]	APM	5ps
[41]	SBR	500fs
[44]	FM	500fs
[51]	FM	0.7ps
[52]	AM	3.73ps
[65]	APM,SESAM	3.8ps
Present work	FM AM (SBR)	0.75ps 1.75ps 49.8fs

4.5 Output pulse shape

Pulse characteristics and shape at each round trip of laser cavity in both normal and anomalous regime were analyzed .This gives a true picture of the pulse evolved along the number of round trips.

It is pertinent to mention that the pulse propagation through nonlinear medium (through it is single mode) case, the pulse undergoes various nonlinear phenomenon, like self phase modulation (SPM) and cross phase modulation (XPM) .

The pulse shape of output laser depended on regimes case .In the anomalous regimes the output pulse is Sech function according the relation in eq(3.17).The pulse grown from zero amplitude in the first round trip to maximum amplitude at 40 round trip. The shape of the pulse can be shown in fig(4.26).

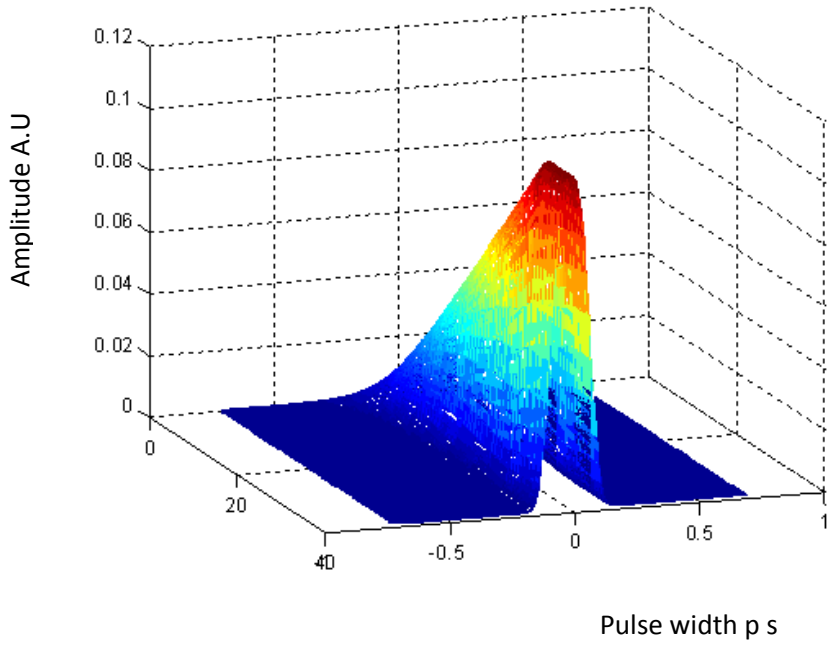

Fig(4.26)the output pulse shape in anomalous regime

In the Normal regimes the output pulse is Gaussian function according to the relation in eq(3-16).The pulse grown from zero amplitude in the first round trip to maximum amplitude at 40 round trip. The shape of the pulse can be shown in fig(4.27).

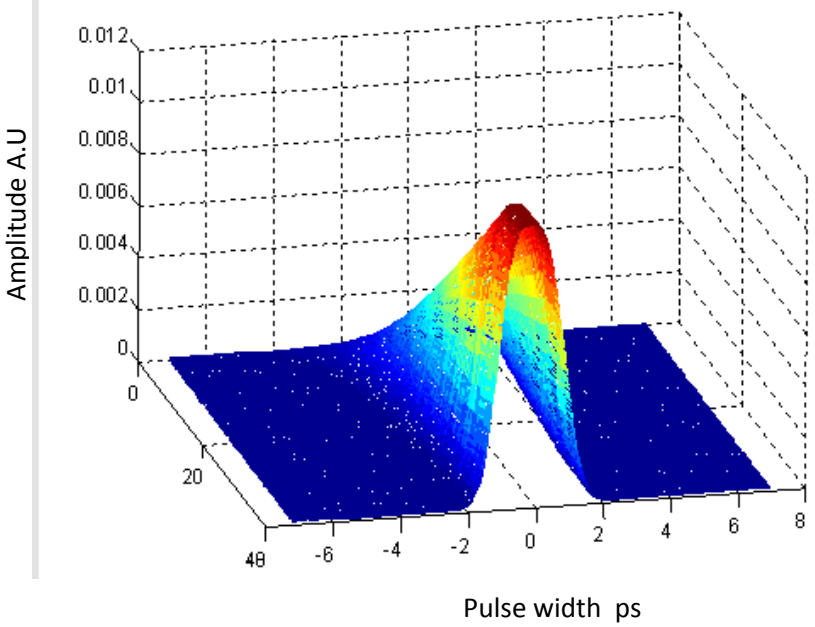

Fig(4.27) the output pulse laser in Normal regime

Chapter Five

Conclusions and Future Work

5.1 Conclusion

From present study and numerical results, many points could be concluded regarding comparison between both dispersion regimes, and modulation frequency, cavity Length, second order dispersion and nonlinear coefficient effect.

1. The study of TOD effect conclude with or without it there are no effect on pulse width, pulse energy and pulse chirp except frequency and temporally shift equal zero without TOD.

2. Anomalous regime pulse compression effect is better than counterpart normal regime due to the combination effect of both negative GVD and nonlinearity.

3. The number of round trip are needed to reaches steady state difference according the mode locking type. In FM mode locking RT>4000, Am mode locking>2000,andAPM mode locking RT>40.

4. Stability is better in anomalous regime and roundtrips required for steady-state values are much less than that for normal regime as shown in the previous plots figures.

5. For variable frequency modulation, it is obvious that it affects on all pulse parameters in addition to the system stability without exception. Modulation frequency does not affect on parameter sign value, since they depend mainly on dispersion regime. In FM the effect value of Fr=5GHz,

AM mode locking Fr=15GHz and APM mode locking Fr=5MHz it is a convert point.

6. In FM mode locking the oscillation is very high to reach to the steady state, in AM mode locking the oscillation is lower, but in APM mode locking is very small.

7. In situation of the length cavity varying, FM, AM mode locking pulse parameter effect directly, but in APM mode locking the pulse energy doesn't effect with varying Lr. The effective length in FM =4m,AM=4m andAPM=4m.

8. Varying nonlinear coefficient effect on all pulse parameter on all mode locking types.

9. Varying the second order dispersion has big effect on pulse parameter. The effective value of β_2 in FM and Am is equals 2ps/m in normal regime and equals -2ps/m in anomalous regime. β_2 doesn't effect in energy and frequency shift in APM ,but the temporally shift and chirp are effect .

10. Comparing of pulse width in three types the shortest pulse can be produced from APM mode locking, and the anomalous regime produces shorter pulse than normal regime.

5.2 Future Work

1. Using another method accurate rather than moment method so as to get exact matching with master equation results.

2. Using another dispersion compensation technique instead of using grating Pairs, which add losses and complicates the system.

3. Studying the effect of variation Modulation depth and pumping power on laser parameter.

4. Studying the stability of pulse mode-locking system and the effect of noise on the output pulse.

5.Using ABCD rule to achieve pulse laser parameter.

Reference

1.C.Guignard,P.Besanard,A.Mihaescu,andN.J.Zheludev"Harmonic Passive Mode-Locking of a single- frequency Semeconductor Laser Submitted to Nonliner Optical Feedback" IEEE J.Quantum Electronics, Vol. 42, No. 12,P 1185-1195, (2006).

2.S. Leprevost and P. Lepoudec" Mode locked fiber laser training kit"ETOP 2005.

3. W. Koechner "***Solid-State Laser Engineering***: Sixth Revised and Updated Edition 2006 Springer Science , New York, Inc.

4. Ronald W. Waynant , Marwood N. Ediger , "***Electro-Optics Handbook***" , McGraw -HILL, Inc. 2nd edition, (2000).

5. Lam Quoc Huy and Le Nguyen Binh, "Implementation and characterization of mode-locked fiber lasers", Department of Electrical and Computer Systems Engineering.

6. G. P. Agrawal," ***Applications of Nonlinear Fiber Optics",*** (Academic Press, New, York, 2001).

7. Cyril C. Renaud, ,J.A.Alvarez-Chavez,J.K.Sahu,J.Nilssion ,D.J.Richardson,and W.A.Clarkson ,"7.7mJ pulses from alarge core Yb-doped cladding pumped Q-switched fiber laser " IEEE Journal of Quantum Electronics, Vol. 37, No. 2,Feb. (2001).

8. Shiquan Yang, Evgueni A. Ponomarev, and Xiaoyi Bao, "80-GHz Pulse Generation From a Repetition-Rate-Doubled FM Mode-Locking Fiber Laser", IEEE Photonics Technology Letts, Vol. 17, No. 2, Feb. (2005).

9. N. G. Usechak, G. P. Agrawal, and J. D. Zuegel, "Tunable, high-repetitionrate, harmonically mode-locked ytterbium fiber laser," Opt. Letts. 29, 1360–1362, (2004).

10. Herman A. Haus, "Mode-Locking of Lasers ", IEEE Journal on Selected Topics in Quantum Electronics, Vol. 6, No. 6, Nov./Dec.(2000).

11. A. B. Grudinin, S.E. Goncharov, I. D. Zalevsky ,O. G. Okhotnikov, L. Gomes, N. Xiang, T. Jouhti,E.M.Dianov, I.A.Bufetov, V.V.Dudin, A.V.Shubin,A.N.Guryanov, M.V.Yashkov, A.A.Umnikov" High Power 980 nm Yb-doped Picosecond Fibre System Pumped by a Cladding Pumped 925 nm Nd-doped Fibre Laser" , IEEE Photonics Technology Letts, Vol. 15, No. 11, Nov.(2003).

12. J. Nathan Kutz , Brandon C. Collings and Keren Bergman , Sergio Tsuda, Steven T. Cundiff, and Wayne H. Knox , Philip Holmes and Michael Weinstein , "Mode-locking pulse dynamics in a fiber laser with a saturable Bragg reflector" , J. Opt. Soc. Am. B ,Vol. 14, No. 10, Oct.,(1997).

Reference

13. Nicholas G. Usechak, Govind P. Agrawal, and Jonathan D. Zuegel , " FM Mode-Locked Fiber Lasers Operating in the Autosoliton Regime ", IEEE Journal of Quantum Electronics , Vol. 41, No.. 6, Jun.(2005).

14.. Geert Morthier, Jinying Sun, Tim Gyselings, and Roel Baets Geert Morthier" A Novel Optical Decision Circuit Based on a Mach–Zehnder or Michelson Interferometer and
Gain-Clamped Semiconductor Optical Amplifiers" IEEE Photonics Technology Letts, Vol. 10, NO. 8, Aug.(1998).

15. W. T. Silfvast,(***Laser Fundamentals***), Cambridge University Press (1998).

16. Nick UsechakNick Usechak," Mode-Locked Fiber Lasers and their Applications "Ph.D. Thesis Proposal, The Institute of Optics, University of Rochester, Rochester, New York, December 9, 2002.

17. H.A.Haus, J.G.Fujmoto and E.P.Ippen "Analytic Theory of additive Pulse and Kerr Lens Mode Locking" IEEE Journal of Quantum Electronics, Vol. 28, No. 10,Oct. (1992).

18.H. A. Haus, E. P. Ippen, and K. Tamura "Additive-Pulse Modelocking in Fiber Lasers "IEEE Journal of Quantum Electronics, Vol. 30, No. 1, JAN.(1994).

19.E.R.Thoen"Development of Ultrashort Pulse fiber Laser for Optical Communication Utilizing Semiconductor Device" Phd.Thesis, Jun(2000).

20. E. A. DeSouza, C. E. Soccolich, W. Pleibel, R. H. Stolen, M. N. Islam, J. R. Simpson, and D. J. DiGiovanni, ''Saturable absorber modelocked polarization
maintaining erbiumdoped fiber laser'' Electron. Lett. 29, 447–449 (1993) .

21. S. Tsuda, W. H. Knox, E. A. de Souza, W. Y. Jan, and J. E.Cunningham, ''Low-loss intracavity AlAs /AlGaAs saturable Bragg reflector for femtosecond modelocking in solid-state lasers,'' Opt. Lett. **20**, 1406–1408 (1995).

22. H. Haus, J. Fujimoto, E. Ippen. "Structures for additive pulse mode locking", J. Opt.Soc. Am. B., Vol. 8, No. 10, pp 2068-2076. 1991.

23. Lynn Elizabeth Nelson, "Mode-locking of Thulium-doped and Erbium-doped Fiber Lasers" ,Doctor Thesis (1997).

24. S. E. HARRIS, and O. P. MCDUFF, "Theory of FM Laser Oscillation," IEEE Journal of Quantum Electronics , VOL QE-1, NO. **6**, SEPTEMBER 1965 .

25. D. J. Kuizenga and A. E. Siegman, "FM and AM mode locking of the homogeneous Laser–Part I: expermental", IEEE J. Quantum Electron.**,** Vol.6, pp 709–715, (1970).

26. H. A. Haus , " Theory of Forced Mode-locking " ,IEEE, J. of Quantum Electronics , Vol.11 , No. 7 , July (1975) .

Reference

27. Hermann A. Haus, and Yaron Silberberg , " Laser Mode Locking with Addition of Nonlinear Index" , IEEE Journal of Quantum Electronics , Vol. QE-22, No. 2, Feb.(1986).

28.G.Geister and R.Ulrich, ”Neodymium-fiber laser with integrated-optic mode locker”,Opt.Comm.Vol.68,pp187-189(1988).

29.M.Hofer,M.H.Ober,F.Haberal,and M.E.Fermann, ”Characterization of ultra –short pulse formation in passively mode-locked fiber lasers”,IEEE.J.Quantum Electronics Electronics,Vol.28,pp720-728(1992)

30. K.Tamura,H. A. Haus,and E.P. Ippen,”Self starting additive pulse mode-locked Errbium fiber ring laser”,Electron.Lett.Vol.28,pp2226-2228(1992).

31. M. E. Fermann, M. J. Andrejco, Y. Silverberg, and M. L. Stock, “Passive modelocking by using nonlinear polarization evolution in a polarizing maintaining erbium-doped fiber,” *Opt. Lett.,* vol. 18, pp. 894–896, (1993).

32. S.Longhi,P.Laporta,S,Taccheo,and O.Svelto,”Third-order harmonic mode-locking of abulk erbium:ytteribium:glass laser at a2.5-Ghz reption rate”Opt.Lett.Vol.23,pp1985-1987(1994).

33. F.X.Kartner,D.Kopf,and U.Keller,”Solitary-pulse stabilization and shorting in active mode-locked laser”,J.Opt.Soc.Am.B.,Vol.12,pp486-496,(1995).

34. Yoshida and M.Nakazawa,”80-200GHz erbium doped fiber laser using a rational harmonic mode-locking technique”Electron.Lett.Vol.32,pp1370-1372,(1996).

35. Brandon C. Collings, Keren Bergman, S. T. Cundiff, Sergio Tsuda, J. Nathan Kutz,, J. E. Cunningham, W. Y. Jan, M. Koch, and W. H. Knox “Short Cavity Erbium/Ytterbium Fiber Lasers Mode-Locked with a Saturable Bragg Reflector, IEEE Journal of Quantum Electronics Vol. 3, No. 4, August(1997).

36. A.B.Grudinin and D.J.Richardson and D.N.Payne,”Passive harmonic mode locking of a fiber soliton ring laser”,Elect.Lett.Vol.29,No.21,pp1860-1861(1997).

37. Kazi Sarwar Abedin, Noriaki Onodera, and Masaharu Hyodo , " Higher Order FM Mode Locking for Pulse-Repetition-Rate Enhancement in Actively Mode-Locked Lasers: Theory and Experiment " IEEE Journal of Quantum Electronics , Vol. 35, No. 6, Jun. (1999).

38. C.X.Yu,H.A.Haus,E.P.Ippen,W.S.Wong,and A.Sysoliatin,”Gigahertz repetition-rate mode-locked fiber laser for continuum generation”,Opt.Lett.Vol.25,pp1418-1320(2000).

Reference

39. Ori Katz, Yoav Sintov, Yehuda Nafcha and Yaakov Glick"Passively Mode-Locked Ytterbium Fiber Laser Utilizing Chirped Fiber Bragg-Gratings for Dispersion Control".

40. C. K. Nielsen, T. V. Andersen, and S. R. Keiding," Stability Analysis of an All-Fiber Coupled Cavity Fabry–Perot Additive Pulse Mode-Locked Laser", IEEE Journal of Quantum Electronics, VOL. 41, NO. 2, Feb. (2005).

41. . Nicholas G. Usechak and Govind P. Agrawal," Rate-equation approach for frequency-modulation mode locking using the moment method", J. Opt. Soc. Am. B/Vol. 22, No. 12/December(2005).

42. Nicholas G. Usechak and Govind P. Agrawal," Semi-analytic technique for analyzing mode-locked lasers", OPTICS EXPRESS, Vol. 13, No. 6, PP2075-2081,March (2005).

43. J.R.Buuckly.S.W.Clark,and F.W.Wise,"Generasion of ten-cycle pulses from an Ytterbiummm fiber laser with cubic phase comprasion",Opt.Lett.Vol.31.pp1340-1342 (2006).

44. Nick G. Usechak, Govind P. Agrawal and Jonathan D. Zuegel" Tunable high-repetition-rate, harmonically mode-locked ytterbium fiber laser" OPTICS LETTERS ,Vol. 29, No. 12 , June (2004).

45. Xiangyu Zhou,Dai Yoshitomi, Yohei Kobayashi, and Kenji Torizuka(Generation of 28-fs pulses from a mode-locked ytterbium fiber oscillator) , OPTICS EXPRESS ,Vol. 16, No. 10 , May (2008).

46. H. Sayinc1, D. Mortag1, 2, D. Wandt1, 2, J. Neumann1, and D. Krach,"Sub-100 fs pulses from a low repetition rate Yb-doped fiber laser", OPTICS EXPRESS ,Vol. 17, No. 7 , March (2009).

47. Mohamed A. Abdelalim, Yury Logvin, Diaa A. Khalil and Hanan Anis"Properties and stability limits of an optimized mode-locked Yb-doped femtosecond fiber laser" OPTICS EXPRESS ,Vol. 17, No. 4, February (2009).

48. Harry J. R. Dutton ***"Understanding Optical Communications"*** , IBM , 1st edition , (1998).

49. J. Swiderski, *et. al* , "Rare-earth doped fiber high power fiber lasers generating in near infrared range " , Opto-Electronics Review Vol. 12 , No. 2 pp 169-173 , (2004).

50. Emmanuel Desurvire, C. Randy Giles, and J.. Simpson, " Gain Saturation Effects in High-speed, Multichannel Erbium-Doped Fiber Amplifiers at $\lambda = 1.53\ \mu m$, Journal of Lightwave Technology , Vol. 7, No. 12, Dec. (1989).

51. Lixin Xu, , L. F. K. Lui, P. K. A. Wai, H. Y. Tam, and M. S. Demokan," 10 GHz actively mode-locked erbium-doped fiber ring laser using an electro-absorption modulator and a linear optical amplifier", O1W34I227.pdf ,2005 Optical Society of America(2005).

Reference

52. Hao Dong, Qiang Wang, Hongzhi Sun, and Niloy K. Dutta," Stable 80-GHz Short Pulse GenerationUsing the Cascaded Polarization-Maintaining Fiber Loop Mirrors", IEEE Photonics Technology Letts. , Vol. 17,No.7, pp1396-1398(2005).

53. G. Keiser, *" **Optical Fiber Communications** "* , McGraw-Hill, Inc., New York, 2nd edition , (1991) .

54. G. P. Agrawal , " ***Fiber-Optics Communication System*** " , By John Wiley & Sons, Inc. 3rd edition (2002).

55. G. P. Agrawal, *" **Nonlinear Fiber Optics** "* (Academic Press, New York, 1995), second edition.

56. T. I. Lakoba and G. P. Agrawal , "Effects of third-order dispersion on dispersion-managed solitons " , J. Opt. Soc. Am. B, Vol. 16, No. 9, Sep. (1999) .

57. Q. Lin and Govind P. Agrawal, , " Effects of Polarization-Mode Dispersion on Cross-Phase Modulation in Dispersion-Managed Wavelength-Division-Multiplexed Systems " , Journal of Lightwave Wave Technology , Vol. 22, No. 4, Apr.(2004).

58. Hermann A. Haus, and Yaron Silberberg , " Laser Mode Locking with Addition of Nonlinear Index" , IEEE Journal of Quantum Electronics , Vol. QE-22, No. 2, Feb.(1986).

59. . G. P. Agrawal "Optical pulse propagation in doped fiber amplifier " , Physical Review A , Vo.44 , No. 11 , Dec. (1991).

60. LEONARD G. COHEN, " Comparison of Single-Mode Fiber Dispersion Measurement Techniques " , Journal of Lightwave Technology , Vol. LT-3, No. 5, Oct. (1985).

61. J.Vasseur,M.Hanna,J.M.Dudley and J.R.Barry "Numerical and Theoretical Analysis of an Alternate Multiwavelength Mode-Locked Fiber Laser" IEEE Photonics Technology Letts, Vol. 17, No. 11, Nov. (2005).

62. Guido H. M. van Tartwijk and Govind P. Agrawal , " Maxwell–Bloch dynamics and modulation instabilities in fiber lasers and amplifiers " J. Opt. Soc. Am. B, Vol. 14, No. 10 , Oct. (1997).

63. Kristin M. Spaulding , Darryl H. Yong , Arnold D. Kim and J. Nathan Kutz ," Nonlinear dynamics of mode-locking optical fiber ring lasers", J. Opt. Soc. Am. B, Vol. 19, No. 5/May 2002 Vol. 19, No. 5,May (2002).

64. Ido Kelson and Amos A. Hardy, " Strongly Pumped Fiber Lasers " , IEEE Journal of Quantum Electronics, Vol. 34, No. 9, Sep.(1998) .

65. Jyhpyng Wang, *"**Fundamental Principles of Lasers and Ultrafast Optics*** " , (1990-2000).

66. Lionel R. Watkins, and Yu Rong Zhou, " Modeling Propagation in Optical Fibers Using Wavelets " , Journal of Lightwave Technology , Vol. 12, N0. 9, Sep. (1994).

Reference

67. J. B. Schlager, , B. E. Callicoatt, R. P. Mirin, , and N. A. Sanford " Passively Mode-Locked Waveguide Laser With Low Residual Jitter " , IEEE Journal of Selected Topics in Quantum Electronics , Vol. 14, No. 9, Sept. (2002).

68. Jennifer J. O.Neil, ‘‘Pulse Dynamics in Actively Modelocking Fiber Optic Lasers, University of Washington, Applied and Computational Mathematical Sciences, Honors Thesis Spring (2002) **.**

69. J. Nathan Kutz, Brandon C. Collings and Keren Bergman ,Sergio Tsuda, Steven T. Cundiff, and Wayne H. Knox,” Mode-locking pulse dynamics in a fiber laser with a saturable Bragg reflector”, J. Opt. Soc. Am. B, Vol. 14, No. 10,pp 2681 – 2690, October (1997).

70 . N. H. Bonadeo and W. H. Knox, Jeffrey M. Roth and K. Bergman,” Passive harmonic mode-locked soliton fiber laser stabilized by an optically pumped saturable Bragg reflector”, OPTICS LETTERS, Vol. 25, No. 19,pp 1421-1423,(2000).

Acknowledgment

All Praise and thanks must be for Almighty Allah for His guidance and help to me to make this work exist.

Also I would like to express my deepest appreciation to my supervisors Dr. Adawiya J. Haider and Dr. Mohammed S.Mehde for his assistance and kind notice and remarks .There encouragement throughout stages of this work made the accomplishment of this thesis possible.

Also I would like to thank Dr.Anwaar.A.Al Dorgazly at Al Nahreen University for her nice assistance, guidance and patience in explaining all problems which faced me during preparation of this thesis.

Special thanks to Dr. Nicholas G.Usechak, at University of Rochester, New York, USA,for his assistance and guidance during my contact with him through internet he showed extraordinary patience and was available for advice whenever needed. His valuable assistance and advice made me understand many diffiticults point s in this thesis.

Also, I would like to thank Dr.Luai K. at collage of science, Bagdad University for his assistance and kind patience in writing Mat-Lab program to perform the numerical solution.

Abstract

Ultra short pulses are very important research field they could be used as a pulsed source for optical fiber or a seed pulse for another laser in medical application .Another important application of ultra short pulses is in high speed optical communication system, where an optical short pulse source with high repetition rate is very important for high bit rate.

In this work, active and passive mode-locking fiber laser are studied. The study is focused on Active Mode-Locking by investigating Frequency Modulation (FM), Amplitude Modulation(AM) Mode-Locking and Passive mode locking by investigating Saturble Bragg Reflector(SBR). The models are studied by using ytterbium-doped, single mode fiber, operating with 1055 nm wavelength with 976 nm optical pump and FM,AM and SBR Mode-Locked by various optical modulators. A dispersion compensation technique (grating pair) is used to compensate the normal dispersion. The effect of both normal and anomalous dispersion regimes on output pulses is investigated .Also, frequency modulation ,nonlinear coefficient , cavity length and dispersion effects on pulse parameters are investigated by driving the modulator into different values .The study shows the stability of working in anomalous dispersion regime and the compression effect is better than counterpart normal regime due to combination effects of both negative(Group velocity dispersion) GVD and nonlinearity .Also it shows the great effect of modulation frequency, nonlinearity, dispersion and cavity length on pulse parameters and stability of the systems. Mode-locking fiber laser master equation is introduced .By using the assumed pulse shapes for both dispersion regimes after modifying (Ginzburg-Landu equation) GLE which is essentially Generalized

Nonlinear Schrödinger equation GNLSE and by applying the moment method ,a set of five ordinary differential equations are introduced. These equations describe pulse parameters evolution during each roundtrip. To solve these equations numerically fourth-fifth order, Runge-Kutta method is performed through Mat-Lab 7.0 computer program.

Result shows that, the output pulse width from the AM mode-Locked equals to τ=1.75ps in anomalous and τ=2.9ps in normal regimes, the pulse width from FM mode locked equals to τ= 0.7ps in anomalous regime and τ=4ps in normal regime and the pulse width from SBR (passive Mode locked) is τ=48.8fs in anomalous regime and τ=50.1fs in normal regime.

Table of Contents

Chapter One

Introduction and Historical Review

Chapter Two

Theoretical & Basic Concept

Chapter Three

Theoretical and their analysis

Chapter Four

Results and Discussions

List of Symbols

Symbol	***Meaning***	***Symbol***	***Meaning***
τ_f	*Lifetime of the upper level of the laser transition*	B_i	*Strength of jth resonance*
ω_0	*Pulse spectrum center frequency*	ω_i	*Resonance frequency*
β_2	*Second order dispersion*	β_1	*First order dispersion*
β_3	*Third order dispersion*	δ_{SA}	*Passive Modulation depth*
D	*Dispersion parameter*	*d*	*Cavity length*
$\bar{\beta}_2$	*Averaged second order dispersion*	$\bar{\beta}_3$	*Averaged third order dispersion*
F_m	*Modulation frequency*	F_r	*Repetition or modulation frequency*
a	*Core radius*	n_g	*Group refractive index*
λ	*Wavelength*	λ_D	*Zero-dispersion wavelength*
k_0	*Wave number*	*c*	*Light velocity*
b	*Optical fiber outer radius*	*N*	*Number of light modes*
Δv_{sep}	*Axial modes frequency spacing*	Δt_{sep}	*Roundtrip duration = (1/Δv_{sep})*
P_T	*Transmitted power*	E_0	*Field amplitude*
P_0	*Launched power*	φ	*Phase shift*

α	*Attenuation constant*	$I(t)$	*Intensity*
α_{dB}	*Attenuation in dB*	a	*Pulse amplitude*
C_R	*Rayleigh scattering constant*	T_R	*Roundtrip time*
α_R	*Rayleigh scattering losses*	$\Delta t_{p,min}$	*Shortest pulse duration*
α_c	*Incident critical angle*	$\bar{E}$	*Electric field vector*
ω	*Optical frequency*	$\bar{H}$	*Magnetic field vector*
$\bar{B}$	*Magnetic flux density vector*	$\bar{D}$	*Electric flux density vector*
$\bar{J}$	*Current density vector*	ρ_v	*Charge density*
$\bar{P}$	*Induced electric polarization*	$\bar{M}$	*Induced magnetic polarization*
μ_0	*Free space permeability*	ε_0	*Free space permittivity*
$\bar{P}_L$	*Linear polarization*	$\bar{P}_{NL}$	*Nonlinear polarization*
χ	*Optical susceptibility*	χ_e	*Electric susceptibility*
$\overline{g}$	*Saturation gain*	$\overline{g}_0$	*Average small-signal gain*
P_{ave}	*Average power*	P_{sat}	*Saturation power*
$A(t,z)$	*Slowly varying envelope of the electric field*	ω_m	*Modulation frequency = 2π (F_r)*
Δ_ω	*Gain medium spectral full width at half-maximum*	T_2	*Spectral width of the finite gain bandwidth*
$M(A,t)$	*Mode-locker term*	*Q - factor*	*Quality factor*
$\bar{\gamma}$	*Average non-linearity*	$\bar{\alpha}$	*Average losses*

T	*Propagation time*	v_g	*Group velocity*
Δ_{FM}	*FM Modulation depth*	t_m	*Delay between the center of the modulation cycle and the temporal window in which the pulses are viewed*
ξ	*Temporal shift*	Ω	*Frequency shift*
τ	*Pulse width*	q	*Chirp*
ΔE	*Variation between maximum and minimum energy value*	$\Delta\xi$	*Variation between maximum and minimum temporal shift value*
E_{max}	*Peak pulse energy*	Ω_{ss}	*Steady-state frequency shift*
L_D'	*TOD dispersion length*	$\Delta\Omega$	*Variation between maximum and minimum frequency shift value*
RT_{ss}	*Steady-state roundtrip*	Δq	*Variation between maximum and minimum chirp value*
q_{ss}	*Steady-state chirp*	ξ_{ss}	*Steady-state temporal shift*
τ_{max}	*Maximum pulse width*	τ_{ss}	*Steady-state pulse width*
RT	*Roundtrip*	RT_{4000}	*Roundtrip at RT=4000*
μm	*Micro-meter*	T_m	*Pulse slot duration*
nm	*Nano meter*	θ	*the angle of incidence*
l_g	*the grating separation*	v_m	*frequency separation*
β′+α	*the diffraction angle*	Δ_{AM}	*AM Modulation depth*

List of Abbreviations

Abbreviations	*Meaning*
AM	*Amplitude Modulation*
APM	*Additive Pulse Mode locking*
CW	*Continuous Laser*
DC	*Direct Current*
EOM	*Electro-Optic Modulator*
FM	*Frequency Modulation*
FBG	*Fiber Bragg Gratings*
FWHM	*Full Width at Half Maximum*
GVD	*Group Velocity Dispersion*
GNLSE	*Generalized Non-Linear Schrödinger Equation*
GLE	*Ginzburg–Landau Equation*
LIDAR	*Light Intensity Detection And Ranging*
LED	*Light Emitting Diode*
MZI	*Mach-Zehnder Interferometer*
NLSE	*Non-Linear Schrödinger Equation*
RF	*Radio Frequency*
SPM	*Self Phase Modulation*
SBS	*Stimulated Brillouin Scattering*
SRS	*Stimulated Raman Scattering*
SA	*Saturable Absorber*
SBR	*Saturable Bragg Reflector*
SESAM	*Semiconductor Saturable Absorbers Mirror*
TOD	*Third Order Dispersion*
PMD	*Polarization Mode Dispersion*
XPM	*Cross Phase Modulation*

Chapter one

Introduction and Historical Review

Chapter Two

Theory and Basic Concept

Chapter Three

Theoretical And Their Analysis

Chapter Four

Results and Discussions

Chapter Five

Conclusion Future Work

جمهورية العراق

وزارة التعليم العالي والبحث العلمي

الجامعة التكنولوجية

قسم هندسة الليزر والبصريات الإلكترونية

التحليل العددي لليزر الليف البصري النبضي

بتقانة قفل النمط الإضافي

رسالة مقدمة إلى

قسم هندسة الليزر والبصريات الإلكترونية في الجامعة التكنولوجية

كأحد متطلبات نيل درجة فلسفة الدكتوراه في هندسة الليزر

مقدمة من قبل

بشرى رزوقي مهدي البياتي

بكالوريوس هندسة إلكترونية 1987

ماجستير هندسة إلكترونية في تطبيقات الليزر 2001

بإشراف

د. محمد صالح مهدي **د. عدوية جمعة حيدر**

شوال 1430 تشرين الاول2009

Ministry of Higher Education & Scientific Research
University of Technology
Laser & Optoelectronics Engineering Department

NUMRICAL ANALYSIS OF ADDITIVE PULSE MODE LOCKING FIBER LASER

A Thesis Submitted to

The Laser and Optoelectronics Engineering Department

University of Technology in partial Fulfillment of the Requirements for the Degree of Doctor of Philosophy in

Laser Engineering

By

Bushra Razooky Mahdi

B.Sc.Electrical Engineering

1987

M.Sc .Electrical engineering in laser applications

2001

Supervised by

Dr.Mohammed S. Mahde

Sptember 2009AD

Dr.Adawiya J. Haider

Shawl 1430 AH

Certification of the Linguistic Supervisor

I certify that this thesis entitled (**Characterization of Additive Pulse Mode Locking Fiber laser**) was prepared under my linguistic supervision.

Its language was amended to meet the style of the English language.

Signature:

Name: Dr. Mohammed S .Ahmad

Title:

Date: / /2009

Supervisor Certification

I certify that this thesis entitled (**Characterization of Additive Pulse Mode Locking Fiber laser**) was prepared under my supervision by (Bushra Razooky Mahdi) at the Laser and Optoelectronics Engineering Department ,University of Technology as partial fulfillment of requirements for the degree of Doctor of Philosophy in Laser Engineering.

Signature:

Name: Dr. Mohammed S .mehde

Title: Assistant Professor

Date: / /2009

Signature:

Name: Dr. Adawiya J. Haider

Title: Assistant Professor

Date: / /2009

In view of the available recommendation, I forward this thesis for debate by the examination committee.

Signature:

Name: Mohammed A. Minshid

Date: / /2009

Assistance to the dean of department

Examination Committee Certificate

We certify that after reading this thesis entitled "**Numerical Analysis of Additive Pulse Mode locking Fiber Laser**" and examined the student "**Bushra Razooky Mahdi**" in its content, and what is related to it ,and that in our opinion,it meets the standard of a thesis for the degree of Doctor of philosophy in Laser Engineering.

Signature:

Prof.Dr. Raad S.Fyath

Data: / / 2009

Signature:

Prof.Dr .Abdul Hadi. AL.Janabi

Data: / / 2009

Signature:

Asst.Prof.Dr. Ziaad T.AL-Dahan

Data: / / 2009

Signature:

Asst.Prof.Dr Kadhim.A.Hubeatir

Data: / / 2009

Signature:

Asst. Prof.Dr. Hani J.Kbashi

Data: / / 2009

Signature:

Prof.Dr Dr. Mohammed S .mehde

Data: / / 2009

(Supervisor)

Signature:

Prof.Dr. Adawiya J. Haider

Data: / / 2009

(supervisor)

Approved for the School of Laser and Optoelectronics Engineering Department

Signature:

Asst. Prof.Dr.Mohammed H. Ali

Data: / / 2009